GENETIC APPROACHES TO THE STUDY OF CORONAVIRUS REPLICATION AND PATHOGENESIS

Damon Joshua Deming

A dissertation submitted to the faculty of the University of North Carolina at Chapel Hill in partial fulfillment of the requirements for the degree of Doctor of Philosophy in the Department of Microbiology and Immunology

Chapel Hill
2006

Approved by,

Ralph Baric, Ph.D.

Mark Heise, Ph.D.

Glenn Matsushima, M.D.

Rick Meeker, Ph.D.

Ronald Swanstrom, Ph.D.

Abstract

DAMON J. DEMING: GENETIC APPROACHES TO THE STUDY OF CORONAVIRUS REPLICATION AND PATHOGENESIS
(Under the direction of Dr. Ralph S. Baric)

The recently developed coronavirus reverse genetic systems have been a tremendous asset for improving our understanding of the viruses' complex replication strategy, pathogenesis, mechanisms of host-range expansion, and in the development of anti-viral therapies. We completed two studies using coronavirus infectious clones. The first evaluated a severe acute respiratory syndrome coronavirus (SARS-CoV) vaccine to protect against an antigenically divergent strain. The second study determined the requirement for proteolytic processing of a highly conserved region of the replicase polyprotein for efficient replication.

Ideally, a SARS-CoV vaccine should confer long-term protection, especially in vulnerable senescent populations, against both the 2003 epidemic strains and zoonotic strains that may yet emerge from animal reservoirs. Using Venezuelan equine encephalitis virus replicon particles (VRP) expressing the 2003 epidemic Urbani SARS-CoV strain spike (S) glycoprotein (VRP-S) or the nucleocapsid (N) protein from the same strain (VRP-N) as candidate vaccines, we tested their ability to protect young and senescent mice when challenged with homologous and heterologous SARS-CoV strains. The novel heterologous SARS-CoV strain (icGDO3-S) was constructed using synthetic biology and reverse genetics to generate a chimeric virus encoding a synthetic S glycoprotein gene of the most genetically divergent human strain, GDO3, which clusters among the zoonotic SARS-CoV, and represents a strain of SARS-CoV that emerged into the human population independently of

the epidemic strain. VRP-S, but not VRP-N, provided protection for both young and senescent mice when challenged with the epidemic strain. When challenged with icGDO3-S, VRP-S protected young mice but only partially protected senescent animals. VRP-N vaccinated mice demonstrated enhanced pulmonary inflammation, which included eosinophils among the cellular infiltrates, following SARS-CoV or icGDO3-S challenge.

The highly conserved region at the carboxy-terminus of the coronavirus replicase ORF1a polyprotein is processed by the main proteinase (M^{pro}) into mature products including nsp7, nsp8, nsp9 and nsp10, proteins with predicted or identified activities involved with RNA synthesis. M^{pro} continuous translation and processing of ORF1ab polyproteins is required for replication, but specific cleavage events may be dispensable. We determined the requirement for the nsp7-10 proteins and their proteolytic processing during the replication of murine hepatitis virus (MHV), which is phylogenetically grouped with the human coronaviruses OC43 and SARS-CoV. Using the MHV reverse genetics system, in frame deletions of the coding sequences for nsp7, 8, 9, and 10 were either deleted, or the flanking cleavage sites ablated, and the effect upon replication determined. Viable viruses were characterized through analysis of M^{pro} processing, subgenomic RNA transcription, and *in vitro* growth fitness. Deletion of any of the four regions encoding nsp7 through 10 was lethal. Disruption of the cleavage sites flanking the protein domains were lethal with the exception of the nsp9/10 cleavage site, which resulted in a mutant virus with severely attenuated replication. In order to determine if a distinct function could be attributed to pre-processed forms of the replicase polyprotein including nsp7-10, the genes encoding nsp7 and nsp8 were rearranged. The mutant virus MHV8/7 was not viable, suggesting that the noncleaved intermediate protein may be essential for replication or proteolytic processing.

TABLE OF CONTENTS

LIST OF TABLES

LIST OF FIGURES

Chapter I

Introduction

The order *Nidovirales* includes a broad group of mammalian, avian and crustacean viruses grouped among the families *Coronaviridae, Arteriviridae*, and *Roniviridae*. The family *Coronaviridae* is further divided into the genera Coronaviruses and Toroviruses. Although nidoviruses differ significantly in genome size, sequence, virion morphology, and host-range specificity, they are grouped within the same order due to several shared traits (reviewed in (66)). All Nidoviruses are positive-stranded RNA viruses with large replicase domains (designated ORF1a and ORF1b) which are functionally conserved and encoded at the 5' end of the genome. Translation of the replicase polyprotein is regulated by a ribosomal frame-shift event which directs the expression of either an ORF1a or an ORF1a/b full-length polyprotein, which is in turn proteolytically processed by virally encoded proteases. Another characteristic unique to nidoviruses is that several structural and nonstructural ORFs are encoded downstream of the replicase polyprotein and expressed by a 3' co-terminal nested set of subgenomic mRNAs (sg mRNAs) generated by a unique strategy of attenuated transcription. There are significant differences between the genome sizes of nidoviruses ranging from the smallest arterivirus genomes of ~13 kb to the largest coronavirus genomes of ~31 kb. The genomes of nidoviruses are infectious, and virus replication is initiated as the genome is delivered to the cytoplasm and the replicase is

translated by host cell ribosomes. For many nidoviruses, including coronaviruses, a typically narrow host range is dictated by the highly specific interaction between the glycoprotein spike displayed on the virion and a particular receptor on permissive cells. However, characteristic high mutation and recombination rates allow these viruses to evolve to infect new cells and expand beyond their normal tissue tropisms and host range limitations.

Coronaviruses are perhaps the most extensively studied of the nidoviruses, due in part to the fact that coronaviruses are the only known nidoviruses to infect humans. The desire to improve our understanding of coronaviruses is further motivated by the fact that several of these viruses present a direct threat to human health and interests. Coronaviruses are associated with human respiratory diseases which induce pathologies ranging in severity from relatively benign cold-like illnesses to fatal pneumonia. The human coronaviruses 229E and OC43 were identified in the 1960's and have been attributed as the cause of ~15% of the common cold in winter (75, 135). In 2003 a new coronavirus was identified (49, 107) which emerged from an animal reservoir(72, 147), most likely bats (113, 118, 149), which was associated with the SARS epidemic and resulted in nearly 8000 confirmed infections and nearly 800 deaths (77). Since then, two new coronaviruses have been isolated from humans exhibiting lower respiratory infections, NL63 (55, 58, 203) and HKU1 (219). Several coronaviruses are responsible for veterinary diseases, usually respiratory or enteric in nature, and are responsible for agricultural economic loss associated with a reduction of animal weights and increased neonatal mortality. Transmissible gastroenteritis virus (TGEV) (162), porcine epidemic diarrhea virus (PEDV) (148), infectious bronchitis virus (IBV) (25), and bovine coronavirus (BCoV) (121) are some of the coronaviruses effecting loss in the swine, poultry, and bovine industries, respectively.

Coronavirus reverse genetic systems were recently developed and have been a tremendous asset as new tools in facilitating our understanding of the viruses' complex replication strategy, pathogenesis, and mechanisms of host-range expansion. Reverse genetics systems are also proving to be useful in the development of safe and effective anti-viral therapies. The small size of the arterivirus, the smallest of the nidoviruses with genomes ranging in size from 13-16kb, facilitated the rapid development of molecular clones as early as 1997 (205). In contrast, the large size of the coronavirus genome and *E. coli* associated toxicity of regions within the polymerase gene had delayed the construction of stable full-length cDNA templates until 2000 (2, 229). Fortunately for coronavirus research, several strategies were successfully employed to overcome these limitations and develop viable reverse genetics systems.

ORF1 Domain Organization and Expression

ORF1, which comprises approximately two-thirds of the 5' portion of the genome, encodes the polycistronic replicase, while the remaining third of the genome codes for the structural and accessory proteins (**Fig. 1**). The organization and composition of the replicase gene is a hallmark of nidoviruses and sets them apart from other RNA viruses (242) (**Fig. 2**). Coronavirus replicases share structurally and functionally conserved domains, despite the fact that there may be limited sequence homology between the elements of the different genera. Several domains of ORF1 are shared by all nidoviruses. Shared features falling within ORF1a include the accessory protease, 3 trans-membrane domains (TM, MP1 and MP2), the main protease, and the ribosomal frame-shift site. Cleavage of the 5' end of the ORF1a polyprotein is mediated by one or two active domains of accessory, or papain-like

cysteine protease, PLP. In some coronaviruses, such as EAV and IBV, the first PLP domain is inactive, suggesting that although proteolytically inactive, they may serve another function in replication. SARS-CoV lacks the first PLP and relies upon the activity of its one PL^{P}, denoted $PL^{pro}2$ due to its position relative to that of other coronaviruses, for cleavage of the 5' end of the replicase polyproteins. The three TMs (TM1, MP1, and MP3) likely anchor the replication complex to intracellular membranes. MP1 and MP2 flank another functionally conserved domain within the ORF1a polyprotein, a papain-like protease responsible for mediating cleavage of most of the replicase polyproteins into its constituent components. These proteases are often referred to as either $3CL^{pro}$, due to their structural and substrate similarity to the picornavirus 3C proteinase, or M^{pro}, the main protease. The M^{pro} designation refers to the fact that these proteases are responsible for processing the majority of the ORF1 polyprotein, including all components of the ORF1b, which encode the major replicative enzymes and most highly conserved domains. A narrowly conserved domain encoding an ADP-ribose 1'-phosphatase (X) was recently identified within the nsp3 of corona- (152, 153) and toroviruses (48).

The -1 ribosomal frame-shift site demarcating the ORF1a/b interface is made up of a "slippery" heptanucleotide sequence followed by a conserved pseudoknot structure which mediates differential ORF1a and ORF1a/b translation. During translation, most ribosomes terminate translation at the 3' end of ORF1a to generate polyprotein 1a (pp1a). However, a relatively small proportion of ribosomes undergo a -1 frame-shift when contacting the "slippery sequence" to read through the translational stop at the end of ORF1a and continue the carboxyl-extension of pp1a to form the fusion polyprotein 1ab (pp1ab) (14, 16, 116). Treatment of infected cells with protease inhibitors interrupts infection, indicating that

constitutive proteolytic processing of the replicase polyprotein is required for replication and suggests that distinct roles may exist for both the fully processed and precursor forms of the polyproteins (13, 45, 103, 165, 168, 243). The necessity for the proteolytic processing of the polyprotein for efficient nidovirus replication has also been demonstrated in equine arteritis virus (EAV) and the mouse hepatitis coronavirus (MHV) by mutation of the cleavage sites recognized by M^{pro} or PLP (46, 206).

Several domains conserved across all nidoviruses fall within ORF1b (**Fig. 2**). In order from N to C-terminus, these elements are the RNA-dependent RNA polymerase (RdRp) (18, 47, 67), the putative Zinc-binding domain (ZBD; Z in **Fig. 2**) (171), a superfamily-1 helicase (Hel) (92, 93, 171), and an endoribonuclease (EndoU; EU in **Fig. 2**) (7, 91). The orientation of the RdRp and Hel domains, with the RdRp N-terminal to that of the Hel, is unique to the nidoviruses among message-sense ssRNA viruses. Also, the ZBD and NendoU domains are unique to nidoviruses and as such are considered hallmark genetic markers for the order (66). Other ORF1 functional domains are conserved over many, but not all, nidoviruses. For example, exoribonuclease (ExoN) (137) and a putative ribose-2'-O-methyltransferase (O-MT; OMT in Fig. 2) are only conserved within the pp1ab of corona-, toro-, and roniviruses (39, 178, 212).

Many elements of the replicase gene have no known function. One such region of the coronavirus genome encodes four small proteins, denoted nsp7 to nsp10 in coronaviruses, are translated from 3' end of ORF1a and are conserved among corona- and toroviruses (66). These proteins are processed by M^{pro} into mature products of 10, 22, 12, and 15 kDa, respectively. The nsp7-10 co localize with the replication complex bound to double membrane vesicles and are presumably involved with RNA synthesis (11, 12, 68, 126, 204).

Although the replicative function of these proteins are yet to be experimentally demonstrated, recent work has provided some insight into their purpose. Structure analyses of SARS-CoV nsp7 and 8 demonstrated that the two proteins form a hexadecameric supercomplex with electrostatic properties favorable for nucleic acid binding that may function as a processivity factor for the RdRp (234). A biochemical report described a primase function associated with the SARS-CoV nsp8 protein, implicating another important role for one of these small proteins in replication (32, 89). The SARS-CoV nsp9 crystal structure has also been resolved and shown to form homodimers possessing single-stranded RNA-binding properties, and it has been suggested that the protein may serve to stabilize nascent and template RNA during replication, transcription, and processing (22, 53). Temperature sensitive mutations localized in nsp10 suggest that the protein may be involved with negative strand synthesis (165). Recent reports describing the refinement of the nsp10 structure have revealed that the protein includes two Zn fingers, exhibits nucleic acid binding affinity (97), and that it may form a spherical dodecameric structure made up of 12 nsp10-11 fused subunits (187). Another recent structural study has described nsp10 crystals that formed monomers and homodimers and possessing nucleic acid binding affinity (97). Collectively, this data implies that the nsp7-nsp10 proteins are important – if not critical – to coronavirus, and likely torovirus, replication.

Organization of the Structural and Accessory protein genes

Genes downstream of ORF1 encode several structural and, for some viruses, non-structural proteins (**Fig. 1**). Although the structural genes vary significantly across the nidoviruses and most likely evolved independently for each family, all viruses of the order

express a single nucleocapsid protein (N) as well as the proteins making up the enveloped virion (66). In coronaviruses, the structural genes maintain the same order: 5'- spike glycoprotein (S), envelope protein (E), membrane spanning integral protein (M), and nucleocapsid (N) - 3' (**Fig. 1**). Some group-2 coronaviruses, such as BCoV, mouse hepatitis virus (MHV), and HCoV-OC43 also include a gene encoding hemagluttinin esterase (HE). SARS-CoV is an exception. In addition to the major structural genes, "accessory" proteins are encoded by ORFs located among, or overlapping with, the structural genes. These proteins, of which coronaviruses typically have between 2 and 8, may or may not be integrated within the mature virion, are not ubiquitously present within viruses of a given group, and are often dispensable for in vitro replication (42, 57, 73, 74, 145, 169, 217, 227). Although not involved with efficient growth in tissue culture, deletion of some of these accessory ORFs have been reported to attenuate pathology in animal models (42, 73, 145).

Expression of ORF2+ Proteins via Subgenomic mRNAs

Nidoviruses express all proteins other than those encoded by ORF1, which are translated directly from genomic RNA, from a 3' co-terminal nested set of mRNAs (**Fig. 3**). These templates are generated by a mechanism referred to as attenuated transcription. As the viral polymerase transcribes the negative sense RNA from the 3' end of the positive sense RNA template, it encounters a conserved sequence, the transcriptional regulatory sequence (TRS), located at the beginning of every ORF (**Fig. 4**, step 1). Upon encountering each TRS there is a chance that the polymerase will dissociate from the RNA template. In this cartoon, considerable distance between the body and leader TRS junction sites are indicated, although some argue that folding of the intervening genomic sequences places the TRS sites in close

proximity. In the case of corona- and arteriviruses, their transcription strategy may more specifically be called discontinuous attenuated transcription. This refers to an additional recombination event that transfers the incomplete negative sense RNA strand to a TRS located near the 5' end of the genomic template (**Fig. 4**, step 2). Transcription continues to include the complementary sequence of the 5' UTR on the newly synthesized minus strand. In turn, the minus sense strand serves as the template for mRNA sense RNAs (**Fig. 4**, step 3). Typically, there is a decreasing chance that the polymerase will retain its association with the genomic template as it progresses past each TRS which leads to a nested set of mRNAs which decreases in relative amount the longer the mRNA.

Nidoviruses as Emerging and Reemerging Infectious Agents

It is estimated that 73% of human emerging and reemerging infectious diseases -- pathogens rapidly increasing in incidence, expanding in geographic range, or extending infection into new host species -- are zoonotic pathogens that have bridged the species barrier (108, 221). At 37% of all emerging and reemerging pathogens, RNA viruses are well represented (221). In order for a virus to expand outside of its normal host range, the virus must evolve the capacity to interact with novel cellular factors and adapt to evade or usurp mechanisms which normally function to ablate virus entry, replication, or transmission in a new host species. An emerging virus requires both the opportunity to interact with a new prospective host as well as possess molecular mechanisms with which to adapt and replicate efficiently within the hostile cellular environment. With a very broad distribution among several different animal species, many of which maintain close contact to humans, coronaviruses are often presented with the opportunity to interact with a new potential host.

With replication characterized by high mutation and recombination rates, coronaviruses also possess the means to rapidly evolve to changing cellular environments and selective pressures.

With established reservoirs in humans, wild and domesticated animals, coronaviruses have plenty of opportunity to make contact with species normally outside of their restricted host range. Many animals hosting coronaviruses are maintained close to other animals or humans, such as in the case of livestock and companion animals, such as equine, swine, bovine, canine, feline, and avian species. Several examples of emergent viruses have been found during the extensive studies of the coronaviruses' ability to expand their host range. For instance, the porcine epidemic diarrhea virus (PEDV), an economically significant cause of severe swine gastroenteritis in Europe and Asia, is closely related to the human coronavirus HCV-229E and is believed to be the result of transmission from humans to swine (15, 51, 148). BCoV is believed to have passed into several species of ruminants including elk (128), waterbuck, sambar deer, and white-tailed deer populations (201), dogs (54), and has been associated with at least one enteric infection in humans (76, 236). Close genetic and antigenic similarities between the group II coronaviruses BCoV, HCoV-OC43, and porcine hemagglutinating encephalomyelitits virus (PHEV) suggests that they may have only recently diverged from a common ancestor (211).

The most significant example of an emerging coronavirus is the severe acute respiratory syndrome coronavirus (SARS-CoV) (49, 107). The epidemic strains of SARS-CoV likely evolved from a zoonotic strain (72, 147) maintained in bats (113, 118, 149). It is believed that the virus crossed into humans through use of a liaison species such as the palm civet or raccoon dog infected while maintained in live-animal markets in close proximity to

other species (72, 119, 180, 202). Similarly, sero-positive wet-market animal handlers who were asymptomatic for signs of SARS suggests that a SARS-like progenitor virus was also transmitted to humans during their contact with animals in the live-animal markets (28, 72, 150)}. Indeed, antibody detected in a low percentage (1.8%) of people in Hong Kong 2 years prior to the epidemic suggests that exposure to SARS-like viruses had infringed into human populations at least 2 years before the virus evolved the ability to efficiently replicate within a human host, cause disease, and spread from human-human (240).

Although nidoviruses have the opportunity to expand their host ranges, they must be able to exploit such opportunities by rapidly adapting to fit their new host. The potential for a virus to successfully adapt to a new host and cross the species barrier involves its ability to adapt to new or changing cellular environments and find new ecological niches via genetic variation (124). Nidoviruses can explore the range of viable genetic variation through two mechanisms, mutation and recombination. As viruses dependent upon a polymerase lacking a proof-reading mechanism, replication introduces approximately $1x10^{-3}$ - $1x10^{-5}$ errors per replication cycle (130), or up to 3 mutations per newly synthesized coronavirus genome. This high rate of error is common for RNA viruses and leads to the generation of genetically variable quasispecies and contributes to their genetic plasticity and ability to rapidly evolve to changes in selective pressure (8, 86, 210). Comparing the sequences of SARS-CoV isolated from live-market animals and early human cases to those of the late epidemic virus illustrates the rapid adaptation and high mutation rate, estimated at approximately two-mutations per human passage (between $1.8x10^{-6}$ and $8.3x10^{-6}$ nucleotide substitutions per site per day or ~0.17 mutations per genome per day) (195, 207, 226).

There is reason to believe that multiple strains of SARS-like CoVs emerged independently into the human population, although not as successful as the Urbani and related epidemic strains in adapting to human hosts. Between December 16, 2003 and January 8, 2004, four patients were independently hospitalized in Guangdong Province, China and confirmed as SARS cases. The patients did not have contact with each other or other SARS patients, and all four patients presented mild symptoms, and likely contacted the SARS-CoV through contact with infected animals from live-markets. Analysis of these isolates showed sequence similarity closer to zoonotic strains than that of the initial epidemic strain (98, 142, 180, 195). Given the facts that they were found relatively late in the epidemic and their sequences did not appear to derive from the epidemic strain, these viruses likely represent an independent reemergence of a SARS-CoV into human populations whose success may have been limited due to the rapid response of the Chinese government to quarantine infected individuals and cull animals suspected of harboring the virus.

A second aspect of coronavirus biology that contributes to remarkably high adaptability to new hosts is a high rate of recombination. In 1995, the high recombination rates of coronaviruses were recognized as an aspect of replication that would likely contribute to these viruses becoming known as a significant threat as emerging pathogens (3). Coronaviruses, along with arteriviruses and toroviruses, rely on homologous recombination as part of their replication strategy to generate subgenomic RNAs from which to express their downstream genes. Using complementation of temperature sensitive mutants, the homologous recombination frequency for the entire genome of the coronavirus mouse hepatitis virus (MHV) was found to approach 20% or more (4, 111). Increasingly higher recombination rates progressing from the 5' to 3' end have also been shown in coronavirus

(61, 62) and arteriviruses (138). The increasing occurrence of recombination moving from the 5' to 3' end of genome is likely a reflection of the increasing number of templates with which recombination can occur as a result of the co-terminal nested set of subgenomic RNA strands formed during replication (61, 129). Indeed, the highly efficient targeted RNA recombination system relies upon the frequent recombination between these RNA templates.

New strains of nidoviruses have been generated by recombination in the lab and in the wild. For example, recombination resulting in viable viruses has been illustrated in experimentally infected animals with murine coronaviruses (100) and in eggs infected with IBV (106). Evidence of homologous recombination between coronaviruses in the wild has also been found in novel strains of IBV (26, 94, 110, 114), including recombination involving vaccine strains (115, 176, 213). Several examples of recombination within feline coronaviruses are also known. A novel serotype of FCoV, serotype II, is the result of a double recombination event with canine coronavirus, CCoV (85). Four FCoV type II strains have been isolated and shown to be the result of independent recombination events (208), suggesting that such recombination events are not rare. SARS-CoV has been postulated to have been derived from multiple recombination events among progenitor coronaviruses of all three groups, although these analyses are more tenuous (157, 184, 185, 237). Critics of the recombinatory origin hypothesis of SARS-CoV point out that these studies are based on the assumption that there is ample opportunity for recombination events to occur between divergent groups, which often exhibit distinctly different host-ranges, and that there is little data to support extensive recombination between different coronavirus groups (64, 131). Evidence of recombination between genotypes of the recently identified HKU-1 may be the first demonstration of coronavirus recombination in humans (220).

Nidoviruses have the opportunity and ability to quickly adapt to new cellular environments, and ongoing studies are devoted to understanding the molecular changes mapping to expanded tropisms. Coronavirus specificity is primarily mediated at binding and entry by the interaction of the spike glycoprotein with specific cellular receptors (23, 37, 44), as transfection of genomic RNA (117, 136) or expression of the appropriate receptor (44, 52, 199, 225) allows infection of otherwise non-permissive cells. Not surprisingly, many of the mutations critical for extended host ranges are the result of mutations within the spike glycoprotein.

Several in vitro models have been developed for studying the molecular determinants of coronavirus cross species expansion. Persistent cell models were developed to identify the genetic alterations that arise in coronaviruses that occur as the viruses and their host cells co-evolve in response to long-term persistent infections (5, 30). In one such model, murine astrocytoma cells (DBT) were infected with MHV-A59 and serially passaged for 210 days. Persistent infection of these cultures by MHV establishes a selective pressure whereby the DBT host cells decrease their ability to be infected by down-regulating expression of the MHV receptor, carcinoembryonic antigen-related receptor glycoprotein (CEACAM) (30, 37). In response, the virus adapts by altering the S gene to alter receptor specificity (30). Changes within MHV S altered its receptor subunit specificity and significantly enhanced viral infectivity of hamster and human cells (30) by increasing its ability to bind the non-murine CEACAM orthologues which are poorly recognized by wild-type MHV S (37). A similar persistent infection model using MHV and murine 17Cl1 cells resulted in an extended host range mutant with affinity for hamster, feline, bovine, rat, monkey, and human cells (166, 167, 193, 194). Such changes occurring over the course of a persistent infection could

account for the altered tropism of viruses such as FCoV. The lethal form of FCoV, feline infectious peritonitis virus (FPIV), likely arises from accumulated mutations within the S gene which alter the tropism of the persistent low virulence feline enteric coronavirus (FECV) from cells of the enteric tract to macrophages (160, 209).

A second in vitro model of coronavirus host range expansion uses persistently infected mixed cell cultures. A culture containing two cell lines, the MHV permissive DBT and the resistant Syrian baby hamster kidney (BHK) were infected with MHV-A59, MHV-JHM, or a combination of the two strains. Although both MHV strains are unable to infect BHK cells, MHV-JHM causes receptor independent fusion between DBT and BHK cells in vitro, and was included in the study for its potential to enhance virus evolution and adaptation to the BHK cells (6, 63). The ratio of the permissive DBTs to resistant BHKs was changed over time with passage, with the relative amount of DBT cells being decreased. This pressure for the virus to adapt to infect the normally non-permissive cells produced an extended host range mutant in the case of the co-infected cultures. After 200 days of virus derived from the MHV-A59/JHM cultures were able to efficiently infect BHK cells. This virus also had adapted the ability to infect human, primate, as well as retaining efficient replication in murine cell lines, further emphasizing the plasticity of the coronavirus genome and demonstrating the ability of these viruses to rapidly evolve new tropisms.

Although the models used to examine host range expansion emphasize the importance of the spike glycoprotein/receptor interaction as determinants for host range expansion, there is evidence that mutation of other regions of the genome can also be critically important for the successful adaptation of a coronavirus to a new host. In an attempt to develop a mouse model for HCoV-229E, mice were genetically engineered to

express the viral receptor, human aminopeptidase N (APN) (199, 218). Although primary cell cultures established from the animals were permissive to infection, mice were resistant to direct infection (218). However, infection of double transgenic mice expressing APN and deficient in *Stat1* were highly susceptible to HCoV-229E infection (112), indicating that the virus was not able to replicate within an immunocompetent animal despite successful binding and entry.

Nidovirus Reverse Genetics Systems

Reverse genetics systems allow viral genomes to be directly manipulated and linked to a given phenotype. The development of reverse genetic systems sparked a revolution in Nidovirus research, significantly contributing to the understanding of gene function and factors that regulate transcription, replication, pathogenesis, assembly and release. The first Nidovirus reverse genetics system was developed by Paul Masters in 1992 based on a targeted recombination system that matured to allow for the ready manipulation of the 3' most ~10Kb of the genome. However, this system didn't allow modification to most of the replicase gene which makes up nearly two-thirds of the viral genome. Modification of the replicase genes required the development of a full length cDNA based infectious clone. An infectious clone provides a cDNA template which can be manipulated by standard molecular biological techniques to alter the viral genome sequence. Virus is generated from the full-length cDNA either by placing a polymerase II promoter or a T7 promoter upstream of the viral sequence. RNA is transcribed from the template, either directly from the DNA transfected into the nucleus of a cell or synthetically in vitro from the T7 promoter. Once the RNA is delivered into the cells cytoplasm, the replicase ORFs are translated into a functional

replication complex that directs the transcription of subgenomic mRNAs and genome length RNA replication, resulting in the production of infectious progeny viruses.

Although an infectious DNA clone for the arterivirus equine arteritis virus (EAV) was reported in 1997, attempts to develop a system for coronaviruses were complicated by the large genome size and cDNA instability when amplified in bacterial vectors. Eventually, stable coronavirus infectious cDNA systems were developed by overcoming the amplification difficulties by one of three different strategies. One strategy, and the first to report the successful generation of infectious virus from a full-length infectious clone, makes use of highly stable bacterial artificial chromosomes. A second strategy disrupts toxic regions encoded within the cDNA copy of the viral genome by separating the clone into contiguous fragments in multiple bacterial plasmids. The full-length cDNA clone is then reconstructed by excising the viral cDNA from the bacterial plasmids and ligating them together in vitro. A more recent approach is stably cloning the full length genome in poxvirus vectors. All three of these systems, targeted RNA recombination, full-length infectious cDNA expressed in stable amplification systems, and infectious clones amplified as multi-component cDNAs, are currently used in research and have relative strengths.

Targeted RNA Recombination

The first nidovirus genetics approach was developed for mouse hepatitis virus (MHV), the prototypic coronavirus (reviewed in (132)). Recognizing the difficulty in developing full length 30 Kb molecular clones, the targeted RNA recombination approach takes advantage of the high recombination rate which occurs during coronavirus replication. The system relies upon a recombination event to transfer genes from a donor construct to a recipient viral

genome, followed by selection conditions which efficiently promote and amplify the replication of recombinants over the parent genome. The earliest version of the system relied upon a temperature sensitive mutant genome recipient, Alb4, which contained a mutation in the nucleocapsid gene (N) that allowed normal replication at permissive temperatures (<34^{o}C) but becomes severely attenuated at higher, or nonpermissive, temperatures (~39^{o}C) (**Fig. 5**). Successful recombination transferred the donor RNA lacking the thermolabile mutation to the host genome and the resulting recombinants were capable of efficient growth and plaqued efficiently at the nonpermissive temperature. Recombinant viruses were selected on the basis of plaque size when grown at the nonpermissive temperature.

Several improvements have been made to the system since its original conception over a decade ago. The original iteration of the targeted RNA recombination system was limited to the production of robust viruses, since selection was made based on the comparison of growth fitness at the nonpermissive temperature. In the case of genetic manipulations resulting in viruses attenuated at the nonpermissive temperature, whether due to their own temperature sensitivity or simply to a loss of growth fitness in general, selection was lost. The target size of the portion of the genome amenable to mutagenesis was mostly limited to the nucleocapsid gene located at the 3' end of the genome. These limitations were overcome by taking advantage of the narrow host ranges of certain coronaviruses. A chimeric donor virus was engineered which expressed the ectodomain of the spike glycoprotein, which determines receptor specificity in coronaviruses, of feline infectious peritonitis virus (FIPV) fused with the c-terminal membrane spanning domain of the MHV S glycoprotein encoded within the MHV genetic background (109) (**Fig. 6**). The chimeric fMHV was able to grow on feline cell lines while wild-type MHV cannot, confirming

previous data that argued that the S glycoprotein was a principle determinant of coronavirus host range. More importantly, fMHV was unable to infect cells derived from mice which are permissive to MHV. However, following successful recombination with a donor construct containing MHV S, the recombinant virus simultaneously lost the ability to infect feline cells and gained the ability to infect murine cells. This system provided a powerful positive selection step (i.e., growth on murine cells) which readily allowed for the isolation of attenuated mutant viruses. Later improvements to the targeted recombinant system include a mechanism for limiting multiple recombination events, especially at the 3' end of the genome. Although successful recombination required that a functional copy of the MHV S gene be selected, there was the possibility of further recombination events occurring (**Fig. 7**). These are particularly likely when an introduced mutation at the 3' end of the genome is debilitating. The likelihood of multiple recombination events occurring was reduced by moving the N gene of the recipient virus immediately downstream of the S gene. In the event of a second recombination event downstream of S, the resulting virus would lack the essential N gene and would be unviable. The targeted recombination system has been extended to MHV-JHM (144), TGEV, and FIPV and remains a powerful technology for altering genes and sequence motifs at the 3'-most 10 Kb of the genome (74).

Infectious cDNA clones

BAC System

The first full-length cDNA infectious clone of a coronavirus was that of the transmissible gastroenteritis virus (TGEV) and was accomplished by the stepwise reconstruction of the full genomic cDNA from a defective minigenome (DI) which required a helper virus to replicate.

The final missing fragment of the TGEV genome, which caused instability in standard bacterial vectors, was added in the last step and the full-length cDNA was transferred to a bacterial artificial chromosome (BAC), which attains a high degree of stability by maintaining a very low plasmid copy number, no more than two copies per cell (2). The full-length genomic cDNA is transfected directly into cells and RNA is transcribed from within the nucleus of a cell from a CMV promoter located upstream of the viral sequence. Notably, the majority of viral RNA does not undergo deleterious mRNA splicing and is transferred from the nucleus of transfected cells into the cytoplasm where the virus replicates normally. After detecting that there was some level of instability in the TGEV BAC system with passage in *E. coli*, the system was further stabilized by inserting an intron into the region of the ORF1 gene responsible for the toxicity in bacteria. Expression of full-length infectious cDNA clones of the human coronaviruses OC43 (186) and SARS-CoV (1) have also been reported using this approach. The full-length cDNA copies of these two clones, however, were not constructed by rebuilding an incomplete DI genome but were pieced together using unique restriction sites either present within the genome or added with the introduction of silent mutations.

Vaccinia Virus Expression System

After reporting difficulty in maintaining cDNA stability in bacterial systems, including BAC, Thiel and associates described a technique by which full-length cDNA of the human coronavirus 229E was amplified in a vaccinia virus cloning vector (196) (reviewed in (197)). The cDNA was systematically assembled and cloned into a vaccinia virus vector. Recombinant vaccinia virus DNA containing the 229E genome cDNA was transfected into

cells and recombinant vaccinia viruses were rescued by co-infection with fowlpox virus. Recombinant vaccinia virus DNA was purified and used as template for the in vitro transcription of genomic RNA, which is then electroporated into cells. Avian infectious bronchitis virus (IBV) (24) was derived from a full-length cDNA by an alternative strategy using vaccinia virus vectors. Following transfection of the vaccinia virus DNA containing the IBV cDNA, cells were infected with fowlpox virus expressing TR RNA polymerase. A T7 promoter was engineered before the IBV cDNA, and viral RNA was transcribed within the cell initiating viral replication.

One of the novel aspects of propagating coronavirus cDNA within the vaccinia virus is the ability to mutate the clone by taking advantage of homologous recombination. There are two recombination steps in the procedure. A donor plasmid DNA containing the desired mutation and containing a dominant selectable marker gene recombines with the recipient cDNA by homologous recombination. Recombinant viruses containing the dominant marker are selected. Next, the selected virus is allowed to grow in the absence of selection. This results in two recombination events: the cDNA reverts to its original sequence or the selectable marker gene is excised and the clone successfully integrates the modification. Isolates containing the mutation are screened by PCR (17). A similar strategy was recently employed for creating and modifying an MHV-A59 infectious clone (36).

A third strategy for producing full-length cDNA infectious clones, and the basis of the systems used for the experiments presented in this manuscript, was presented in 2000 from the Baric Lab. The stability problems in bacterial amplification systems were overcome by breaking up the viral genome into several smaller contiguous subclones. The components of the genome are propagated individually in bacterial vectors and full-length cDNA clones

generated after the genome fragments are excised from the plasmid vectors and ligated. Synthetic RNA is produced in vitro through the use of a polymerase promoter at the 5' end of the construct and electroporated into cells. This strategy was first applied to the development of a six-component TGEV infectious clone (229). Subclones were flanked by BglI or BstXI, restriction enzymes that recognize symmetric palindromes but cleave within asymmetric sites resulting in a 3- or 4- nucleotide complementary overhang. Use of these enzymes allows for a high degree of variability among different BglI digests, unique complementation, and high-specificity between contiguous fragments.

The first full-length infectious clones of MHV-A59 (231), SARS-CoV (230), and IBV (228) were also generated by using the multi-component approach. The development of molecular clones for the group II coronaviruses had been complicated by the presence of several toxic regions within the cDNA copy of the viral genome. Toxic regions were identified by systematically removing viral sequence until plasmid stability had been achieved, then engineering BsmBI or BglI restriction sites to allow reassembly between adjacent fragments. As a result, regions of the genomic cDNA that were toxic in bacteria could be specifically disrupted by separating the region into two genomic segments (Figure 7). Following digestion with the restriction enzyme, cDNA fragments could be seamlessly ligated to generate the full-length cDNA copy of the viral genome from which RNA could be transcribed and electroporated into cells to form virus.

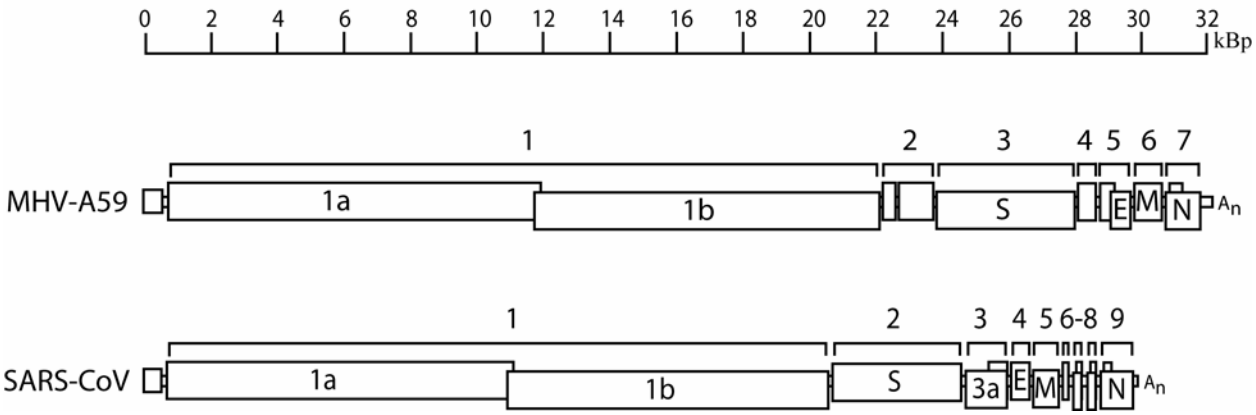

Figure 1. Genome organization of MHV-A59 and SARS-CoV. The 5' two-thirds of the genome encode the polycistronic replicase protein in ORF1. Two polyproteins are expressed from ORF1, pp1a and 1ab. Pp1ab is a c-terminal extension of pp1a which is dependent upon a -1 ribosomal frame-shift event at a conserved pseudoknot structure. The primary structural genes, Spike glycoprotein (S), Envelope associated protein (E), Membrane protein (M), and Nucleocapsid (N), as well as a series of virus specific accessory proteins are encoded within the 3' one-third of the genome from ORFs 2-7 for MHV-A59 and ORFs 2-9 in SARS-CoV.

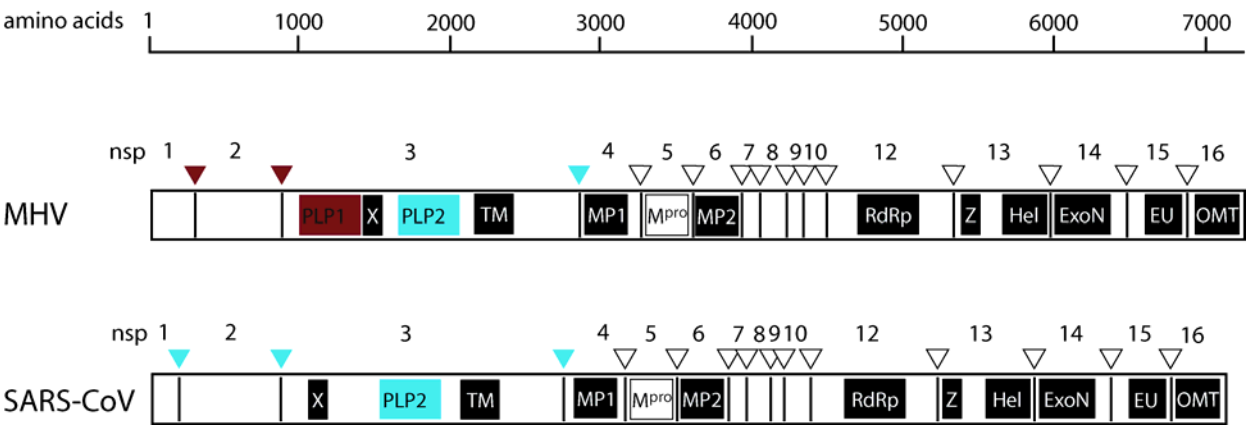

Figure 2. ORF1ab polyprotein: Proteolytic processing and conserved elements. Cleavage is mediated by three proteases in MHV or by two in SARS-CoV. The box color for each proteolytic domain and triangles at each nsp interface are color coordinated to the protease which cleaves at each position (red for $PL^{pro}1$, blue for $PL^{pro}2$, and white for M^{pro}). MHV and SARS-CoV conserved domains are shown, including the accessory protease (PL^{P}), ADP-ribose 1'-phosphatase (X), transmembrane domains (TM, MP1 and MP2), main protease (M^{pro}), RNA dependent RNA polymerase (RdRp), zinc-binding domain (Z), helicase (Hel), exoribonuclease (ExoN), an endoribonuclease (EU), and ribose-2'-O-methyltransferase (OMT).

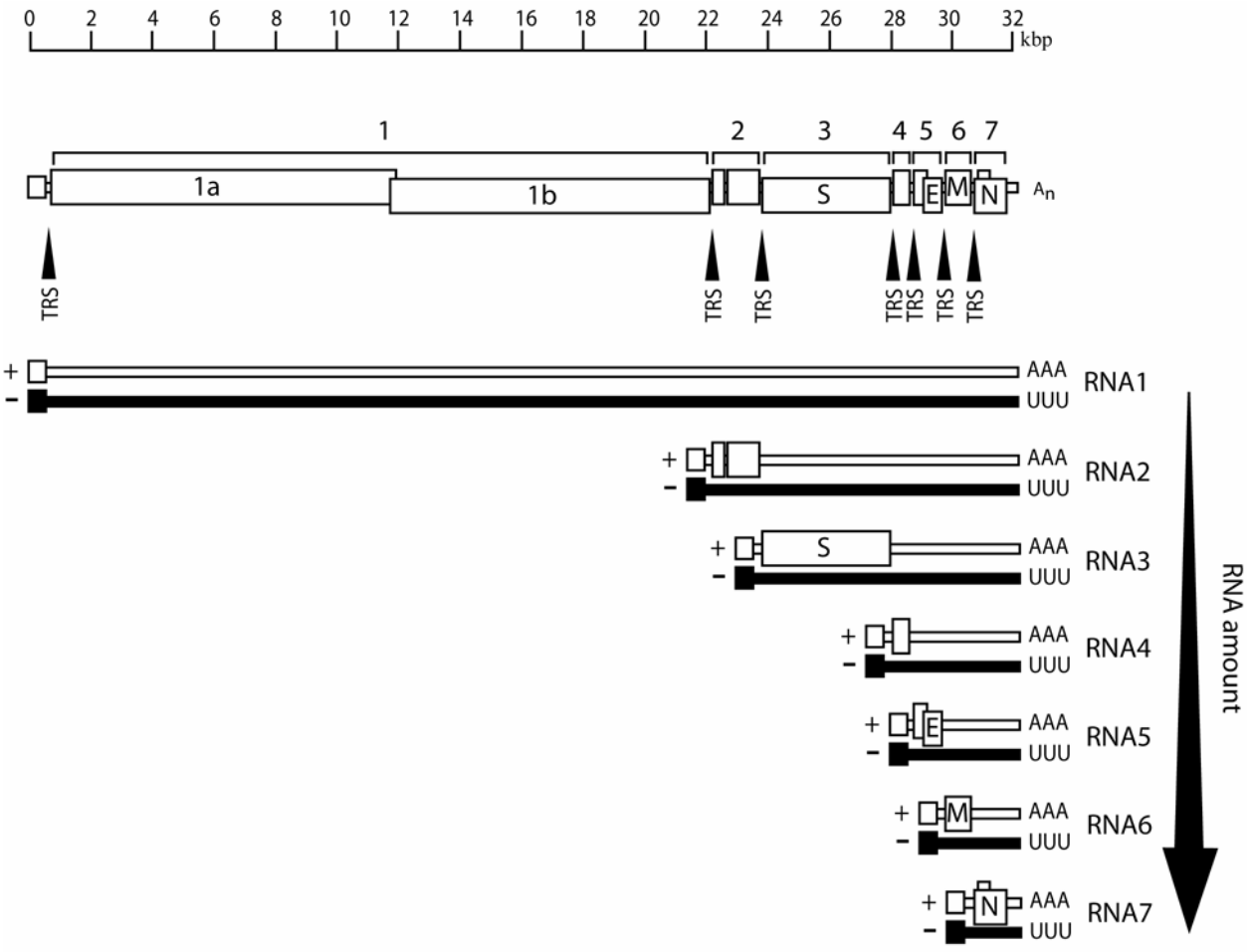

Figure 3. Expression of ORF2+ from subgenomic RNAs. A nested set of RNA sharing co-terminal ends is generated during coronavirus replication for expression of the structural and accessory proteins. Each subgenomic RNA is associated with one ORF defined by a conserved transcriptional regulatory sequence (TRS) at the beginning of its encoded protein. Each subgenomic RNA generally only expresses the protein expressed at the 5' end of the RNA template. The relative abundance of each RNA species typically increases progressing from longer to shorter molecules.

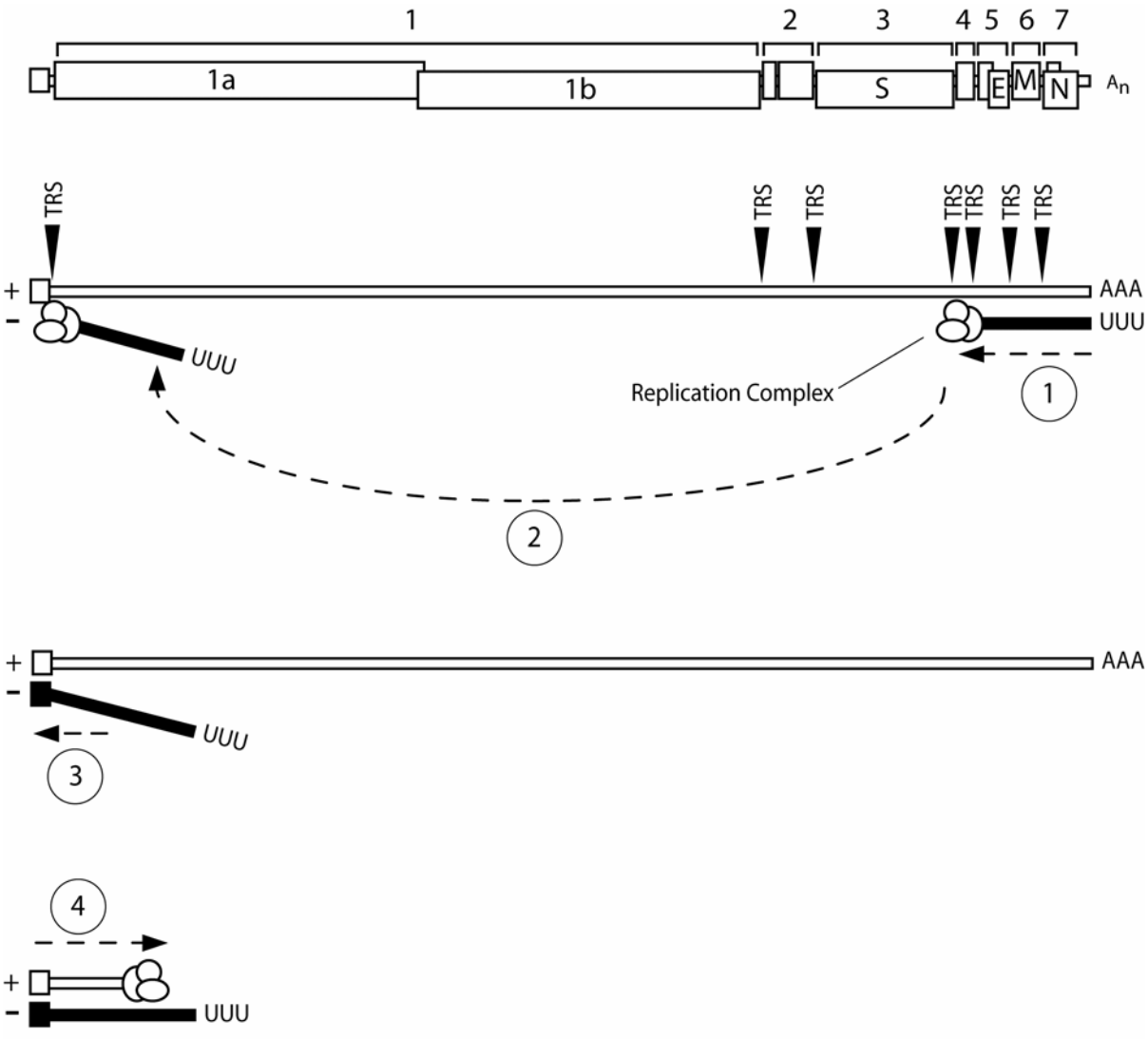

Figure 4. Generation of subgenomic RNA by discontinuous attenuated transcription. (1) The replication complex begins to transcribe the negative strand from the genomic RNA template. (2) The polymerase has a chance of disassociating from the template upon encountering transcriptional regulatory sequences (TRS) located immediately upstream of each ORF and reannealing with the genomic template at the 5'-most TRS. (3) After reassociating with the template, the polymerase continues to transcribe the complement to the 5' leader. (4) The subgenomic negative strand then functions as template for message sense RNA.

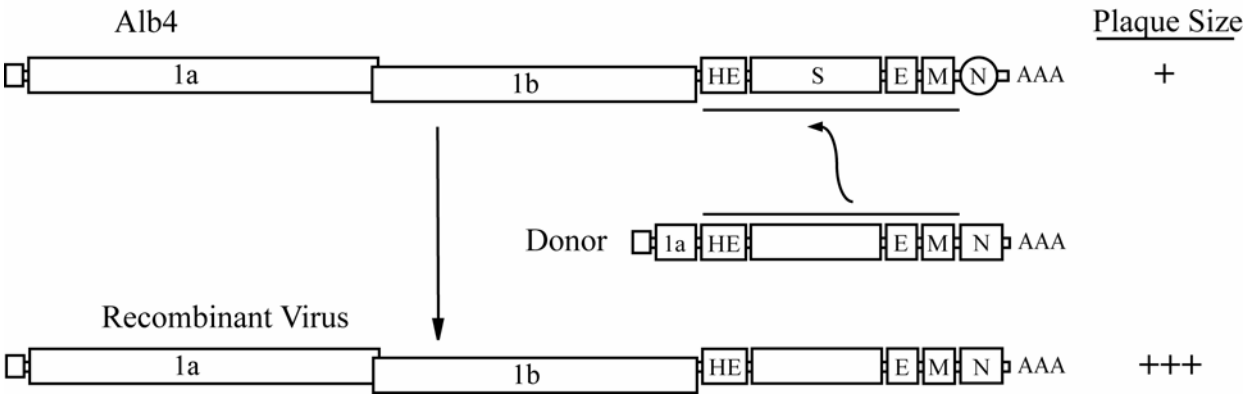

Figure 5. Initial version of targeted recombination reverse genetics system for coronaviruses. Alb4 produced a limited number of small plaques at the nonpermissive temperature. Following transfection of subgenomic mRNA 7 and infection of Alb4, RNA recombinants would be generated that resulted in wildtype plaque phenotypes, evidenced by large plaques that could be easily distinguished from Alb4.

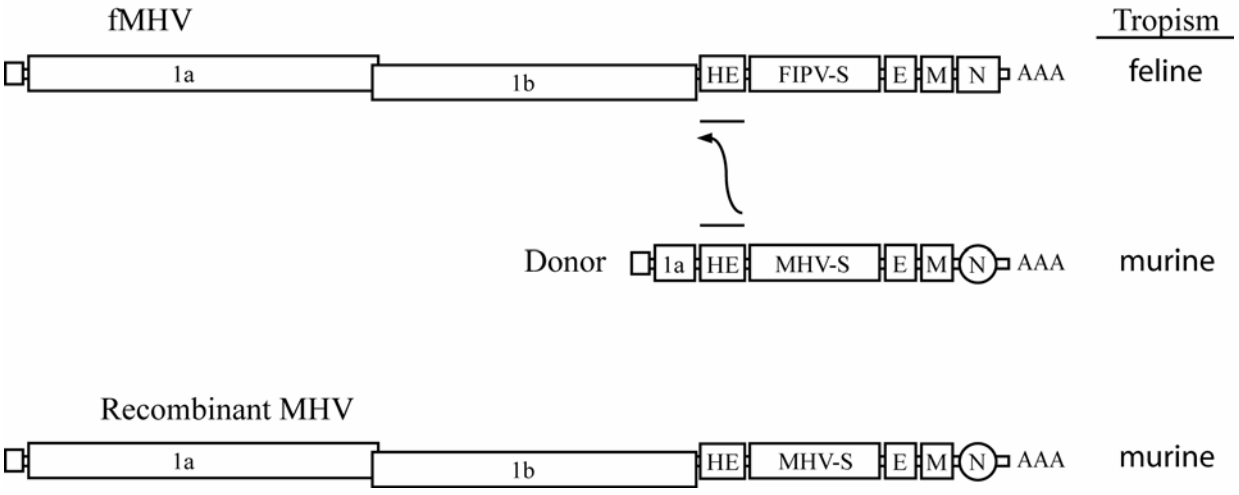

Figure 6. Improved targeted recombination system using cell specificity for screening. A chimeric virus of MHV, fMHV, expressing the S of FIPV infects feline cells transfected with RNA from a donor molecule, pMH54, bearing a mutated MHV spike glycoprotein. Successfully recombined virus is screened by growth on murine cells.

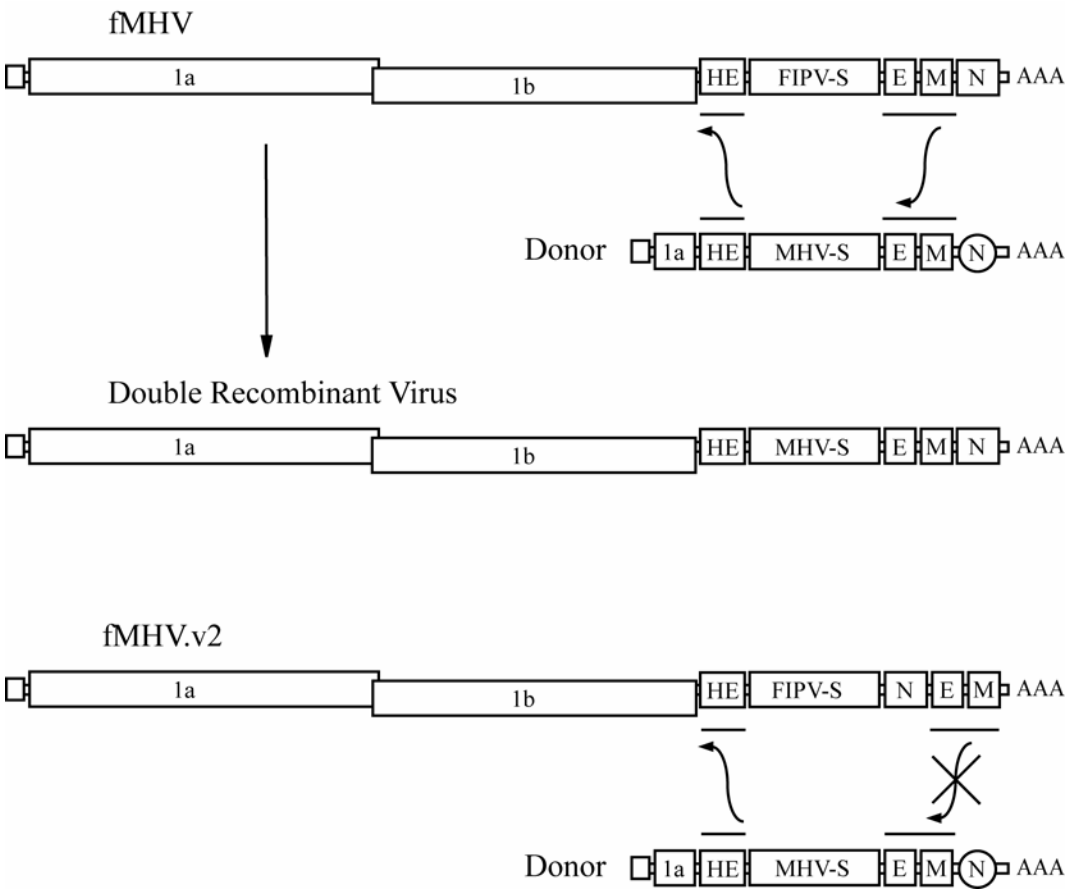

Figure 7. Rearrangement of structural genes to limit the occurrence of multiple recombination events. The first generation of the target recombinant fMHV system could undergo a second recombination event which could exclude introduction of the desired mutation (round N gene) while integrating the MHV-S gene. By moving N gene position immediately downstream of S (fMHV.v2), downstream recombination events will often be lethal as they exclude critical genes encoding major structural genes.

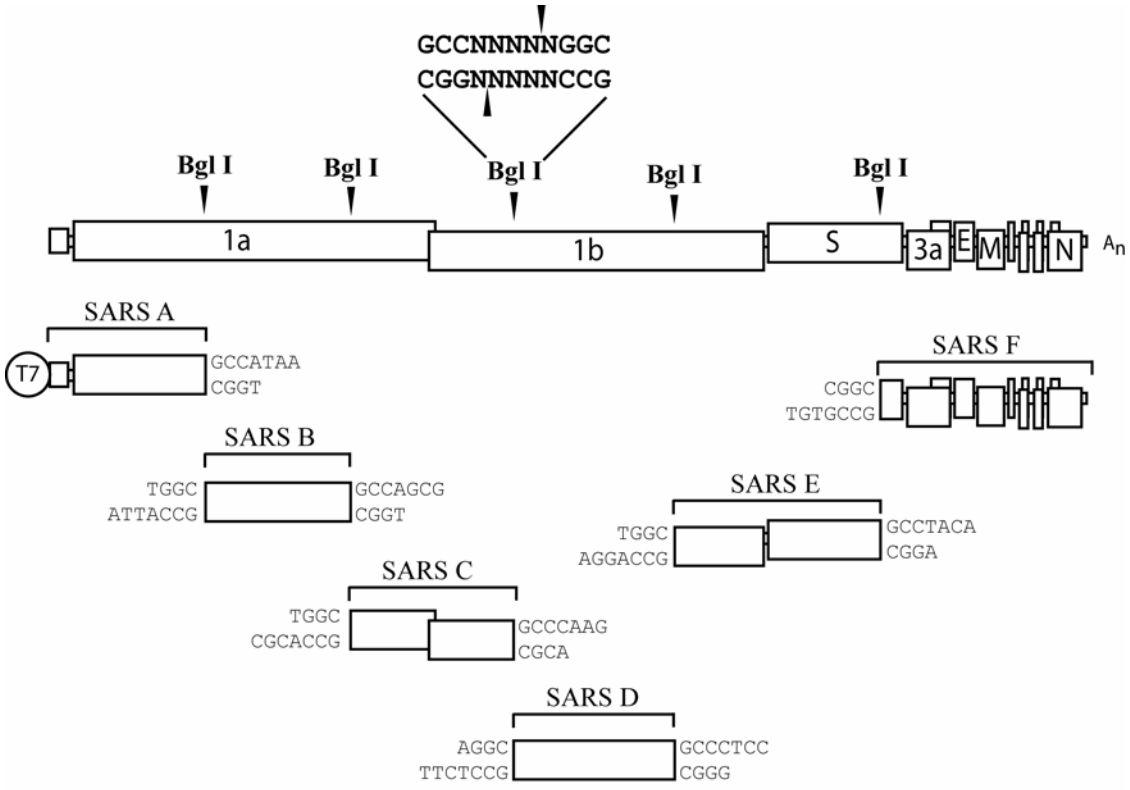

Figure 8. Multi-component reverse genetics system for SARS-CoV. cDNA stability in *E. coli* DNA amplification vectors is maintained by separating the viral genome over several overlapping constructs. Each fragment is ligated to form a full-length cDNA copy of the genome from which to drive transcripts through use of a T7 promoter at the 5' end of the construct and unique overlapping nucleotides left by digestion with Bgl I.

CHAPTER II

Vaccine Efficacy in Senescent Mice Challenged with Recombinant SARS-CoV Bearing Epidemic and Zoonotic Spike Variants

Abstract

In 2003, severe acute respiratory syndrome coronavirus (SARS-CoV) was identified as the etiological agent of severe acute respiratory syndrome, a disease characterized by severe pneumonia that sometimes results in death. SARS-CoV is a zoonotic virus that crossed the species barrier, most likely originating from bats or from other species including civets, raccoon dogs, domestic cats, swine, and rodents. A SARS-CoV vaccine should confer long-term protection, especially in vulnerable senescent populations, against both the 2003 epidemic strains and zoonotic strains that may yet emerge from animal reservoirs. We report the comprehensive investigation of SARS vaccine efficacy in young and senescent mice following homologous and heterologous challenge. Using Venezuelan equine encephalitis virus replicon particles (VRP) expressing the 2003 epidemic Urbani SARS-CoV strain spike (S) glycoprotein (VRP-S) or the nucleocapsid (N) protein from the same strain (VRP-N), we demonstrate that VRP-S, but not VRP-N vaccines provide complete short- and long-term protection against homologous strain challenge in young and senescent mice. To test VRP vaccine efficacy against a heterologous SARS-CoV, we used phylogenetic analyses, synthetic biology, and reverse genetics to construct a chimeric virus (icGDO3-S) encoding a synthetic S glycoprotein gene of the most genetically divergent human strain, GDO3, which

clusters among the zoonotic SARS-CoV. icGD03-S replicated efficiently in human airway epithelial cells and in the lungs of young and senescent mice, and was highly resistant to neutralization with antisera directed against the Urbani strain. This work tests the hypothesis that vaccination of young and old mice with VRP-S and VRP-N provide protection from replication by epidemic and heterologous strains of SARS-CoV. Although VRP-S vaccines provided complete short-term protection against heterologous icGD03-S challenge in young mice, only limited protection was seen in vaccinated senescent animals. VRP-N vaccines not only failed to protect from homologous or heterologous challenge, but resulted in enhanced immunopathology with eosinophilic infiltrates within the lungs of SARS-CoV–challenged mice. VRP-N–induced pathology presented at day 4, peaked around day 7, and persisted through day 14, and was likely mediated by cellular immune responses. This study identifies gaps and challenges in vaccine design for controlling future SARS-CoV zoonosis, especially in vulnerable elderly populations. The availability of a SARS-CoV virus bearing heterologous S glycoproteins provides a robust challenge inoculum for evaluating vaccine efficacy against zoonotic strains, the most likely source of future outbreaks.

Introduction

Severe acute respiratory syndrome coronavirus (SARS-CoV) infection results in severe acute respiratory disease, pneumonia, and sometimes death (49, 107). The disease was reported in Guangdong Province, China, in 2002 and spread to more than 30 nations within a few months. Disease severity was linked to age and other comorbidities, with mortality rates increasing with age and exceeding 50% in individuals over 65 y (77). SARS-CoV is a zoonotic virus that crossed the species barrier, most likely originating from

bats(113, 118, 149) or from other species including civets, raccoon dogs, domestic cats, swine, and rodents(72). New zoonotic variants may emerge as evidenced by sporadic cases of human disease in late 2003 and early 2004, which arose from strains distinct from that of the epidemic (195). In 2004, several laboratory-acquired infections were reported, including secondary spread resulting in fatal disease (141). Given the significant health and economic impact, the development of an effective vaccine strategy that is protective against both epidemic and zoonotic SARS-CoV strains is highly desirable.

Attenuated and killed SARS-CoV, DNA, and viral vectored vaccines are being evaluated in a number of animal models including mouse, ferret, hamster, and primate (9, 20, 21, 81, 90, 99, 170, 181, 183, 192, 215, 223, 232, 238), and have demonstrated that the SARS-CoV spike (S) glycoprotein is the principal component of protective immunity (20, 155, 161). Although strong immune responses are elicited against both S glycoprotein and nucleocapsid (N) protein (20, 154, 215, 241), passive transfer studies have illustrated that only anti-S antibody confers protection from SARS-CoV replication in the mouse model (9, 99, 188). Vaccine development faces a series of potential concerns including reversion or recombination repair of attenuated vaccine strains, induction of immune-mediated enhancement of pathology, waning immune protection, lack of cross-protection for heterologous strains, and limited vaccine efficacy within senescent populations. Furthermore, immune enhancement has been demonstrated with another coronavirus, feline infectious peritonitis coronavirus (143), and more recently with a modified vaccinia vector expressing SARS-S that exacerbated hepatitis in ferrets while failing to protect from infection (216). Notably, some antibodies against the epidemic Urbani strain increased the infectivity of lentiviruses pseudotyped with an animal SARS-S glycoprotein in an in vitro

model, raising the specter of vaccine-mediated immune enhancement of disease following heterotypic challenge (224). Another potential problem is that SARS vaccines might fail to induce antibodies that protect from infection with divergent strains of SARS-CoV. The S glycoprotein of SARS-CoV contains about 2%–20% amino acid variation between zoonotic and the 2003 epidemic strains (195, 224), possibly limiting the effectiveness of monotypic SARS-S vaccines. Finally, studies measuring the duration of protective immunity or vaccine efficacy in animals greater than 4 mo post-boost have not yet been reported (99).

In this report, the efficacy of Venezuelan equine encephalitis virus replicon particle (VRP) vaccines expressing the Urbani SARS-CoV S glycoprotein (VRP-S) and N protein (VRP-N), either individually or in combination (VRP-S+N), are determined in young and senescent mouse models. We tested whether the senescent mouse model, which exhibits an age-related susceptibility to SARS-CoV similar to that seen in the human disease (158), will provide a sensitive measure of vaccine efficacy and reveal potential complications in SARS-CoV vaccine development for vulnerable elderly populations. We evaluated the duration of protective immunity following homologous and heterologous SARS virus challenge, examining the impact of waning immunity on long-term protection. Through the use of publicly available SARS-CoV sequence databases, bioinformatics approaches, synthetic biology, and reverse genetics, we constructed a viable heterologous challenge virus to test the ability of current vaccine regimens to protect against zoonotic strains; the likely source of future epidemics (195).

Methods

Viruses and Cells. The Urbani, Tor-2, recombinant Urbani (icSARS), and a recombinant chimeric virus encoding the S gene of GDO3 SARS-CoV (icGD03-S), strains were propagated on VeroE6 cells in Eagle's MEM supplemented with 10% fetal calf serum, kanamycin (0.25 μg/ml), and gentamycin (0.05 μg/ml) at 37 °C in a humidified CO_2 incubator. For virus growth, cultures of VeroE6 cells were infected at a multiplicity of infection (MOI) of 1 for 1 h, the monolayer washed twice with 2 ml of PBS and overlaid with complete MEM. Virus samples were harvested at different times post-infection and titered by plaque assay. Plaques were visualized by neutral red staining and then counted.

Human nasal and tracheobronchial epithelial cells were obtained from airway specimens rejected from patients undergoing elective surgery under University of North Carolina (UNC) Institutional Review Board–approved protocols by the UNC Cystic Fibrosis (CF) Center Tissue Culture Core. Briefly, primary cells were expanded on plastic to generate passage 1 cells and plated at a density of 250,000 cells per well on permeable Transwell-Col (T-Col, 12-mm diameter; Corning [http://www.corning.com]) supports. Human airway epithelium (HAE) cultures were generated by provision of an air–liquid interface for 4–6 wk to form well-differentiated, polarized cultures that resemble in vivo pseudo-stratified mucosciliary epithelium, and infected with wild-type or recombinant SARS-CoV as previously described by our laboratory (174). All virus work was performed in a biological safety cabinet (BSC cabinet) in a biosafety level three (BSL3) laboratory containing redundant HEPA-filtered exhaust fans. Personnel were double gloved and wore Tyvek suits with hoods supplied with HEPA-filtered air by a powered air-purifying respirator (PAPR).

Construction and Isolation of the icGDO3-CoV Variant Virus. The GD03-S glycoprotein sequence has been reported. A synthetic DNA containing the 5′-most GD03 mutations was purchased (Blue Heron Biotechnology [http//www.blueheronbio.com]) and inserted into the SARS-E fragment. The plasmid clone (SARS-E GD03) was fully sequenced and shown to contain all of the appropriate mutations. The remaining GDO3 mutation was incorporated by PCR mutagenesis (5′ amplicon A: 5′-CTGTTTTCCCTGGGATCGC-3′; 3′ amplicon A: 5′-NNNNNNCACCTGCTTTTGGGCAACTCCAATGCC-3′; 5′ amplicon B: 5′-NNNNNNCACCTGCAGTTGCCCAAAATGTTCTCTATGAGAAC-3′; 3′ amplicon B: 5′-CATAAATTGGATCCATTGCTGG), followed by seamless ligation of the amplicons as previously described (230) into the SARS-F subclone. The final construct (SARS-F GD03) was fully sequenced and found to contain the appropriate set of GD03-S glycoprotein alleles.

The icGDO3-S was generated as previously described. Infectious clone fragment plasmid DNA was prepared in *Escherichia coli* (TOP-10, Invitrogen [http://www.invitrogen.com]), isolated, and purified (Qiagen [http://www.qiagen.com]). Infectious clone fragments B, C, D, and E were digested with BglI. Infectious clone fragments A and F were digested with EcoRI and NotI, respectively. Infectious clone fragments A and F were then dephosphorylated and then digested with BglI. Individual cDNA fragments were gel purified (Qiagen) and ligated (Roche [http://www.roche.com]) to form a full-length genomic cDNA and then chloroform extracted and EtOH precipitated. N cDNA and full-length viral genomic cDNA were then used as templates for in vitro transcription reactions (Ambion [http://www.ambion.com]). N and full-length viral genomic transcripts were then electroporated into Vero cells. Cell culture media containing virus was

harvested 48 h post-electroporation. Virus was plaque purified and then passaged twice in Vero cells. The resultant stock was plaque titered and cyropreserved at −80 °C.

Western Blot Analysis. Twelve hours post-infection, Urbani–, icSARS-CoV–, SARS-CoV–, Tor-2–, and icGD03-S–infected cells were washed in 1X PBS, lysed in buffer containing 20 mM Tris-HCL (pH 7.6), 150 mM NaCl, 0.5% deoxycholine, 1% nonidet-p-40, 0.1% sodium dodecyl sulphate (SDS), and post-nuclear supernatants added to an equal volume of 5 mM EDTA/0.9% SDS, resulting in a final SDS concentration of 0.5%. Samples were then heat inactivated for 30 min at 90 °C in the BL3 prior to removal. At BL2, samples were again heat inactivated for 30 min at 90 °C before use. Equivalent sample volumes were loaded onto 4% to 20% Criterion gradient gels (BioRad [http://www.bio-rad.com]) and then transferred to PVDF membrane (BioRad). Blots were probed with polyclonal mouse antisera directed against the Urbani-S glycoprotein diluted 1:200 or human sera 1128 diluted 1:400 and developed using electrogenerated chemiluminescence (ECL) reagents (Amersham Biosciences [http://www5.amershambiosciences.com]). Patient sera #1128 was collected from a patient infected during the second disease outbreak in Toronto, Canada.

Plaque Reduction Neutralization Titer Assays. One-hundred plaque forming units (pfu) of either icSARS-CoV or icGDO3-S were treated with heat-inactivated serum diluted to final concentrations of 1:100, 1:200, 1:400, 1:800, or 1:1,600 and incubated at 37 °C for 30 min, and the resulting titer determined by plaque assay. Plaque numbers formed by virus treated with each dilution of sera from individual mice vaccinated with VRP-S or VRP-S+N were compared to the average number of plaques formed after treatment with a given dilution of sera from VRP expressing the influenza A HA protein (VRP-HA)- or PBS-vaccinated mice

and expressed as the relative percentage. The dilution at which 80% of plaques were neutralized was determined for each VRP-S– or VRP-S+N–vaccinated animal.

Mice. Female BALB/c mice (Charles River Laboratories [http://www.criver.com]) were anesthetized with a ketamine (1.3 mg/mouse) and xylazine (0.38 mg/mouse) mixture administered intraperitoneally with a 50-μl volume. Each mouse was intranasally (i.n.) inoculated with 50 μl of virus at a concentration of 2×10^6 pfu/ml of virus. Four days post-infection, the right lung was removed and frozen at −70 °C for later plaque assay determination of viral titers. Half of the left lung was placed into Trizol Reagent (Invitrogen) for RNA extraction. The second half of the left lung was fixed in 4% PFA in PBS (pH 7.4) for at least 7 d prior to paraffin imbedding and sectioning for histopathological analysis. All mice were housed under sterile conditions, and sentinel mice were used to verify that the colony was mouse hepatitis virus (MHV) negative. Experimental protocols were reviewed and approved by the Institutional Animal Care and Use Committee at UNC Chapel Hill. Young mice refer to those challenged with SARS-CoV at ages equal or less than 5 mo old, whereas old or senescent mice are those animals with ages greater than 1y at the time of challenge.

Plaque Assay Titration of Virus from Lungs. Lungs were weighed and homogenized in four equivalent volumes of PBS to generate a 20% solution. The solution was centrifuged at 13,000 rpm on a tabletop centrifuge for 5 min, the clarified supernatant serially diluted in PBS, and 200-μl volumes of the dilutions placed onto monolayers of Vero cells in 60-mm

dishes. Following a 1-h incubation at 37 °C, cells were overlaid with 1% agarose-containing medium. Two days later, plates were stained with neutral red and then plaques counted.

VRP-S and VRP-N. The VRP constructs were made in two rounds of PCR, the first to generate two amplicons, and a second round of overlapping PCR to fuse them together. The fused DNA was digested with ApaI and AscI, and ligated into the similarly digested pVR21 plasmid. PCR reactions were performed with Expand Long Taq (Roche Molecular Biochemicals http://www.roche-applied-science.com) in 30 cycles of 94 °C for 30 s, 55 °C for 30 s, and extensions at 68 °C for 1 min. The first amplicon, which was used in the construction of both VRP-S and VRP-N, was generated with primers 5′nsp4Sw (5′-GATTGAGGCGGCTTTCGGCG) and 3′26S (5′-TTAATTAAGTCAATCGGCGCGCCCTTGGCGGACTAGACTATGTC) using pVR21 as template. The N-gene–specific amplicon was produced using primers V5′SARNg (5′-AGTCTAGTCCGCCAAGATGTCTGATAATGGACCCCAATC) and 3′SARSNg (5′-NNNNTTAATTAATTATGCCTGAGTTGAATCAGC) with SARS-F plasmid for template. The S-gene–containing amplicon was made with V5′SARSg (5′-AGTCTAGTCCGCCAAGATGTTTATTTTCTTATTATTTCTTACTCTCAC) and SARS3′Sg (5′-NNNNTTAATTAATTATGTGTAATGTAATTTGACACCC) using ligated SARS-E and -F fragments. The VRP-S and VRP-N cDNA templates were sequenced for verification and replicon particles produced as previously described (40). Mice were vaccinated with 10^6 infectious units (IU) of VRP in a 10-μl volume in the left rear footpad.

Lung Histopathology. Lungs were fixed in 4% PFA in PBS for 7 d before being submitted to the Histopathology Core Facility (UNC, Chapel Hill) for paraffin imbedding, sectioning at 5-μm thickness, and hematoxylin and eosin staining. Approximately one-quarter of the total lungs were sectioned, with four to six sections mounted from cuts taken at five different depths within the paraffin-imbedded tissue. Lung pathology was scored in a blinded manner, in which six to ten sections per animal were evaluated and scored using the following scale. 1.0 to 2.0 = no to mild inflammation, 2.0 to 3.0 = mild to moderate inflammation, 3.0 to 4.0 = moderate to severe inflammation in less than half of the tissue section, and 4.0to 5.0 = severe inflammation in more than half of the tissue section. The same sets of tissues were also evaluated qualitatively by a respiratory pathologist (author JH).

In Situ Hybridization. The 5 μm–thick paraffin-embedded sections were probed with ^{35}S UTP-labeled riboprobes complementary to the N gene of SARS-CoV (Urbani) or the HA gene of the A/PR8 strain of influenza as a negative control using previously described methods (83). In brief, following treatment to prevent nonspecific probe binding, the tissues were incubated overnight with either probe at 5×10^4 cpm/μl in hybridization buffer at 42 °C. The slides were then washed, dehydrated, and coated with NBT emulsion (Kodak [http://www.kodak.com]), and incubated at −80 °C. for 1 wk prior to development. Positive signal, as determined by silver grain deposition, was then evaluated.

Enzyme-Linked Immunosorbent Assay. Antibody titers were determined by standard indirect enzyme-linked immunosorbent assay (ELISA). High-binding 96-well round-bottom plates (Corning [http://www.corning.com]) were coated with 10 μg/ml of SARS-S, SARS-N, or

inactivated influenza A diluted in carbonate buffer containing 32 mM sodium carbonate, 68 mM sodium bicarbonate, pH 9.6 at 4 °C overnight. Mouse sera, diluted 1:100 in casein blocking buffer (Sigma [http://www.sigmaaldrich.com]), were added to wells in duplicate, and 2-fold serial dilutions were performed, followed by incubation for 2 h at 37 °C. Plates were then incubated for 1 h with goat anti-mouse IgG with alkaline phosphatase (AP) conjugate (Sigma), developed with *p*-nitrophenyl phosphate (*p*NPP; Sigma), and the optical density (OD) at 405 nm was measured (Bio-Rad Model 680 microplate reader). Log_{10} half-maximum ELISA titers were calculated with Sigmaplot (Systat [http://www.systat.com]) for the dilution at which an absorbance of 2.1, half that of the maximum measurable absorbance, was achieved. Since very low amounts of antibody were being measured in the passive transfer experiment, log_{10} OD = 0.2 ELISA titers were calculated.

Passive Sera Transfer. Mice were inoculated with 10^6 IU of VRP-HA, VRP-S, or VRP-N at 7 wk of age, boosted 4 wk later, and terminally bled via cardiac puncture 3 wk post-boost. The sera of each group were pooled and 150 µl transferred by tail vein injection into mice at 7 or 43 wk of age. Mice receiving sera were bled and i.n. challenged with 10^5 pfu of icSARS.

Statistical Analysis. Unless otherwise noted, two-tailed Mann-Whitney tests were used for statistical comparisons. The Fischer exact tests were completed by comparing the number of animals positive for viral replication within the lungs of a group of animals vaccinated with VRP-S or VRP-S+N to that of the negative control group, VRP-HA or PBS. Values outside

the limit of detection were assigned a value equal to the limit of detection for any analysis. The plus or minus (±) symbol is used to refer to standard deviation.

An amino acid multiple alignment was generated for the entire S gene of viral sequences representing early, middle, and late phases of the SARS epidemic in humans, as well as animal strains of SARS-CoV isolated from civets and raccoon dogs found in Chinese live animal markets or housed on farms in China that supplied the markets. The sequences were aligned using ClustalX 1.83 with default settings (33). A phylogenetic tree was generated using Bayesian inference as implemented in the program MrBayes v3.0b4 (87). Briefly, the alignment was exported in the nexus format, the amino acid substitution model was set to JTT (96) using the lset command, and Markov chain Monte Carlo simulation (87) was used to approximate the posterior probabilities of trees with sampling conducted on four chains over 500,000 generations (159). Trees were sampled every 100 generations, and the 5,001 trees collected were summarized with the sumt command set to a burnin of 1,000, which generated a consensus tree using the 50% majority rule (159). The burnin value was determined using the sump command with an arbitrary burnin of 250, which demonstrated that stationarity occurred prior to the 100,000th generation, indicating that a burnin of 1,000 was appropriate for the sumt command (159).

Results

Venezuelan Equine Encephalitis Virus Replicon Particles Expressing SARS-CoV S and N. The SARS-CoV S glycoprotein gene and N protein gene were PCR cloned, sequence verified, and inserted into Venezuelan equine encephalitis VRPs. VRP-S and VRP-N constructs were packaged to give titers greater than 10^9 IU per ml and shown to express

antigenically relevant recombinant proteins. VRP-infected cell lysates were probed with antiserum 1128, derived from a convalescent human SARS patient. Western blot analysis of VRP-S–infected lysates revealed the expected S glycoprotein doublet of approximately 180–210 kDa, whereas that of VRP-N–infected lysates revealed a major product of less than 50 kDa, the expected sizes for SARS-S and -N, respectively (**Fig. 9A**). VRP-S was inoculated into BALB/c mice and tested for its ability to induce antigen-specific antibody. Western blots were performed with Vero cell lysates infected with Urbani, SARS-CoV Tor-2, icSARS-CoV (the Urbani recombinant virus), and icGD03-S, a chimeric SARS-CoV expressing the S glycoprotein of the heterologous GDO3 strain. Blots were probed with anti–VRP-S mouse serum, 1128 human convalescent serum, or with anti–VRP-N mouse serum. The Western blots demonstrated that probing with human serum resolved bands corresponding to the major SARS antigens S (a doublet at ~180–210 kDa) and N (triplet at <50 kDa), as well as other unidentified SARS-CoV proteins (**Fig. 9B**). Serum from mice vaccinated with VRP-S only identified SARS-S (**Fig. 9C**), whereas serum from mice vaccinated with VRP-N recognized SARS-N in addition to another SARS-CoV protein that is probably a dimer of N (**Fig. 9D**).

VRP Vaccine Efficacy against icSARS-CoV Replication in the Mouse Model. As a general measure of vaccine efficacy (Table 1, experiment 1), six 4-wk-old BALB/c mice were vaccinated with either 10^5 IU of VRP-S or VRP-HA, boosted 4 wk later with an equal amount of VRP, and then i.n. challenged with 10^5 pfu of icSARS-CoV 8 wk post-boost. Consistent with other studies that made use of vectored SARS-S–expressing vaccines to induce protective responses (9, 21, 31, 56), vaccination with VRP-S also prevented the

replication of icSARS-CoV following challenge. No virus was detected by plaque assay (250 pfu/g limit of detection) in the lungs of VRP-S–vaccinated animals at 2 d post-infection, whereas the VRP-HA–vaccinated mouse lung had a mean titer of 6.7 ± 0.5 $\log_{10}$ pfu/g (**Fig. 10A**). Vaccination with VRP-S demonstrated significant protection at the time of peak lung titer relative to VRP-HA–vaccinated control animals ($p = 0.007$ Fisher exact test).

A second vaccine experiment was completed to evaluate long-term VRP protection. Five-week-old BALB/c mice were vaccinated with 10^5 IU of VRP-HA, VRP-S, VRP-N, or a combination of VRP-S and VRP-N (VRP-S+N), and boosted 5 wk later. Fifty-four weeks post-boost, mice were i.n. challenged with 10^5 pfu of icSARS-CoV and lungs removed 4 d post-infection (summarized in Table 1, experiment 2). Although day 2 post-challenge demonstrates peak viral titers, day 4 was chosen to harvest lungs because it is the time at which the highest level of pathology is evident in senescent mice (158). Titers in the lungs (**Fig. 10B**) of animals vaccinated with VRP-S or the combination of VRP-S+N were below the limit of detection (250 pfu/g). In contrast, the lung titers of VRP-HA–vaccinated animals were 5.8 ± 0.6 $\log_{10}$ pfu/g, comparable to the VRP-N–vaccinated animal titers of 5.3 ± 0.6 $\log_{10}$ pfu/g ($p = 0.2$). These plaque assay results were confirmed by SARS-CoV–specific in situ hybridization on lung tissues from the infected mice (**Fig. 10C**). Radiolabeled riboprobes complementary to the SARS-CoV N gene were hybridized to sectioned lungs of five mice from VRP-HA, VRP-N, VRP-S, or VRP-S+N vaccinated groups. Lung sections from VRP-HA (unpublished data) and VRP-N (**Fig. 10C**, image a) vaccinated animals exhibited extensive in situ signal (arrows), whereas only one of five sections from VRP-S–vaccinated (**Fig. 10C**, image b) and zero of five sections from VRP-S+N–vaccinated (**Fig. 2C**, image c) mice exhibited SARS-CoV N-specific signal. Both VRP-S and the

combination of VRP-S+N provided complete long-term protection against challenge with the homologous vaccine strain of SARS-CoV at 4 d post-infection ($p < 0.001$ Fisher exact test for both VRP-S- and VRP-S+N–vaccinated groups relative to VRP-HA).

Protection against Heterologous Challenge. To perform cross-protection efficacy studies, it was necessary to construct a heterologous SARS-CoV. Selection of a likely candidate strain was made after Bayesian analysis of the SARS-CoV S glycoprotein, which demonstrated three main phylogenetic branches. Two of the branches include viruses isolated from animals, such as the palm civet and raccoon dog, and low pathogenic viruses sporadically isolated from humans, such as GDO3 and GZ0401. Viruses representing the 2003 early, middle, and late phases of the epidemic strains form the third branch in the SARS-S phylogenetic tree (**Fig. 11A**). We resurrected the S glycoprotein of GDO3, a virus reported from a sporadic SARS case on December 22, 2003. Although GDO3 was not successfully isolated, its S glycoprotein was sequenced and reported. Compared to epidemic strains, GDO3 likely represented an independent introduction, was reported to be less pathogenic, and its S glycoprotein sequence is among the most divergent of all human strains (195). The GDO3-S glycoprotein contains 17 amino acid changes relative to Urbani-S (**Fig. 11B**), many of which map within neutralizing epitopes between amino acids 130–150 and 318–510, part of the receptor binding domain (RBD) (31, 34, 50, 71, 82, 101, 190, 200, 214). Importantly, polyclonal antibody directed against the late-phase Urbani strain was less effective at neutralizing pseudotyped viruses bearing GDO3-S glycoproteins than those bearing Urbani-S (224). The Urbani-S glycoprotein was removed from the SARS-CoV molecular clone, replaced with a synthetic cDNA encoding the GD03-S sequence, and used to generate

recombinant virus (230). Sequence analysis of plaque-purified icGDO3-S recombinant virus confirmed the presence of the GDO3-S glycoprotein and two additional changes in the S gene relative to Urbani-S (F7L and D613G), which likely arose as tissue-culture adaptations. The chimeric icGDO3-S, which only differs from Urbani SARS-CoV in its S glycoprotein, and wild-type icSARS-CoV recombinant viruses replicated in Vero cells to comparable titers that approached 10^7 PFU/ml within 24 h (unpublished data) and their proteins were both detected in Western blots with human antiserum from convalescent patients (**Fig. 9B**). Given the reduced amount of N present in the lysate of icGDO3-S–infected cells, the reduced intensity of the GDO3-S band probed with either anti–VRP-S mouse sera or the convalescent human serum is most likely due to the presence of lower GDO3-S protein rather than a marked difference in antibody specificity between GDO3-S and Urbani-S. icGD03-S replicated efficiently in HAE cells, although its maximum titer was approximately 1 log lower than that of icSARS or Urbani (**Fig. 11C**). To compare the growth of icSARS and icGDO3-S in animals, 6-wk-old BALB/c mice were i.n. infected with 10^5 pfu of either icSARS or icGDO3-S. At 2 d post-infection, icSARS-CoV mean lung titer was 6.8 ± 0.5 $\log_{10}$ pfu/g, whereas icGDO3-S titers were lower at 6.3 ± 0.2 $\log_{10}$ pfu/g ($p = 0.04$). The mean lung titer of icSARS-CoV–infected mice on day 4 was 4.5 ± 0.5 $\log_{10}$ pfu/g compared to icGDO3-S titers of 3.7 ± 0.3 ($p = 0.04$). By the seventh day, virus replication in the lungs of three of five mice infected with icSARS-CoV and four of five mice infected with icGDO3-S fell below the limit of detection (50 pfu/g). Average icSARS-CoV and icGDO3-S titers were similar on day 7 with 1.7 ± 0.1 $\log_{10}$ pfu/g and 1.8 ± 0.1 $\log_{10}$ pfu/g ($p = 0.9$), respectively (**Fig. 11D**).

To evaluate VRP protection against short-term heterologous challenge, groups of eight animals were primed at 7 wk of age with 10^6 IU of VRP-S, VRP-N, VRP-S+N, or VRP-HA, boosted 3 wk later, and then challenged 7 wk post-boost with 10^5 pfu of icGD03-S (summarized in Table 1, experiment 3). Lungs were harvested 2 d after challenge. VRP-S and VRP-S+N protected ($p < 0.001$ Fisher exact test for both VRP-S and VRP-S+N groups relative to VRP-HA) against heterologous icGD03-S recombinant virus replication (**Fig. 12A**). Although high titers of virus were detected in VRP-N– and mock-vaccinated animals with mean titers of 6.3 ± 0.1 and 7.0 ± 0.1 $\log_{10}$ pfu/g, respectively, the VRP-N–vaccinated animals had a lower mean titer ($p < 0.001$).

SARS-CoV vaccines should confer protection to elderly subjects who face infection with a new variant of the virus. To model this scenario, we vaccinated 6-mo-old to 1-y-old BALB/c retired breeders with 10^6 IU of VRP-S, VRP-N, VRP-S+N, or PBS, boosted them 4 wk later, and then challenged them 32 wk post-boost with 10^5 pfu of icGDO3-S (summarized in Table 1, experiment 4). At 4 d post-infection, mean titers in the lungs of animals vaccinated with VRP-N and PBS were similar at 4.4 ± 0.5 and 4.7 ± 0.6 $\log_{10}$ pfu/g ($p = 0.2$), respectively (**Fig. 12B**). VRP-S vaccination provided partial protection when compared to the PBS control group ($p = 0.026$ Fisher exact test), with the lungs of three of eight animals positive for viral replication at a mean titer of 2.9 ± 1.8 $\log_{10}$ pfu/g. All eight of the lungs harvested from the VRP-S+N–vaccinated animals were positive for viral replication, although a mean titer of 3.5 ± 1.2 $\log_{10}$ pfu/g was comparable to the mean titer for VRP-S–vaccinated mice ($p = 0.4$) and reduced relative to the PBS control ($p = 0.02$). The presence of SARS-CoV replication in the lungs of control and vaccinated animals was confirmed by in situ hybridization (**Fig. 12C**). SARS-CoV N-specific riboprobe was hybridized to lung

sections of mice from PBS-, VRP-N–, VRP-S–, and VRP-S+N–vaccinated groups (**Fig. 12C**). All tested lung sections from PBS mocks (unpublished data) and VRP-N–vaccinated (**Fig. 12C**, image a) animals exhibited in situ signal (arrows), although the signal did not appear to be as intense as that of the icSARS-CoV–infected animals (**Fig. 10C**). Lungs of the VRP-S–vaccinated animals (**Fig. 12C**, image b) had two of five slides exhibiting SARS-CoV–specific signal above background levels, whereas VRP-S+N (**Fig. 12C**, image c) had three of four slides.

Senescence and VRP-S Immune Responses. Because neutralizing antibody has been reported to confer protection from SARS-CoV replication within the lungs of mice (9, 188, 223), it was of interest to determine whether the VRP-S vaccine established high neutralizing antibody levels that persisted until challenge. Plaque reduction neutralization titer (PRNT) of serum samples harvested prior to vaccination showed no neutralization of icSARS-CoV; similar results were noted from serum collected from mice vaccinated with the negative controls, VRP-HA or PBS (unpublished data). The 80% PRNT values ($PRNT_{80}$), the dilution of serum at which plaque numbers are reduced by 80% relative to virus treated with control sera, for VRP-S– and VRP-S+N–vaccinated animals at 5 and 53 wk post-boost against both icSARS-CoV and icGDO3-S were compared (Fig. 13A and Table S1). The mean reciprocal dilutions for the $PRNT_{80}$ of VRP-S and VRP-S+N against icSARS were measured at 796 ± 307 at 5 wk post-boost and 628 ± 363 at 53 wk. Sera from mice vaccinated with the combination of VRP-S+N had mean reciprocal $PRNT_{80}$ of 1,091 ± 361 and 370 ± 179 at 5 and 53 wk, respectively. The initial neutralizing response in animals vaccinated with VRP-S and VRP-S+N was similar ($p = 0.2$ at 5 wk post-boost), and although there was not

significant waning of the icSARS-neutralizing activity over the 48-wk period in the VRP-S–vaccinated animals ($p = 0.3$ Wilcoxin matched pairs signed-rank test), VRP-S+N serum was diminished by about 3-fold ($p = 0.03$ Wilcoxin matched pairs signed-rank test). All tested sera remained above the lower limit of detection (1:100) and were sufficient to prevent icSARS replication within the lungs of challenged animals (**Fig. 10B**). The neutralizing activity of sera from the vaccinated animals was more effective against the vaccine strain than against heterologous icGDO3-S virus for both sera harvests and vaccine combinations. The reciprocal dilutions for the $PRNT_{80}$ of the VRP-S samples at 5 wk post-boost were below the limit of detection, whereas two samples of the week 53 bleed were measured above the limit of detection with a mean value of 112 ± 28. The icGDO3-S $PRNT_{80}$ measurements for VRP-S+N at weeks 5 and 53 post-boost were below the limit of detection with one exception for each time point: one mouse was measured to have a $PRNT_{80}$ of 124 at 5 wk, for an average titer of 103 ± 8, and another a $PRNT_{80}$ of 107 at 53 wk post-boost, an average of 101 ± 3.

Given that the VRP-S vaccine's ability to provide long-term protection was likely due to the strong SARS-CoV–neutralizing response induced in vaccinated mice, we measured the $PRNT_{80}$ of the VRP-S immune sera from mice vaccinated when old (Table 1, experiment 4) to determine if the incomplete protection seen in that study could be linked to a reduced neutralizing antibody response in the senescent animals (**Fig. 13B** and Table S1). Against the vaccine strain, the reciprocal dilutions of the mean $PRNT_{80}$ were 170 ± 82 with two of six samples falling below the limit of detection for VRP-S mice at 12 wk and 142 ± 65 at 29 wk post-boost with four of six falling below the limit of detection. Sera from the VRP-S+N–inoculated mice had $PRNT_{80}$ values falling near or below the limit of detection with only one

measurable sample at 114, for an average of 103 ± 6 and no icSARS-neutralizing ability detected at week 29. Against icGDO3-S, the VRP-S $PRNT_{80}$ values were below the limit of detection with the exception of a single VRP-S–vaccinated animal showing a neutralizing titer of 179 at 12 wk post-boost, for an average dilution of 116 ± 35 for the group. Sera harvested from these animals exhibited a marked reduction in neutralizing ability when compared to the response in animals vaccinated when young, even against the vaccine strain ($p = 0.008$ for VRP-S week 5 versus VPP-S week 12 post-boost; $p = 0.006$ VRP-S+N week 5 versus VRP-S+N week 12 post-boost). A strong anti–SARS-CoV neutralizing response was not induced by the VRP vaccines when administered to senescent mice.

ELISAs for total IgG specific for SARS-S and influenza-HA were performed to compare the VRP vaccines' ability to induce antibody to those antigens in mice vaccinated when young or senescent. ELISA for SARS-S was performed on sera collected prechallenge from the VRP-S– and VRP-S+N–vaccinated mice of experiments 2 and 4 (**Fig. 14A**). Mice vaccinated young with VRP-S (experiment 2) had an average $\log_{10}$ half-maximum ELISA titer of 2.6 ± 0.6 at 53 wk post-boost, whereas that of the senescent animals was approximately a log lower at 1.5 ± 0.9 at 29 weeks post-boost ($p = 0.007$). The difference between animals of the two age groups was even more striking when anti-S IgG levels were compared in the VRP-S+N mice. The animals vaccinated young with VRP-S+N had an average titer of 2.6 ± 0.3, whereas the average for senescent animals was at the limit of detection of 0.02 $\log_{10}$ half-maximum ELISA titer. To verify that the reduced ability of the senescent animals to mount specific antibody responses was not limited to the SARS-S antigen; anti-HA IgG titers were compared in mice vaccinated with VRP-HA. The average anti-HA titer of animals vaccinated when young was 4.7 ± 0.2, whereas the titer of the

vaccinated senescent mice was approximately one-tenth the size with a mean titer of 3.7 ± 0.8 ($p < 0.001$). The reduced ability of sera harvested from senescent animals to neutralize virus correlates to a general reduction in antigen-specific antibody production.

Pathologic Findings in Mice. Lungs from the vaccinated senescent mice challenge studies (Table 1, experiments 2 and 4) were sectioned, hematoxylin and eosin stained, and analyzed for pathology. Though there was some animal-to-animal variation, in general only minor inflammatory changes were observed in the senescent control mice challenged with either icSARS or icGDO3-S (**Fig. 15**, panel C, and **Fig. 16**, panels A and B). However, following SARS-CoV challenge in senescent mice, the N-vaccinated groups exhibited more marked bronchiolitis and alveolitis, as well as a conspicuous perivascular and peribronchiolar interstitial accumulation of numerous mononuclear leukocytes (mainly lymphocytes and plasma cells; i.e., lymphoplasmacytic cuffing) and increased numbers of widely scattered eosinophils (**Fig. 15** images b and c; **Fig. 16** images c and d). Upon SARS-CoV challenge, the animals vaccinated with S+N also exhibited a similar, but less severe, lymphoplasmacytic infiltration around pulmonary vessels and bronchiolar airways, although alveolitis and eosinophil infiltration were not a prominent feature in these animals (**Fig. 15** panel F and **Fig. 16** panels G and H). The lungs of animals vaccinated with VRP-S were similar to VRP-HA– or PBS mock-vaccinated animals with minimal lymphoplasmacytic cell accumulations (**Fig. 15** image e; **Fig. 16** images e and f). Therefore, not only did N vaccination fail to control SARS-CoV replication within the lungs, but N vaccination also resulted in an enhanced immunopathology in the lungs of the senescent animals upon viral challenge.

Duration of N-Induced Pathology. In order to determine the kinetics of the VRP-N–associated immunopathology and whether this effect was age dependent, young and old VRP-N– or VRP-HA–vaccinated mice were challenged with icSARS and sacrificed on days 2, 4, 7, and 14 post-challenge. Young (8 wk of age) or senescent (53 wk of age) female BALB/c mice were vaccinated with 10^6 IU of VRP-N or VRP-HA, boosted 7 wk later, then i.n. challenged with 10^5 pfu of icSARS-CoV 4 wk post-boost. Lungs were harvested on days 2, 4, 7, and 14, titered, and processed for histology (Summarized in Table 1, experiments 5 and 6). In young mice, day 2 average lung titers were 7.5 ± 0.2 $\log_{10}$ pfu/g and 8.1 ± 0.1 $\log_{10}$ pfu/g for the VRP-N– and VRP-HA–vaccinated animals, respectively. Day 4 average titers were 5.5 ± 0.3 $\log_{10}$ pfu/g for VRP-N–vaccinated and 5.7 ± 0.1 $\log_{10}$ pfu/g for VRP-HA–vaccinated mice. SARS titers in the VRP-N–vaccinated mice lungs had dropped to the limit of detection by day 7, with two of the three lungs from VRP-HA–vaccinated mice showing measurable titers at a mean of 3.2 ± 0.3 $\log_{10}$ pfu/g. By day 14, virus was undetectable in either group. In senescent animals, the day 2 average lung titers were 8.2 ± 0.2 and 8.5 ± 0.1 $\log_{10}$ pfu/g for the VRP-N– and VRP-HA–vaccinated animals, respectively. By day 4, the mean titers had dropped to 5.4 ± 0.6 $\log_{10}$ pfu/g for VRP-N–vaccinated animals and 5.7 ± 0.5 $\log_{10}$ pfu/g for the VRP-HA controls. On day 7, one VRP-N–vaccinated mouse had a detectable titer of 3.7 $\log_{10}$ pfu/g, whereas the lungs of two VRP-HA–vaccinated mice were positive for replication with a titer of 3.7 ± 0.5 $\log_{10}$ pfu/g. No virus was detected in either group on day 14 post–challenge.

Though enhanced inflammation was observed in a subset of the VRP-N–vaccinated animals at day 2 post–infection (**Fig. 17** panel B), the inflammatory infiltrates were readily apparent in both young and senescent animals at day 4 post-infection (**Fig. 17** panel D and

unpublished data) and were maintained at days 7 and 14 post-infection (**Fig. 17** panels F and H). As had been noted previously, VRP-HA– and VRP-N–vaccinated animals also differed by the presence of eosinophils (**Fig. 18**). At day 2 post-infection, eosinophils were rarely seen in either VRP-HA– or VRP-N–vaccinated mice (**Fig. 18**, panels A and B, respectively). In VRP-N–vaccinated animals, but not HA–vaccinated animals, eosinophils were widespread on days 4 and 7 (**Fig. 18**. panels D and F), but had largely cleared from the lungs by day 14 (**Fig. 18**, panel H). There was no apparent difference in severity between the young and senescent animals, suggesting that the immune pathology was specific to pre-existing N immunity, but was not age dependent (unpublished data).

Anti–SARS-N Antibody and Inflammation. A passive transfer of anti-N, anti-HA, or anti-S sera into naive mice was performed to determine if the increased inflammatory response could be attributed to N-specific antibody, and to confirm that protection in S-vaccinated animals was mediated by S-specific antibody. Hyperimmune sera against VRP-HA (5.26 $\log_{10}$ OD = 0.2 ELISA titer), VRP-N (5.6 $\log_{10}$ OD = 0.2 ELISA titer), or VRP-S (5.5 OD = 0.2 ELISA titer) were intravenously transferred in 150-µl volumes to groups of 8-wk-old or 43-wk-old naive BALB/c mice prior to challenge with 10^5 pfu of icSARS. Prior to challenge, serum was collected from mice and antigen-specific IgG titered to verify successful transfer. Young mice receiving anti–VRP-HA (n = 4) had a mean ELISA serum titer of 2.8 ± 2.4 $\log_{10}$ OD = 0.2, whereas senescent mice (n = 4) had a 2.9 ± 1.8 $\log_{10}$ OD = 0.2 ELISA titer. The average serum titers for mice injected with anti–VRP-N were 2.7 ± 2.4 $\log_{10}$ OD = 0.2 ELISA titer in young (n = 4) and 2.3 ± 1.9 $\log_{10}$ OD = 0.2 ELISA titer in senescent animals (n = 4). The anti–VRP-S $\log_{10}$ OD = 0.2 ELISA titers were 3.1 ± 3.1 in

young animals (n = 3) and 2.9 ± 2.3 in senescent mice (n = 3). Lungs were harvested 4 d post-challenge, virus titers determined, and processed for histological analysis. Virus titers in the young mice were 5.0 ± 0.1 $\log_{10}$ pfu/g in the anti–VRP-HA group, 5.2 ± 0.1 in the anti VRP-N group, and below the limit of detection (2.4 $\log_{10}$ pfu/g) in animals injected with the anti–VRP-S. Titers in the senescent mice were 5.3 ± 0.3 $\log_{10}$ pfu/g in the anti–VRP-HA group, 5.6 ± 0.6 in animals receiving the anti–VRP-N, and below the limit of detection in mice inoculated with anti–VRP-S. None of the mice displayed the enhanced inflammation noted in VRP-N–vaccinated animals (unpublished data), indicating that the observed immunopathology was not the result of antibody-dependent enhancement.

Discussion

VRP vaccine vectors induce robust mucosal and cellular immune responses against a large number of foreign antigens (40, 41) and were evaluated as candidate vaccines against homologous and zoonotic SARS-CoV challenge in young and senescent animals. Inoculation of mice with VRP-S induced antibody that recognized the epidemic SARS-CoV S glycoprotein as well as the S of a highly divergent strain, GDO3. The VRP-S vaccine induced long-term protection against challenge with the vaccine strain, complete short-term protection against icGDO3-S challenge, and partial protection against the divergent virus in the senescent mouse model. In contrast, vaccination with VRP-N failed to inhibit viral replication within the lungs of either young or senescent animals, resulted in enhanced immunopathology following viral challenge, and did not provide any measurable benefit when combined with VRP-S. The data suggest that vaccine regimens eliciting complete protection against antigenically heterologous forms of SARS-CoV in healthy individuals may

not be sufficient for higher risk groups, including vulnerable elderly populations, and that there is a need for further testing of candidate vaccines that induce an anti-N response.

VRP-S vaccination generated a strong neutralizing antibody response ($PRNT_{80}$ > 1:600) that persisted for over a year and provided complete protection against challenge with the vaccine strain. In humans, neutralization titers have been measured from 1:12 to 1:512 with a geometric mean titer of 1:61 (235). In a study evaluating an inactivated virus vaccine, neutralizing antibody titers greater than 1:114 resulted in complete protection against challenge (181). Mice inoculated with vesicular stomatitis virus vectors expressing SARS-S developed lower average neutralizing titers of 1:32, which were nevertheless protective against SARS-CoV infection for up to 4 mo after vaccination (99). We followed animals for over 1 y after boost. To our knowledge, these are the first assays illustrating waning immune responses to a SARS-CoV candidate vaccine. On average, mice vaccinated when young with VRP-S did not show a significant reduction in neutralizing titers up to 53 wk post-boost, whereas mice vaccinated with the combination of VRP-S+N experienced about a 3-fold reduction over the same period of time. Although it is problematic to compare our neutralizing antibody titers to those induced by other SARS vaccines due to the use of different assays, we demonstrate protection from challenge with either vaccine or heterologous challenge virus strains in animals with an icSARS $PRNT_{80}$ greater than 1:114, near the assay's limit of detection. Vaccines that induce robust neutralizing titers against the homologous strain will likely confer protection against zoonotic reintroductions, especially in younger populations.

As reported with other SARS-N–expressing DNA and vectored vaccines (20, 155), VRP-N did not protect mice from SARS-CoV replication, and no benefit to vaccination with

a cocktail of both VRP-S and VRP-N was observed, although an approximately half-log reduction in viral titers within the lungs of some VRP-N–vaccinated mice was occasionally observed. Although any reduction in SARS-CoV titer can be interpreted as a positive aspect of a potential vaccine, given the relationship between viral titer and SARS disease severity (35, 88), the increased number of lymphocytic and eosinophilic inflammatory infiltrates, which are also characteristic of the immune pathology observed with respiratory syncytial virus (RSV) infection following vaccination with formalin-inactivated RSV (43, 78), raises concerns that vaccination with N alone will not only fail to effectively protect against SARS-CoV replication, but may result in vaccine-enhanced pulmonary disease (102). N-induced pathology has not been previously reported, probably because most studies examined young mice at 2–3 d post-infection, prior to the infiltration of inflammatory cells into the lung. VRP-N–induced pathology was clearly evident by day 4 and persisted for 1–2 wk following wild-type virus challenge, suggesting the potential for serious complications in lung physiology and function. This finding has particular significance for SARS-N and inactivated SARS-CoV vaccines currently under development that also induce anti-N antibody and T cell responses (104, 122, 170, 181, 192, 222, 233, 241), because they may lead to adverse effects. Therefore, caution is merited with respect to the inclusion of SARS-CoV N protein in any vaccine formulation. The passive transfer of anti-N antibody did not contribute to inflammation and leads us to hypothesize that it is the activity of SARS-N–specific T cells in the absence of effective neutralizing anti–SARS-CoV antibody that mediates the adverse response. It is interesting that a T_h2–skewed cytokine profile is a hallmark of the RSV vaccine-enhanced disease, which raises the possibility that the N-specific immune response is skewed in a similar manner (95).

SARS-CoV strain diversity was mostly confined to China where many human and animal isolates were not successfully cultured in vitro (195). Consequently, most available experimental strains, like Urbani, are nearly identical and do not reflect natural diversity (156, 175). Recent advances in synthetic biology used to reconstruct extinct viruses, or specific genes of those viruses, de novo from their nucleotide sequences (29, 105, 177) provide the means for expanding the number of available SARS-CoV test strains. Using a comprehensive SARS-CoV genetic database (195, 224), we resurrected the divergent GDO3-S glycoprotein in the Urbani genetic backbone. The icGD03-S recombinant virus was identical to the molecular clone except for the presence of two mutations in S that likely evolved after transfection of full-length RNA and virus passage in Vero cells, similar to the cell culture adaptations reported in S for other SARS-CoV strains isolated from human clinical specimens and passaged in vitro (182). The icGDO3-S CoV's sequence divergence from Urbani, efficient in vitro replication in HAE and Vero cultures, and robust in vivo replication in the mouse model, make it an excellent heterologous challenge inoculum for vaccine studies. The GD03 RBD is also present in many zoonotic isolates described in civets and raccoon dogs, supporting its use as a zoonotic model strain (195). Furthermore, the reduced replication in HAE cultures of icGDO3-S compared to Urbani-CoV is consistent with the reduced pathogenesis noted in the GDO3 human case (35, 88, 195).

Consistent with previous work comparing the susceptibility of pseudotyped lentiviruses bearing the S glycoproteins of various SARS strains to neutralization by anti-S (Urbani) IgG (224), anti–VRP-S antibody demonstrated reduced neutralization of icGDO3-S relative to the vaccine strain. In spite of this, the VRP-S vaccine successfully provided short-term protection against the divergent virus. Vaccination of senescent animals produced

significantly reduced antibody responses compared with younger mice, and when challenged with the heterologous icGDO3-S virus, protection was incomplete. However, any animal with a $PRNT_{80}$ value above 1:114 against icSARS showed reduced viral replication within the lungs following challenge with either the vaccine or icGDO3-S strains. As noted for the homologous challenge studies, the combination of VRP-S+N did not enhance protection from heterologous challenge, but may actually have weakened it, with senescent animals showing even lower anti-S antibody responses and an even higher rate of viral replication, albeit with reduced titers, and increased lung pathology. One possible cause for vaccine failure is the emergence of an escape mutant in an environment of suboptimal neutralization. However, initial data comparing the neutralization susceptibility of viruses isolated from these mice to the challenge stock refute this conjecture (unpublished data). Incomplete protection by a vaccine in immunosenescent animals and humans is well documented and is more likely the result of an age-related compromise in one or more stages of the immune response to the vaccine. For instance, antibody responses in the immunosenescent tend to offer less protection with limited switching to secondary isotypes, lower antibody levels in general, and production of antibody with lower affinities (59, 84, 134, 139, 179, 239). Although we have not tested single-vaccine dose regimens, previous studies have demonstrated that these are efficacious against SARS-CoV challenge in young animals (99). Given the low antibody titers following boost in senescent populations, single-vaccine dose formulations will likely prove ineffective. Rather, improving the VRP-S efficacy in older vaccinees may require additional vaccine boosts, the use of adjuvants, or other additional therapies (60). Another likely contributing factor to vaccine failure in older animals was the resistance of icGDO3-S to neutralization relative to the vaccine strain, icSARS-CoV. At

least three neutralizing sites have been identified in the SARS-CoV S glycoprotein, two of which map at the N-terminus and in the RBD of the S glycoprotein, and one to a weak third site near the carboxy-terminus of S. Given that most of the GD03 mutations map in and around the N-terminus and RBD in S1 (224), it is possible that either one or both of these critical epitopes are significantly different in icGD03-S, and likely explains the resistance to neutralization with antisera against Urbani-S. These data suggest that robust neutralizing titers should be induced by candidate vaccines to provide long-term protection from SARS-CoV infection, especially in the vulnerable senescent population and against heterologous strains.

Earlier work had indicated that antibodies to the Urbani strain of SARS-CoV enhanced the in vitro infectivity of pseudotyped viruses bearing the S glycoprotein of zoonotic strains, primarily with strains SZ16 and SZ3, and raised the specter of S-vaccine–induced complications with newly emergent strains (224). In contrast, it was shown that monoclonal, but not polyclonal, antibodies that neutralized the epidemic strain may enhance the infectivity of pseudotyped viruses bearing GD03-S glycoproteins, although the enhanced infection was marginal at best (224). Our research with antibody directed against Urbani-S indicated that the polyclonal antibody neutralized icGD03-S on Vero cells, although less efficiently than the vaccine strain, which is consistent with the previous report (224). Moreover, in the young and senescent mouse models, VRP-S–vaccinated animals challenged with homologous or heterologous icGD03-S recombinant viruses did not display vaccine-mediated enhancement of virus replication or enhanced pathology. Because VRP-S vaccines induce broad neutralizing antibody responses that likely target multiple epitopes across the S glycoprotein, it is possible that the noted enhancement of infectivity with monoclonal

antibodies is nullified. Indeed, recent work showed that antibody specific for the RBD of Tor-2–S, GDO3–S, and SZ3–S glycoproteins did not reproduce enhanced infectivity in pseudotyped viruses bearing SZ3-S and identified conserved epitopes that allowed all three strains to be effectively neutralized, raising hope that a single vaccine could be effective against widely divergent strains of SARS-CoV (80). Clearly, additional studies are needed with more heterologous strains in alternative animal models before the possibility of vaccine-induced enhancement of infection and pathology can be discounted.

To our knowledge, this study is the first to demonstrate that a SARS-CoV vaccine conferred long-term protection into the period in which a host is most susceptible to SARS-CoV pathology: senescence. Furthermore, the VRP-S vaccination of young animals protected against challenge with a divergent strain of SARS-CoV, indicating that current vaccines may also provide protection from many zoonotic strains that might emerge in the future. Such cross protection has been observed among other vaccines, such as HA formulations for influenza virus (38) and VRP vaccines against norovirus (123). Inducing robust immune responses in older animals is more challenging, but VRP-S vectors provided some protection from icGDO3-S challenge, and did so without the enhanced pathology induced by the VRP-N vaccine.

Because human infections have not been reported since 2004, animal models are essential for the development of SARS-CoV vaccines. The young mouse model provides readily available animals on a homogenous genetic background and efficient replication within the respiratory tract. The senescent mouse model adds the benefit of enhanced pathogenesis and mimics the age-related susceptibility seen in humans (158). Although aging decreases B and T cell immunity and innate immune function in humans and mice,

characterization of these immune deficiencies is incomplete in both species. SARS-CoV infection in senescent mice provides a key model to evaluate the mechanisms by which aging deters immune responsiveness to highly pathogenic emerging viruses like SARS-CoV and influenza virus, and develop key intervention approaches to enhance vaccine efficacy in the elderly. The expense and limited availability of other senescent species makes the mouse model invaluable.

Important caveats must be considered while evaluating this work. Murine models of SARS disease have limitations. The disease progression in mice is faster than in humans, rodents and humans do not share the same symptoms, and virus infection is less severe; limitations that are also evident in the hamster, primate, and ferret models (189). These shortcomings necessitate that vaccine candidates be tested in other animal systems and underscore the critical need for the development of highly pathogenic challenge models for vaccine and therapeutic testing. This report does not provide a mechanism for the VRP-N–induced pathology nor provide solutions for minimizing potential risks associated with it. Although the passive transfer of anti–SARS-N serum did not reproduce the inflammation seen in VRP-N–vaccinated animals, these results must be interpreted with caution because the anti-N antibody levels in the recipient mice were lower than those of mice directly immunized by VRP-N.

The data presented in this manuscript do reveal critical needs and potential complications in vaccine design, laying the foundation for continuing and future studies to improve the quality, safety, and efficacy of SARS-CoV vaccines. Our model systems provide a means for identifying the host factors that contribute to immune senescence and will allow us to evaluate whether changes in vaccine design or regimen will improve vaccine

efficacy in senescent animals. The models provide clear rational to test candidate SARS vaccines in the hamster, ferret, and primate models in which pathology and clinical disease are more prominent following wild-type virus challenge. Our research provides a model for future experiments designed to characterize the components and inducers of the VRP-N–enhanced pulmonary inflammation, and suggests that vaccine regimens that contain N protein should be used with caution in human populations until further testing. The successful resurrection of a novel recombinant SARS challenge virus bearing zoonotic S glycoproteins suggests that it might be feasible to reconstruct other rare zoonotic SARS-CoVs that have never been successfully cultured, providing novel challenge viruses for vaccine and therapeutic drug testing against potential future zoonotic SARS introductions into human populations. Finally, these studies should encourage the development of senescent animal models of human disease and encourage vaccine testing and design against influenza, West Nile virus, and other pathogens that produce disproportionate disease burdens in the elderly (27, 140).

Table 1. Summary of Vaccine Groups and Select Results for Mouse Experiments

Exp	n	Vaccine	Age Vaccinated (weeks)	Age Boosted (weeks)	Challenge Virus	Age Challenged (weeks)	Lungs Harvested (days post challenge)	Lung Titer	+ for viral replication
1	6	VRP-S	4	8	icSARS	16	2	0	0/6
	6	VRP-HA	4	8	icSARS	16	2	6.7±0.5	6/6
2	8	VRP-S	5	10	icSARS	64	4	0	0/8
	8	VRP-N	5	10	icSARS	64	4	5.3±0.6	7/7
	8	VRP-S+N	5	10	icSARS	64	4	0	0/8
	7	VRP-HA	5	10	icSARS	64	4	5.8±0.6	8/8
3	8	VRP-S	7	10	icGDO3-S	17	2	0	0/8
	8	VRP-N	7	10	icGDO3-S	17	2	6.3±0.1	8/8
	8	VRP-S+N	7	10	icGDO3-S	17	2	0	0/8
	8	VRP-HA	7	10	icGDO3-S	17	2	7.0±0.1	8/8
4	8	VRP-S	>26	>30	icGDO3-S	>62	4	5.0±0.9	3/8
	7	VRP-N	>26	>30	icGDO3-S	>62	4	4.4±0.5	8/8
	8	VRP-S+N	>26	>30	icGDO3-S	>62	4	3.7±1.2	8/8
	8	PBS	>26	>30	icGDO3-S	>62	4	4.9±0.6	8/8
5	3	VRP-N	8	15	icSARS	19	2	7.5±0.2	3/3
	3	VRP-HA	8	15	icSARS	19	2	8.1±0.1	3/3
	3	VRP-N	8	15	icSARS	19	4	5.5±0.3	3/3
	3	VRP-HA	8	15	icSARS	19	4	5.7±0.1	3/3
	3	VRP-N	8	15	icSARS	19	7	0	0/3
	3	VRP-HA	8	15	icSARS	19	7	3.2±0.5	2/3
	3	VRP-N	8	15	icSARS	19	14	0	0/3
	2	VRP-HA	8	15	icSARS	19	14	0	0/2
6	3	VRP-N	53	60	icSARS	64	2	8.2±0.2	3/3
	2	VRP-HA	53	60	icSARS	64	2	8.5±0.1	2/2
	3	VRP-N	53	60	icSARS	64	4	5.4±0.6	3/3
	3	VRP-HA	53	60	icSARS	64	4	5.7±0.5	3/3
	2	VRP-N	53	60	icSARS	64	7	3.7	1/2
	2	VRP-HA	53	60	icSARS	64	7	3.7±0.5	2/2
	3	VRP-N	53	60	icSARS	64	14	0	0/3
	2	VRP-HA	53	60	icSARS	64	14	0	0/2

Table S1. Titers and $PRNT_{80}$ Dilutions for Individual Senescent Mice

Experiment	Vaccine	Mouse	Challenge Virus	Lung Titer (log_{10}pfu/g)	icSARS-CoV		icGDO3-S	
					$PRNT_{80}$ week 5	$PRNT_{80}$ week 53	$PRNT_{80}$ week 5	$PRNT_{80}$ week 53
2	VRP-S	1	icSARS	ND	500	526	<100	<100
	VRP-S	2	icSARS	ND	938	755	<100	<100
	VRP-S	3	icSARS	ND		1417		<100
	VRP-S	4	icSARS	ND	585	159	<100	<100
	VRP-S	5	icSARS	ND	695	493		114
	VRP-S	6	icSARS	ND	1260	574	<100	181
	VRP-S	7	icSARS	ND		652		<100
	VRP-S	8	icSARS	ND		445	<100	<100
	VRP-N	1	icSARS	6.1				
	VRP-N	2	icSARS	4.9				
	VRP-N	3	icSARS	5.2				
	VRP-N	4	icSARS	4.2				
	VRP-N	5	icSARS	5.8				
	VRP-N	6	icSARS	5.6				
	VRP-N	7	icSARS	5.4				
	VRP-N	8	icSARS	5.1				
	VRP-S+N	1	icSARS	ND	>1600	549	<100	<100
	VRP-S+N	2	icSARS	ND	628	150	<100	<100
	VRP-S+N	3	icSARS	ND	1417		124	
	VRP-S+N	4	icSARS	ND	775	308	<100	<100
	VRP-S+N	5	icSARS	ND	1159	346	<100	107
	VRP-S+N	6	icSARS	ND		594	<100	<100
	VRP-S+N	7	icSARS	ND	1243	487	<100	<100
	VRP-S+N	8	icSARS	ND	817	159	<100	<100
	VRP-HA	1	icSARS	5.2				
	VRP-HA	2	icSARS	6.2				
	VRP-HA	3	icSARS	5.8				
	VRP-HA	4	icSARS	6.1				
	VRP-HA	5	icSARS	6.6				
	VRP-HA	6	icSARS	5.2				
	VRP-HA	7	icSARS	5.2				

Table S1. Titers, $PRNT_{80}$ Dilutions, and Inflammation Scores for Individual Senescent Mice (continued)

Experiment	Vaccine	Mouse	Challenge Virus	Lung Titer (log_{10}pfu/g)	icSARS-CoV		icGDO3-S	
					$PRNT_{80}$ week 12	$PRNT_{80}$ week 29	$PRNT_{80}$ week 12	$PRNT_{80}$ week 29
4	VRP-S	1	icGDO3-S	ND	237	100	100	<100
	VRP-S	2	icGDO3-S	ND	106	100	<100	<100
	VRP-S	3	icGDO3-S	4.3				<100
	VRP-S	4	icGDO3-S	ND				<100
	VRP-S	5	icGDO3-S	ND	185	237	179	<100
	VRP-S	6	icGDO3-S	6.0	100	100	<100	
	VRP-S	7	icGDO3-S	ND	291	212		
	VRP-S	8	icGDO3-S	4.7	100	100	<100	
	VRP-N	1	icGDO3-S	3.6				
	VRP-N	2	icGDO3-S	4.6				
	VRP-N	3	icGDO3-S	4.5				
	VRP-N	4	icGDO3-S	5.3				
	VRP-N	5	icGDO3-S	3.8				
	VRP-N	6	icGDO3-S	4.3				
	VRP-N	7	icGDO3-S	4.6				
	VRP-S+N	1	icGDO3-S	4.7				<100
	VRP-S+N	2	icGDO3-S	4.0		<100		<100
	VRP-S+N	3	icGDO3-S	2.2	<100	<100	<100	<100
	VRP-S+N	4	icGDO3-S	4.3	<100	<100	<100	<100
	VRP-S+N	5	icGDO3-S	2.4	114	<100	<100	<100
	VRP-S+N	6	icGDO3-S	4.8	<100	<100	<100	
	VRP-S+N	7	icGDO3-S	3.5	<100		<100	
	VRP-S+N	8	icGDO3-S	1.7				
	PBS	1	icGDO3-S	4.9				
	PBS	2	icGDO3-S	5.0				
	PBS	3	icGDO3-S	4.7				
	PBS	4	icGDO3-S	4.6				
	PBS	5	icGDO3-S	5.1				
	PBS	6	icGDO3-S	4.9				
	PBS	7	icGDO3-S	5.2				
	PBS	8	icGDO3-S	3.2				

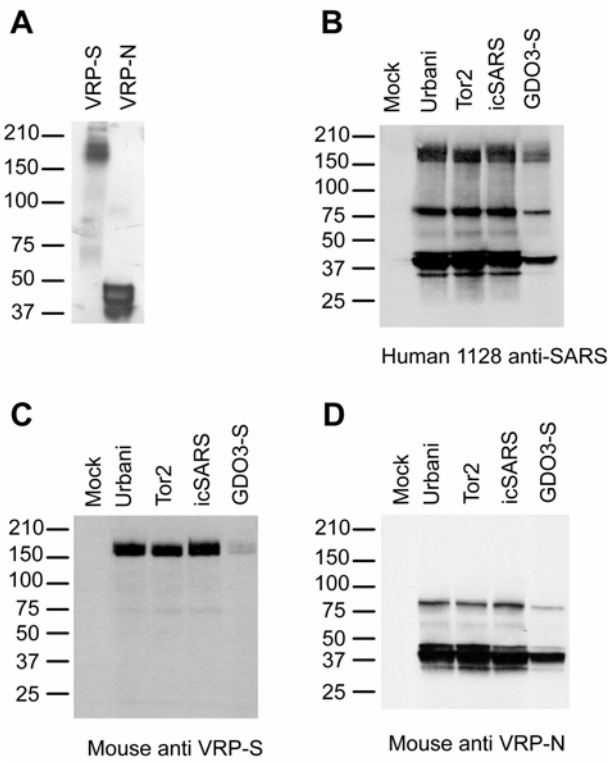

Figure 9. VRP Expression of SARS S and N and VRP-S Induction of Anti-SARS S Antibody. (A) Western blot of cell lysates infected with VRP-S or VRP-N and probed with human serum collected from a convalescent SARS patient, 1128. (B) Western blot of lysates from cells infected with the SARS-CoV strains Urbani, Tor2, icSARS, or icGDO3-S and probed with human convalescent serum, 1128, (C) mouse anti–SARS-S serum from VRP-S–vaccinated animals, or (D) mouse serum from a mouse vaccinated with VRP-N.

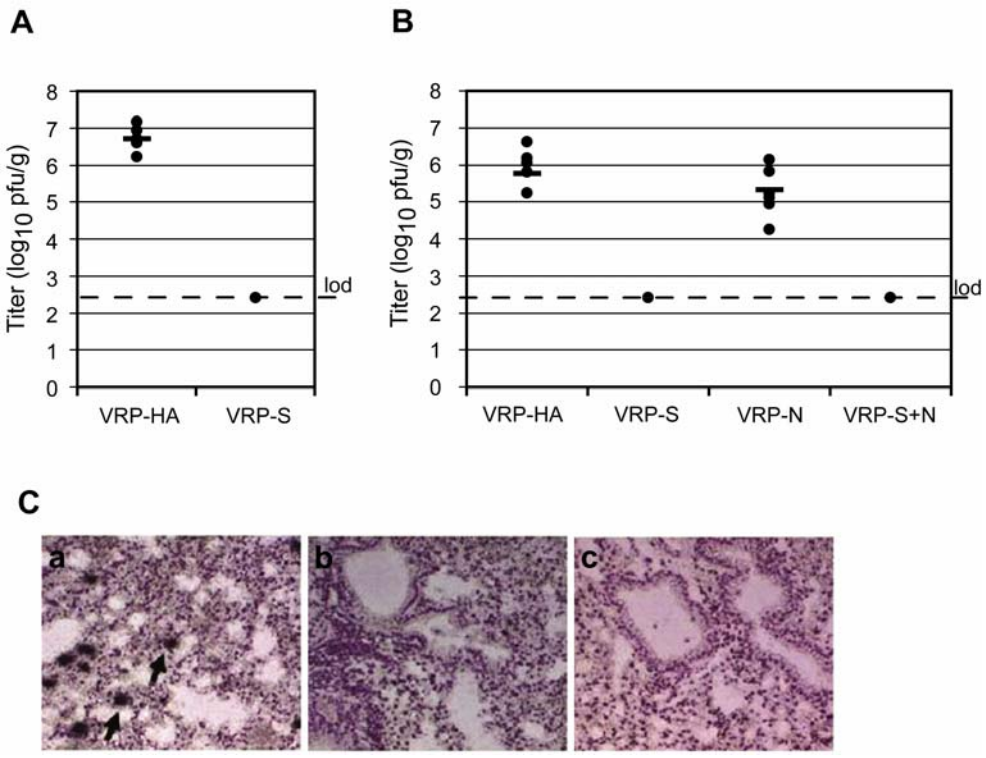

Figure 10. VRP-S Induces Short- and Long-Term Protection against icSARS-CoV Challenge. icSARS titers are expressed as the $\log_{10}$ plaque forming units per gram (pfu/g) of lung. Tissues were homogenized in PBS to form a 20% suspension and titered on Vero monolayers. The titers for individual mice are shown as a filled circle, and the mean titer for the group is represented by a solid bar. Limit of detection (lod) is 2.4 $\log_{10}$ pfu/g. (A) Lung titers of16-wk-old BALB/c mice harvested 2 d after being i.n. infected with 10^5 PFU of icSARS-CoV ($n = 6$). (B) Lung titers of BALB/c mice vaccinated and boosted with 10^6 infectious units (IU) of VRP expressing the influenza HA (VRP-HA), SARS-S glycoprotein (VRP-S), SARS-N protein (VRP-N), or a combination of VRP-S and VRP-N (VRP-S+N). Mice ($n = 7$ VRP-HA, $n = 8$ for other groups) were vaccinated at 5 wk of age, boosted 5 wk later, then i.n. challenged with 10^5 pfu of icSARS-CoV 54-wk post-boost. Lungs were harvested 4 d later and titered. (C) Plaque assay results were confirmed by in situ hybridization to sectioned lungs of five mice from each vaccinated group with a radiolabeled riboprobe complementary to the SARS CoV N gene. In senescent mice challenged with the icSARS-CoV, representative lung sections from VRP-HA– (unpublished data) and VRP-N–vaccinated (a) animals exhibited extensive in situ signal (black arrows), whereas only one of five sections from VRP-S–vaccinated (b) and zero of five sections from VRP-S+N–vaccinated (c) mice exhibited SARS-CoV–specific signal above background levels.

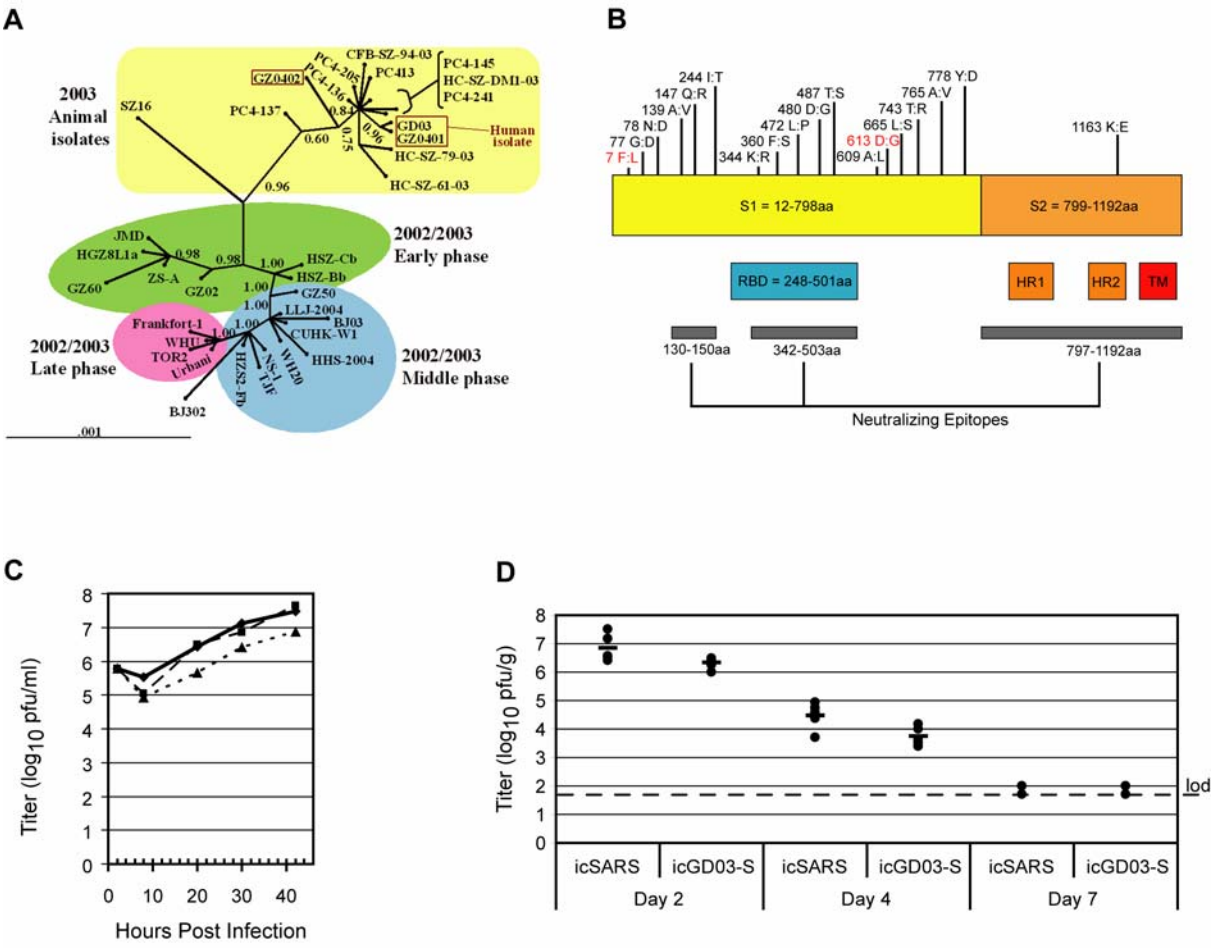

Figure 11. Synthetic Reconstruction of icGD03-S. (A) Unrooted phylogenetic gene tree of 35 SARS isolates ranging from early, middle, and late phases of the 2002–2003 epidemic to 2003–2004 animal isolates. Branch confidence values are shown as posterior probabilities. The three human isolates that fall within the cluster otherwise isolated from animals (shown in boxes), GZ0402, GD03, and GZ0401, may represent infections in which a human acquired the virus from a Himalayan palm civet. (B) The GDO3- S glycoprotein. Amino acid changes unique to the GDO3-S with the GDO3-S amino acid listed on the left and the corresponding Urbani to the right. The GDO3-S amino acid changes are shown in relation to the S1 and S2 subunits, the receptor binding domain (RBD), heptad repeats one (HR1) and two (HR2), the transmembrane domain (TM), and known neutralizing epitopes. Two mutations that arose during tissue culture passage of the chimeric icGDO3-S are shown in red. (C) Growth curves of the Urbani strain of SARS-CoV (diamond, solid line), the recombinant Urbani icSARS (squares, dashed line), and the recombinant chimeric virus icGDO3-S (triangles, dotted line) in human airway epithelial cells. (D) Comparing growth of icSARS-CoV to icGDO3-S in the lungs of mice. Six-week-old female BALB/C mice were infected with icSARS-CoV or icGDO3-S (n = 5 per group). The individual titer of each mouse is represented by a filled circle, and the mean titer of the group is represented as a solid bar.

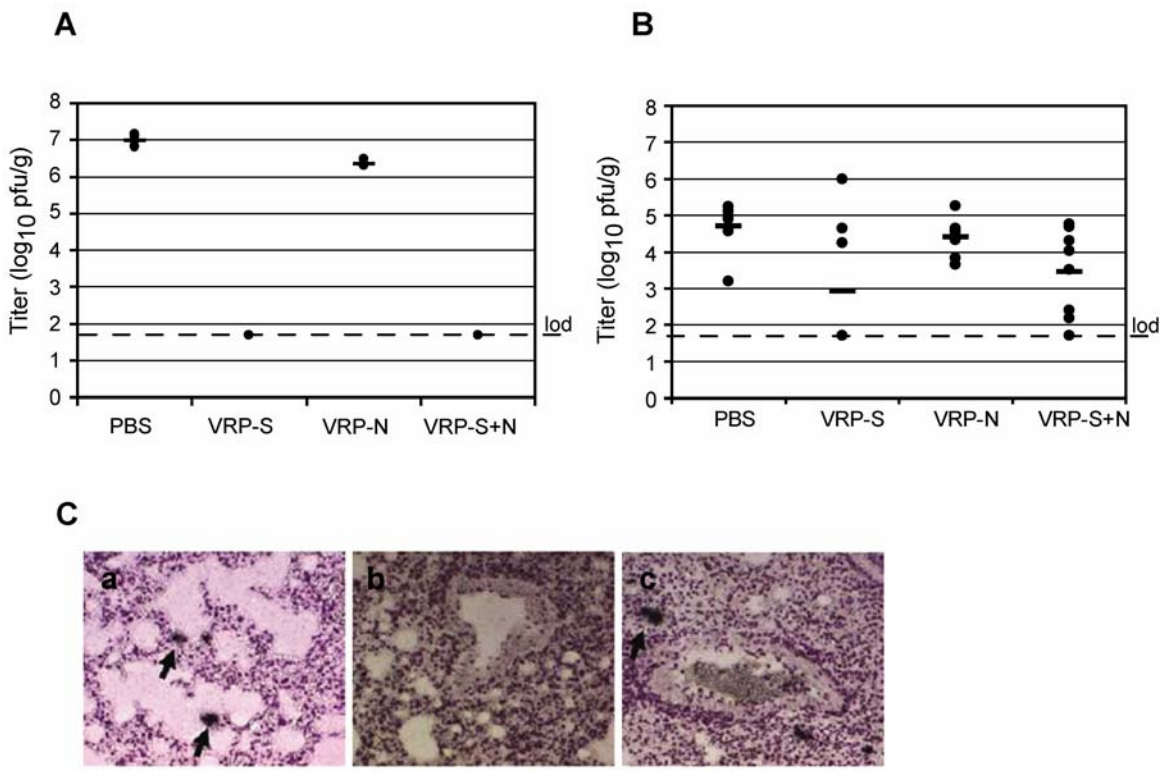

Figure 12. VRP-S Induces Short-Term Protection against icGDO3-S in Young and Partial Protection in Old Mice. (A) Lung titers of BALB/c mice vaccinated and boosted with 10^6 IU of VRP-S, VRP-N, a combination of VRP-S plus VRP-N (VRP-S+N), or mock vaccinated with PBS, then challenged with 10^5 pfu of icGDO3-S challenge (n = 8 per group). Lungs were harvested 2 d post-challenge. (B) Lung titers of aged BALB/c mice vaccinated at greater than 26 wk of age, boosted 4 wk later, then challenged 12 wk post-boost with icGDO3-S (n = 7 VRP-N, n = 8 for other groups). Tissue was harvested 4 d post-challenge. (C) SARS CoV specific in situ signal (black arrows) was observed in the lungs of senescent mice that were vaccinated with PBS (unpublished data) or VRP-N (a) and challenged with icGDO3-S, although overall, the signal appeared to be less intense than that observed in the icSARS challenge animals (Figure 10C). Vaccination with VRP-S (b) or VRP-S+N (c) failed to induce complete protection from icGD03-S challenge, as sections from two of five S- and three of four S+N-vaccinated animals exhibited signal above that of uninfected controls.

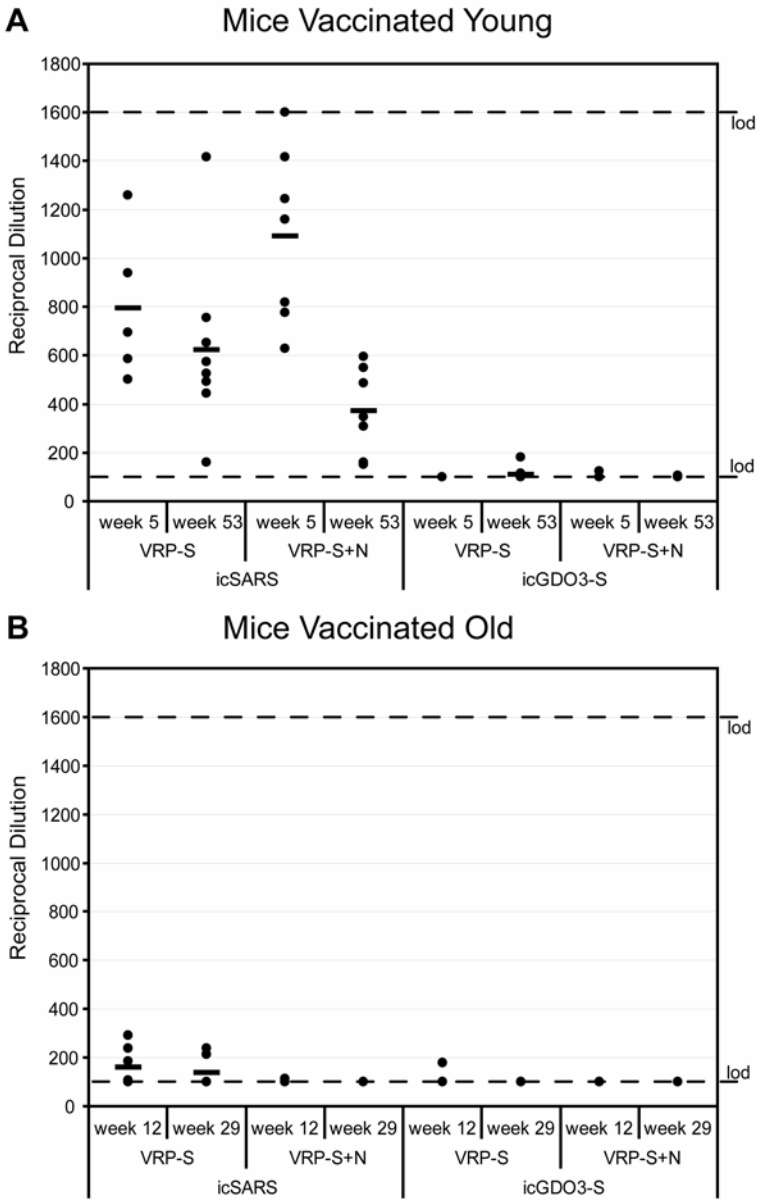

Figure 13. An 80% Plaque Reduction Neutralization Titers ($PRNT_{80}$) for VRP-S and VRP-S+N Hyperimmune Serum. (A) Mice vaccinated young: icSARS-CoV (left) and icGDO3-S (right) $PRNT_{80}$ for VRP-S immune serum (experiment 2) collected at 5 wk post-boost ($n = 5$) and 53 wk post-boost ($n = 8$). (B) Mice vaccinated old: icSARS (left) and icGDO3-S (right) $PRNT_{80}$ values for VRP-S and VRP-S+N immune serum (experiment 4) at 12 and 29 wk post-boost ($n = 6$ for icSARS; $n = 5$ for icGDO3-S). The $PRNT_{80}$ values for individual animals are show as black circles, and the mean value is shown as a solid bar. The limits of detection (1:1,600 upper and 1:100 lower) are represented by horizontal dotted lines.

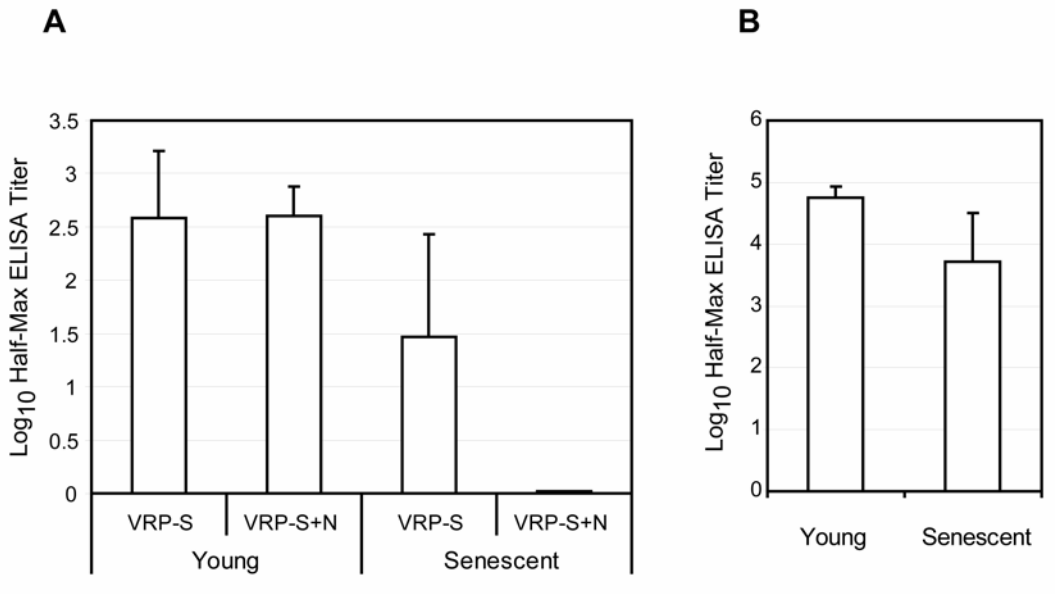

Figure 14. ELISA Titers for Anti-S and Anti-HA IgG in Vaccinated Animals. (A) Log_{10} half-maximum ELISA titers for anti-S IgG antibody in aged mice vaccinated with VRP-S or VRP-S+N when young (Table 1, experiment 2) or senescent (Table 1, experiment 4). Values represent mean values, and error bars indicate standard deviation. (B) Log_{10} half-maximum ELISA titers for anti-HA IgG antibody in aged mice vaccinated when young (experiment 2) or senescent (experiment 4).

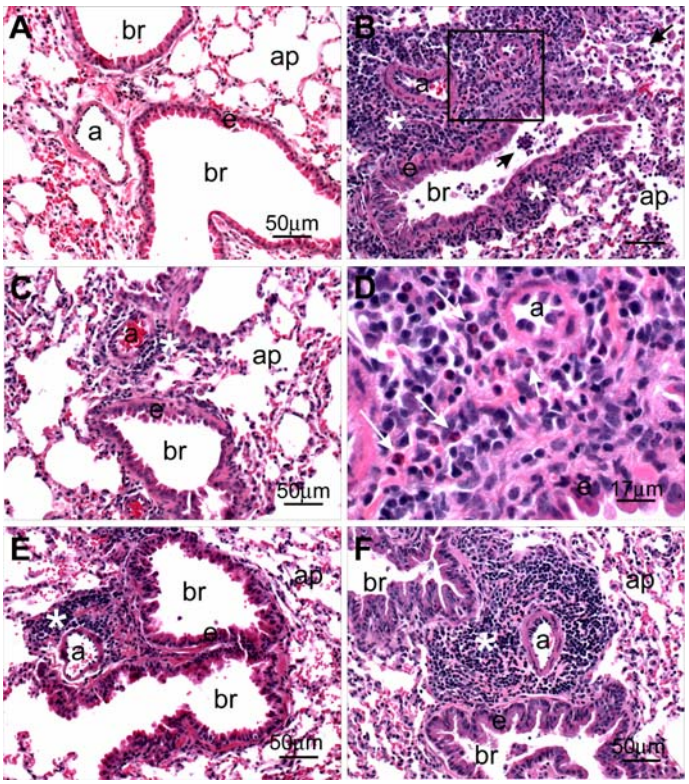

Figure 15. Pathogenic Findings Following Homologous Challenge. Light photomicrographs of representative histologic lung sections (Table 1, experiment 2) taken from an untreated control mouse (A), a VRP-N–vaccinated mouse (B) and (D), a VRP-HA–vaccinated mouse (C), a VRP-S–vaccinated mouse (E), and a VRP-S– and VRP-N–treated mouse (F). No histopathology was evident in (A). A marked mixed inflammatory infiltrate composed mainly of mononuclear leukocytes (lymphocytes and plasma cells) and widely scattered eosinophils are evident in the perivascular and peribronchiolar interstitium (asterisk) in (B). Similar inflammatory cells are also present in bronchiolar (br) airways and alveolar airspaces along with enlarged and vacuolated alveolar macrophages (arrows). The box in (B) denotes the site of the light photomicrograph (D) that was taken at a higher magnification to better illustrate the lymphoplasmacytic inflammatory cell infiltrate with lesser numbers of eosinophils (arrows). Similar, but slightly less severe, perivascular inflammatory infiltrates (asterisk) are also present in (F), but without accompanying alveolitis. Minimal lymphoplasmacytic cell accumulations around the pulmonary arteriole (a) are evident in (C) and (E). All tissues were stained with hematoxylin and eosin. Bars denote the scale of the magnification. a, pulmonary arteriole; ap, alveolar parenchyma; br, bronchiolar lumen; e, surface epithelium of the bronchiole.

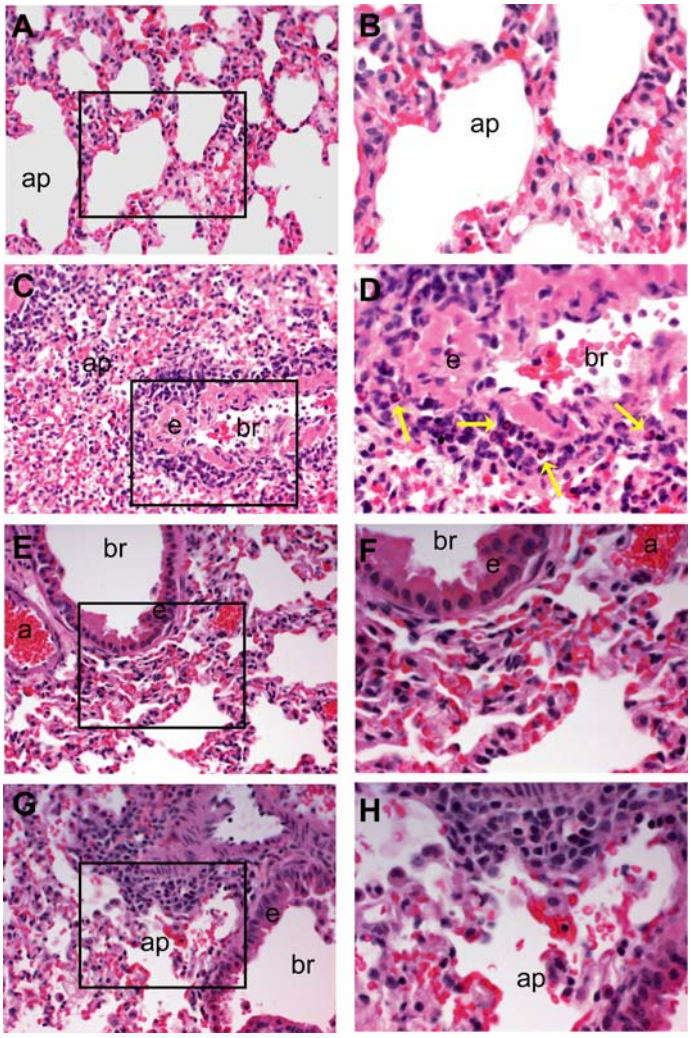

Figure 16. Pathogenic Findings Following Heterologous Challenge. Light photomicrographs of representative histologic lung sections (Table 1, experiment 4) taken from a mock PBS–vaccinated mouse (A) and (B), a VRP-N–vaccinated mouse (C) and (D), a VRP-S–vaccinated mouse (E) and (F), or a VRP-S+N–vaccinated mouse (G) and (H). The boxes in (A), (C), (E), and (G) (200× magnification) denote the site of the light photomicrograph that was taken at a higher magnification (400×) to better illustrate the lymphoplasmacytic inflammatory cell infiltrates including eosinophils (yellow arrows). All tissues were stained with hematoxylin and eosin.

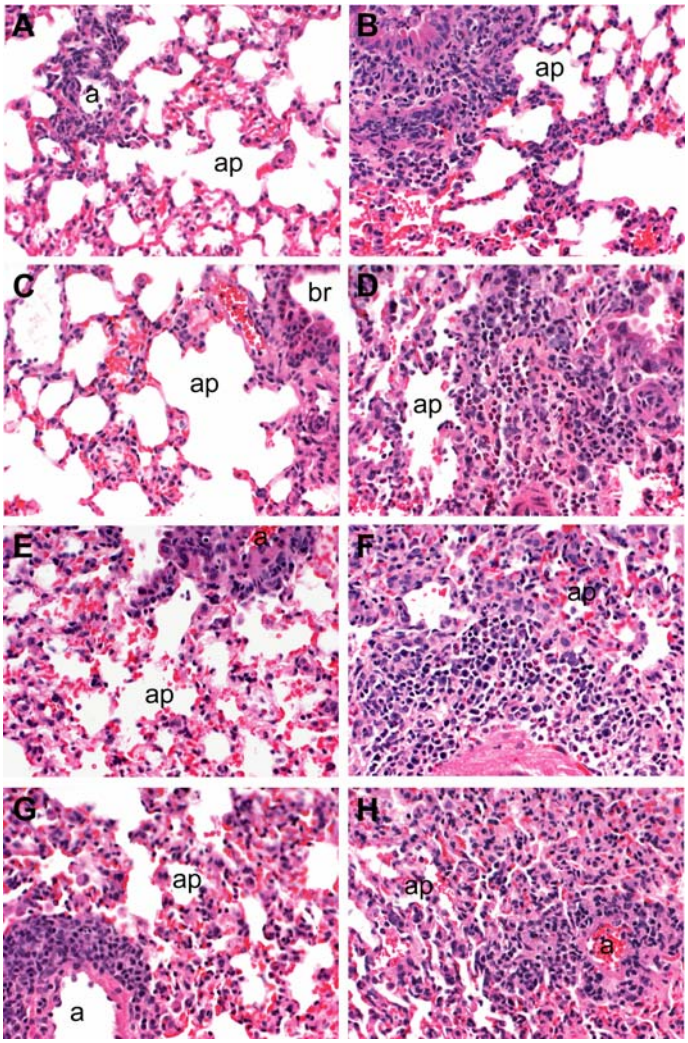

Figure 17. Kinetics of VRP-N–Associated Inflammation. Light photomicrographs of lung sections taken from VRP-HA– and VRP-N–vaccinated mice harvested at days 2, 4, 7, and 14 post–icSARS-CoV challenge (Table 1, experiment 5). Representative lung sections (200× magnification) comparing pulmonary inflammation between VRP-HA–vaccinated (A), (C), (E), and (G) and VRP-N–vaccinated (B), (D), (F), and (H) mice. Enhanced inflammation was evident by day 2 (A) and (B) in some VRP-N–vaccinated animals relative to lung sections of VRP-HA–inoculated mice. By day 4 post-infection (C) and (D), increased inflammation in VRP-N–vaccinated animals was widely apparent and was maintained through days 7 (E) and (F) and 14 (G) and (H).

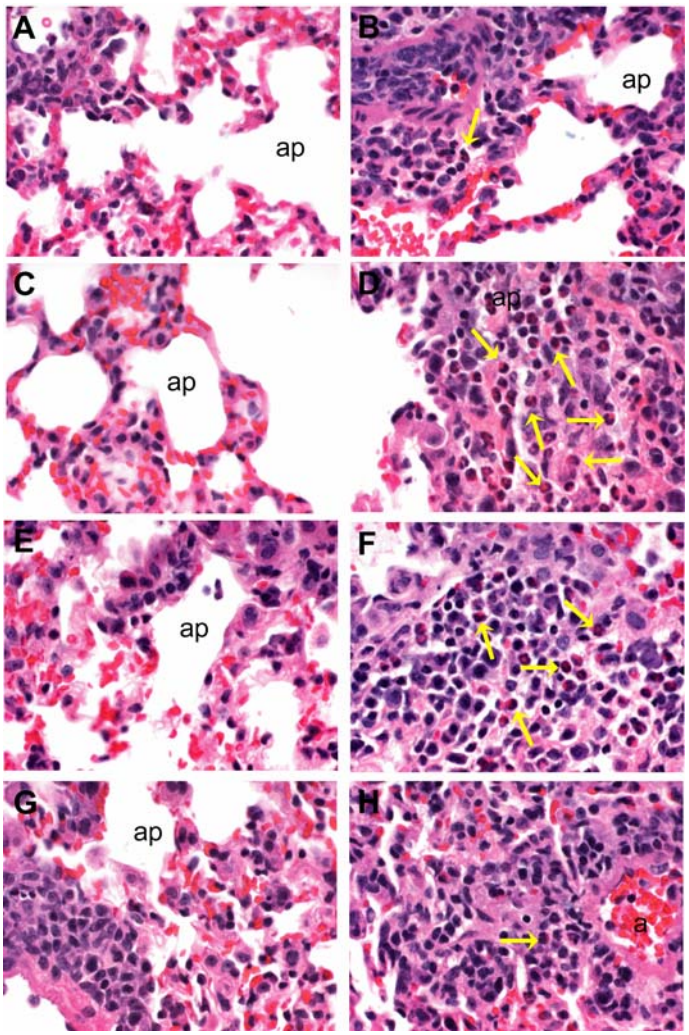

Figure 18. Identifying Eosinophils among Inflammatory Infiltrates. The 400 × magnification comparing eosinophil infiltration within the lung sections of VRP-HA–vaccinated (A), (C), (E), and (G) and VRP-N–vaccinated (B), (D), (F), and (H) mice (Table 1, Experiment 5). At day 2 post-infection (A) and (B), eosinophils are rarely evident in the lungs of either VRP-HA (A) or VRP-N (B) mice. Day 4 post-infection (C) and (D), extensive eosinophils (yellow arrows) are present within the lungs of VRP-N–vaccinated mice. Widespread eosinophils are seen at day 7 post-challenge in VRP-N–vaccinated (F), but not VRP-HA–vaccinated (E) mice. By day 14 (G) and (H), eosinophils are rarely found among inflammatory cells of VRP-N–vaccinated mice. An identical experiment in old animals was performed simultaneously (Table 1, experiment 6), showed results indistinguishable from those of young mice (unpublished data). All tissues were stained with hematoxylin and eosin.

Chapter III

MHV-A59 ORF1A REPLICASE PROTEIN NSP7-NSP10 PROCESSING IN REPLICATION

The coronaviruses express ORF1a and 1b polyproteins from which are processed 16 nonstructural proteins (nsps). The highly conserved region at the carboxy-terminus of the coronavirus ORF1a is processed by the nsp5 proteinase (3CLpro or M^{pro}) into mature products including nsp7, nsp8, nsp9 and nsp10, proteins with predicted or identified activities involved with RNA synthesis. M^{pro} continuous translation and processing of ORF1ab is required for replication, but specific cleavage events may be dispensable. We test the hypothesis that the nsp7-10 proteins, and their efficient processing by M^{pro}, are required for replication. We determined the requirement for the nsp7-10 proteins and their processing during murine hepatitis virus (MHV) replication. Using an MHV reverse genetics system, in frame deletions of the coding sequences for nsp7-10 were either deleted, or the flanking cleavage sites ablated, and the effect upon replication determined. Viable viruses were characterized through analysis of M^{pro} processing, RNA transcription, and growth fitness. Deletion of any of the regions encoding nsp7-10 was lethal. Disruption of the cleavage sites were lethal with the exception of the nsp9-10 site, which resulted in a mutant virus with severely attenuated replication. Serial passage of the attenuated nsp9-10 cleavage mutant increased fitness to near wild-type kinetics without reverting to a virus with the ability to process nsp9-10. We also confirm the presence of a second cleavage site between nsp7-8. In order to determine if a distinct function could be attributed to pre-processed forms of the

polyprotein including nsp7-10, the genes encoding nsp7 and nsp8 were rearranged. The mutant virus was not viable, suggesting that the uncleaved protein may be essential for replication or proteolytic processing.

Introduction

Coronaviruses were identified in the 1960's and have since been isolated from almost all species of animals tested, including humans. Disease in animals is often severe and contributes to significant agricultural and economic loss. Until an emergent coronavirus was identified as the etiological agent of the SARS outbreak in 2003 (49, 107), human coronaviruses were typically associated with mild upper respiratory tract infections in winter (75, 135). In addition to the more severe SARS-CoV (49, 107), two new human coronaviruses were found associated with more severe lower respiratory disease, NL-63 and HKU-1(55, 58, 203, 219). Since the SARS epidemic, new research into coronaviruses has been driven by the desire to better understand coronavirus replication, pathology, mechanisms of host range expansion, and spurred development of anti-coronavirus therapies in the event of another deadly emergence.

Coronavirus replication is mediated by a complex of cellular and virus-encoded proteins of the first open reading frame (ORF1), which comprises the first two-thirds of the viral 27-to-32 kb positive strand RNA genome (**Fig. 19A**). Translation of ORF1 produces two polyproteins, designated ORF 1a and ORF 1ab (**Fig. 19B**). The larger of the two polyproteins, pp1ab, is a carboxyl-extension of pp1a that depends upon a minus 1 ribosomal frame-shift at a pseudoknot structure to read through the translational stop at the end of ORF 1a and translate through ORF1b (14, 116). For murine hepatitis virus (MHV) the

polyproteins are processed into intermediate and mature nonstructural proteins (nsps) by two papa in-like proteinase activities in nsp3 (PLP1 and PLP2) and by the nsp5 proteinase (3CLpro or M^{pro}) (65, 67, 125, 127, 198). Continuous translation and proteolytic processing of the polyproteins is required for productive infection, making the proteases attractive targets for antiviral therapies, and suggesting that distinct roles may exist for both the mature and intermediate precursor forms of the proteins (13, 45, 103, 120, 165, 224).

The components of the coronavirus replication complex and their individual roles have only partially been defined. Processing of pp1a and pp1ab by nsp3 and nsp5 of most coronaviruses, MHV and SARS-CoV, yields 16 nsps that are associated with the replication complex (**Fig. 19B**) (67, 151, 172, 173, 242, 243). Although functions have been assigned to many of these proteins by comparative sequence or biochemical analysis (10, 65, 67, 116), several are either poorly understood or unknown. In addition to the proteinases, putative or known functions of ORF1a derived proteins include hydrophobic trans-membrane domains in nsp3 (TM) (79), nsp4 (MP1), and nsp6 (MP2) that likely anchor the replication complex to cellular membranes. An ADP-ribose-1"-phosphate (Appr-1”-p; X in **Fig. 19B**) domain has also been identified in nsp3 (152, 153, 163). The proteins encoded by ORF1b have been associated directly with transcription of the viral genes. These include the RNA-dependent RNA polymerase (RdRp) in nsp12 (18, 47, 67), putative zinc-binding domain (ZBD; Z in **Fig. 19B**) (171), nucleoside triphosphatase and superfamily-1 helicase (Hel) in nsp13 (92, 93, 171), 3’ to 5’ exonuclease (ExoN) in nsp14 (137), an endoribonuclease (EndoU; EU in **Fig. 19B**) in nsp15 (7), and an S-adenosylmethionine-dependent ribose 2’-O-methyltransferase (OMT) in nsp16 (178).

Among the poorly understood replicase proteins are the "cassette" of nsp7, nsp8, nsp9 and nsp10 (nsp7-10) near the 3' end of ORF 1a (**Fig. 19B**). These proteins are present in all coronaviruses with significant identity and similarity, and are processed by M^{pro} into mature products of 10, 22, 12.7, and 15 kDa, respectively. The nsp7-10 co-localize with the replication complex and are presumably involved with viral RNA synthesis (11, 12, 68, 126, 204). Although the exact function of these proteins is unknown, recent work has provided some insight into their purpose. Structure analyses of SARS-CoV nsp7 and nsp8 demonstrated that the two proteins form a hexadecameric supercomplex with electrostatic properties favorable for nucleic acid binding that may function as a processivity factor for the RNA-dependent RNA polymerase (234). Nsp8 has also been shown to possess a low fidelity primase activity and was proposed to provide the RNA primers required by the nsp12 RdRp during replication (32, 89). The SARS-CoV nsp9 crystal structure has also been resolved and shown to form homodimers possessing single-stranded RNA-binding properties, and it has been suggested that the protein may serve to stabilize nascent and template RNA during replication, transcription, and processing (22, 53, 191). Putative temperature sensitive mutations localized within nsp10 suggest that the protein may be involved with negative strand synthesis (165). Recent reports describing the refinement of the nsp10 structure have revealed that the protein includes two Zn fingers (97, 133), exhibits nucleic acid binding affinity (97, 133), and can crystallize to form a spherical dodecameric structure made up of 12 nsp10-11 subunits (187) or nsp10 monomers and homodimers (97). Collectively, this data implies that nsp7-10 is important – if not critical – to coronavirus replication.

In this report we describe the requirement for nsp7-10 and their proteolytic processing in MHV replication. Using the established MHV reverse genetics system (231), we

individually deleted the genes encoding each protein and disrupted each of the cleavage sites associated with the nsp7-10 and evaluated whether the protein domain was essential for productive virus infection. For all viable mutants, we characterized virus growth and RNA synthesis in cultured cells, transcription function, and *in vitro* growth fitness. A potential second cleavage site at the interface of nsp7-8 in class 2 coronaviruses was previously identified (**Fig. 19C**) (126), and we determined if ablation of either or both of the putative cleavage sites affects replication. We also determined if the precursor protein containing the nsp7-10 performs a distinct role in viral replication by attempting to rescue viable virus by rearranging the nsp7 and nsp8 genes within the infectious clone. This work contributes to the growing body of data indicating that these small proteins are intimately involved with and critical to viral replication, and as such, are attractive targets for both research aimed at understanding the intricacies of the coronavirus replication complex and as the focus of anti-viral therapies.

Methods

Cells. The viruses were generated from infectious clones using delayed brain tumor (DBT) and baby hamster kidney cells stably expressing the MHV receptor (BHK-MHVR) as previously described (231). DBT cells were maintained in Eagle's minimum essential medium supplemented with 10% fetal clone II, 5% tryptose phosphate broth, 0.05 μg of gentamicin/ml, and 0.25 μg of kanamycin/ml. BHK-MHVR cells were maintained in alpha minimum essential medium supplemented with 10% fetal calf serum, 10% tryptose phosphate broth, 0.05 μg of gentamicin/ml, 0.25 μg of kanamycin/ml, and 800 μg/ml of Geneticin (G418 sulfate; Sigma).

Assembly of a full-length MHV-A59 and mutant infectious cDNA templates. Viruses were produced from the MHV infectious clone as previously described (231). Plasmids containing the viral genome were grown to a high concentration, isolated, and digested with *Esp*3I, *Bgl*I, or *Not*I according to the manufacturer's directions (New England Biolabs). Viral cDNA inserts were visualized in 1% agarose gels in TAE buffer (Tris-acetate-EDTA) on a Darkreader (Claire Chemical Research, Denver, Colo.) and isolated with the QIAquick Gel Extraction Kit (Qiagen Inc., Valencia, Calif.). The concentration of the individual MHV A-G DNA fragments were measured, pooled in stoichiometrically equivalent amounts to 1 ug total DNA, and ligated with T4 DNA ligase (15 U/100 μl) at room temperature overnight in 30 mM Tris-HCl (pH 7.8)-10 mM $MgCl_2$-10 mM dithiothreitol-1 mM ATP. The ligated products were purified by phenol-chloroform-isoamyl alcohol (1:1:24) and chloroform extraction, ethanol precipitated, and resuspended in H_20. Efficient ligation was confirmed by gel electrophoresis prior to in vitro transcription reactions.

Transcripts of the MHV N gene were co-electroporated with full-length transcripts of the genome. The N-gene transcripts were driven from a T7 promoter at the 5' end of a DNA template generated by PCR from the MHV-G plasmid. The T7 bearing 5' primer (5′-ATGCAT TAATACGACTCACTATAGGGAGAATGTCTTTTGTTCCTGGGCAAG-3′) (5'T7MHV-N) and the poly-A containing 3' primer (5′-TCCGGA$(TTT)_{8}$-TTACACATTAGAGTCATCTTCTAACC-3′) (A59Ng3′(−)).

RNA transfection. Full-length transcripts of the MHV-A59's constructs were generated in vitro with some modification to the manufacturer's instructions (Ambion, Austin, Tex;

mMessage mMachine). Reactions were performed for 3 h at 37°C with 20-µl reaction mixtures supplemented with 3 µl of a 30 mM GTP stock for a 1:1 ratio of GTP to cap analog. The transcripts were treated with DNase I, precipitated in the provided LiCl solution, and resuspended in H_20. Full-length transcripts were verified by electrophoresis in 0.5% agarose gels in TAE buffer containing 0.1% sodium dodecyl sulfate (SDS). Subconfluent cultures of BHK-R and DBT cells were trypsinized, washed twice with ice-cold PBS, and resuspended in PBS at 10^7 cells/ml. Full-length RNA transcripts were mixed with N-gene transcripts and electroporated into 800 ul of the BHK-R cell suspension with three pulses at 850 V and 25 µF in a Bio-Rad Gene Pulser II electroporator. The transfected BHK-MHVR cells were diluted 1:10, 1:100, and 1:1000 in 5 ml volumes of fresh media, mixed with 10^5 DBT cells, seeded in 60-mm-diameter cell culture dishes, and incubated at 37°C. Three hours later, the media was removed from each dish and replaced with 5 ml of 1% agarose melted in 10% FCS MEM. The overlaid plates were then incubated at 37°C in 5% CO_2 and checked for plaques the next day. Plaques were isolated at 24 or 48 h post electroporation and amplified on DBT monolayers in 60-mm-diameter cell culture dishes. The virus containing media was removed 18 to 24 h post infection, aliquoted, and frozen at -70°C until titered. RNA was isolated from the monolayers for sequence analysis of the plaque purified viruses by RT-PCR. If plaques were not visible by 72 hours post electroporation the transfection was repeated and the cells were transferred to a single $75cm^2$ flask with 10^5 DBT cells and passaged 1:10 (cells and media) every 2-3 days. RNA was extracted from cells during each passage and analyzed for leader containing transcript.

Cloning of the MHV deletion and cleavage mutants. Overlapping PCR was employed for constructing the mutant cDNA templates. Mutations were introduced with two rounds of PCR. The first round generated two amplicons which were then fused by a second round of PCR using the 5' primer for amplicon 1, the 3' primer of amplicon 2, and the two overlapping amplicons for template. The first round of PCR consisted of 35 cycles of 94^{o}C annealing for 30 seconds, 55^{o}C annealing for 30 seconds, and 68^{o}C extension for 30 seconds. The second round of PCR increased the extension time to 1 minute. The fused overlapped PCR products were purified (Qiagen, PCR Purification Kit), digested at two unique restriction sites, purified a second time (PCR Purification Kit), and ligated into a similarly digested MHV plasmid. Primers, template DNA, restriction sites, and the plasmid backbone the PCR product was ligated into are included in Table 2. Mutations inserted into the MHV infectious clone were verified by sequence analysis.

Rearranging nsp7 and nsp8 genes. DNA encoding rearranged nsp7 and nsp8 genes were synthesized (Bio Basic Inc., Ontario, Canada), digested with PstI and HindIII according to the manufacturer's instructions (NEB), and ligated into the similarly digested MHV-D plasmid. The mutated template was verified by sequence analysis and assembled as part of the infectious clone.

Plaque Assay Titration of Virus Titer. DBT cells in 60-mm-diameter cell culture dishes (~10^6 cells) were infected with 200 ul of serially diluted virus in PBS. After 1 hour incubation at 25^{o}C, cells were washed 3X with PBS and then overlaid with 5 ml of 1%

agarose melted in 10% FCS MEM and incubated at 37°C in 5% CO_2. The next day, plates were stained with neutral red and plaques counted.

RTPCR verification of non-viable mutants. Mutants failing to generate plaque forming viruses were tested for their ability to generate leader containing transcripts, whose presence would indicate at least low levels of replication even in the absence of cytopathic effects. RNA harvested from passaged cells was used as template for generating cDNA by reverse transcription using superscript II (Ivitrogen) and random hexamers (Invitrogen) by the manufacturer's instructions. Following cDNA synthesis, PCR was completed using the primers (5'-AAGAGTGATTGGCGTCCGTA-3') (MHV-4), which anneals to the leader sequence of MHV, and (5'-GCAGTAATTGCTTCTGCTG-3') (30019c), which is complementary to the N-gene. Simultaneous PCR for GAPDH was also run as RNA quality and RT controls using primers GAPDHF (5'-CATGGGGAAGGTGAAGGTCG-3') and GAPDHR (5'-TTGATGGTACATGACAAGGTGC-3').

Northern Blot Analysis. DBT cells in 60-mm-diameter cell culture dishes (10^6 cells) were infected with MHV-A59 or one if the recombinant viruses at an MOI of 0.01. At 12 hrs post infection, intracellular RNA was isolated using TRIzol Reagent (Invitrogen) as directed by the manufacturer, and 0.05 μg of total mRNA was treated with glyoxal and separated on agarose gels using NorthernMax®-Gly according to the manufacturer's directions (Ambion). The RNA was transferred to BrightStar-Plus membrane (Ambion) for 3.5 hrs and then cross-linked to the membrane by UV light. The blot was prehybridized and probed with a labeled RNA complementary to ~200 bp of the 5' portion of the N gene. The RNA probe was generated by PCR using the primers (5'-ATGTCTTTTGTTCCTGGGCAAG-3') (MHV-5'N)

and (5'ATATAT

TAATACGACTCACTATAGGGAGACCAGAAAACCAGGAGTAATGG-3') (T7-30019c). RNA transcripts were driven from the T7 promoter included in the 3'primer. RNA was biotinylated with the BrightStar® Psoralen-Biotin Nonisotopic Labeling Kit as directed by the manufacturer (Ambion). Following prehybridization, blots were hybridized overnight, and washed with low and high stringency buffers as recommended by the manufacturer (Ambion). Filters were incubated with the chemi-illuminescent substrate CDP-STAR (Ambion). The blots were overlaid with film and developed.

Radiolabeling MHV proteins and immunoprecipitation of cell lysates. DBT cells in 60-mm-diameter cell culture dishes (3×10^6 cells) were infected with MHV, one of its mutants, or mock infected with PBS. At 4.5 h.p.i., the medium was replaced with fresh 5% FCS DMEM lacking methionine and cysteine and containing actinomycin D (20 μg/ml). At 6 h.p.i. [^{35}S]methionine-cysteine (100 uCi/ml) was added and incubated at 37C for 3 hours. Cells were washed with 1 M Tris and then lysed in 1 ml of lysis buffer (150 mM NaCl, 1% NP-40, 0.5% deoxycholate [DOC], 50 mM Tris, pH 8.0). Immunoprecipitations were performed in a final volume of 1 ml, using protein A-Sepharose beads (Sigma), 100 μl of radiolabeled lysate and 2 to 10 μl of polyclonal antiserum specific for one of the nsp7-10 proteins (12) after the lysate was boiled for 5 min in 1% SDS, in buffer C (150 mM NaCl, 1% NP-40, 1% DOC, 1% SDS, 10 mM Tris, pH 7.4). Protein-bead conjugates were washed three times in the same buffer used for immunoprecipitations, and the proteins were eluted from the beads, followed by boiling for 5 min in 2× protein loading buffer (200 mM dithiothreitol, 100 mM Tris, pH 6.8, 0.04% bromophenol blue, 20% glycerol). The proteins

were resolved by SDS-PAGE in 5 to 18% polyacrylamide gradient gels and analyzed by fluorography. The [^{14}C] high-molecular-weight standard (Gibco) and full-range rainbow marker (Invitrogen) were used as molecular weight standards.

Immunofluorescence assays and confocal microscopy. DBT cells grown on glass coverslips were infected with MHV or PBS mock and then rocked at 25°C for 30 min. Following virus adsorption, the infected medium was replaced with fresh prewarmed 10% FCS MEM, and the cells were incubated at 37°C. At 8 h.p.i., the cells were fixed and permeabilized with 100% methanol cooled to -20^{o}C. Indirect immunofluorescence assays were performed as previously described (12). Secondary antibodies conjugated to fluorophores were used at 1:1,000 dilution and included α-guinea pig-Alexa 546, α-rabbit-Alexa 488, and α-mouse-Alexa 633. Immunofluorescence was detected using a Zeiss LSM 510 laser scanning confocal microscope with a 40× oil immersion objective. Image analysis and merging was performed using Adobe Photoshop version 7.0.

Results

Viability of nsp7-10 deletion mutants. M^{pro} targets amino acid sequences (L,F,I)Q↓(S,N/,A) and cleaves after the essential Gln at position 1 (P1) (116). Individual protein domains were deleted from the MHV genome while preserving functional cleavage sites by fusing the N-terminal P1 amino acid to the carboxyl P1' residues of the flanking proteins (Table 3). Virus was produced from cDNA templates as previously described (231) and viability was determined by syncytia formation in cells electroporated with in vitro-transcribed mutant genome RNA. All of the deletion mutants failed to yield virus or produce

viral cytopathic effect. A series of MHV temperature-sensitive mutants have been described where viruses only grow at a lower permissive temperature (165). With this in mind, a second attempt to generate non-viable viruses was made and electroporated cells incubated at 32^{o}C instead of 37^{o}C. However, none of the deletion mutants demonstrated the temperature-sensitive phenotype; no viable viruses were detected at 32^{o}C even after several passages spanning at least a week, and no leader-containing transcripts indicative of subgenomic mRNA synthesis were detected in transfected cultures by RTPCR indicating that these deletions were truly lethal for replication.

Viability of cleavage site-disrupted mutants. To evaluate the requirement of nsp7-10 proteolytic processing on virus replication, cleavage sites flanking nsp7, nsp8, nsp9 and nsp10 were individually disrupted by substituting the P1 Gln with Ala (Table 4). There are two potential cleavage sites at the nsp7-8 interface, an LQ↓A and LQ↓S (present at positions P5-P3 and P2-P1' in Table 2, respectively). Although the LQ↓S has been shown to be cleaved during nsp7-8 processing (126), it is possible that the upstream LQ↓A site is also functional. To address this possibility, both sites were substituted, either individually (MHV7/8A and MHV7/8B) or in combination (MHV7/8AB).

Full length cDNAs of each of the seven cleavage site mutants were assembled using standard techniques and transcripts were electroporated into cells. Viability was determined by syncytia formation and, for viruses that failed to produce syncitia, detection of leader containing transcripts by RT-PCR of transfected cell RNA harvested at each of three passages (**Fig. 20**). Following electroporation of mutant genome RNA into cells, no syncytia or infectious virus was detected from mutants MHV6/7, MHV7/8AB, MHV8/9, and

MHV10/11. A second attempt to generate non-viable viruses was made with incubations at 32°C, but none of the cleavage mutants failing to grow at 37°C were rescued by growth at the lower temperature. These data indicated that disruption of cleavage sites nsp6-7, both sites at nsp7-8, nsp8-9, and nsp10-11 were lethal to viral replication. In contrast, disruptions of either of the nsp7-8 or the nsp9-10 cleavage sites were not lethal and recombinant viruses of each were plaque purified for future use. Plaque morphology of MHV7/8A and MHV7/8B were similar to wildtype, but MHV9/10 displayed a small plaque phenotype (data not shown). Sequence analysis of RNA from virus infected cells demonstrated the presence of the appropriate mutations in each of the viable viruses. Growth kinetics of these viable viruses were compared to wild-type MHV in DBT cells at a MOI of 0.01 pfu/cell (**Fig. 21A**). MHV, MHV7/8A, and MHV7/8B reached peak titers at 18 hours post infection of 7.4±0.1, 7.3±0.2, and 7.4±0.1 $\log_{10}$ pfu/ml, respectively. The MHV9/10 mutant displayed an attenuated growth phenotype with peak titers almost two logs lower titer at the 18 hour time point (5.5±0.1 $\log_{10}$pfu/ml).

Stability of the replication-attenuated MHV9/10 mutation was tested by successive blind serial passage on DBT cells for 15 passages, followed by 3x plaque-purification of the resulting virus. The growth kinetics of two passage-15 isolates, MHVp15-1 and MHVp15-3, were compared to that of MHV (**Fig. 21B**). In contrast to the parent mutant virus, the passage 15 isolates displayed near wild-type growth kinetics in DBT cells, MHVp15-1 and MHVp15-3 reached peak titers of 6.8±0.1 and 6.9±0.1 that approached that of MHV (7.2±0.1 $\log_{10}$pfu/ml).

Sequence analysis of the nsp7-10 region of the revertant viruses illustrated that the inserted mutation did not revert to wild-type sequence at the nsp9-10 cleavage site. Two

patterns of mutations were found. Three of the six plaque isolates sequenced, including MHVp15-1, had mutated the guanosine at nt 13164 to an adenosine, changing the introduced alanine at P1 of the nsp9-10 cleavage site to a threonine (Table 5). The other mutants, including MHVp15-3, maintained the alanine at the P1 position, but had a guanosine instead of a adenosine at nt 13102, producing an arginine instead of lysine 21 amino acids upstream of the nsp9-10 P1 position.

Three mutants were constructed to determine if the changes found in nsp9 of the passage 15 isolates could be attributed to the improved fitness of the viruses (Table 5). Engineered mutant MHV_{Q4319T} contained the P1-Gln4319Thr, reproducing the nsp9 sequence found in MHVp15-1. In order to determine if the Lys4298Arg substitution in nsp9 identified in MHVp15-3 affects viral replication in DBT cells, the single mutation was introduced in the wild-type infectious clone and used to produce the mutant virus, MHV_{K4298R}. The final mutant, $MHV9/10_{K4298R}$, possessed the nsp9 Lys4298Arg substitution in addition to the P1-Gln4319Ala introduced to disrupt nsp9-10 cleavage, giving it an nsp9 sequence identical to MHVp15-3. Viable viruses were recovered for all three and growth curves of plaque purified viruses indicated that neither of the changes in nsp9 of MHVp15-1 or MHVp15-3 were solely responsible for the improved growth kinetics of the passage 15 revertants (**Fig. 22**). MHV_{Q4319T} reached a titer of 6.3±0.2 $\log_{10}$ pfu/ml at 30 h.p.i., comparable to that of MHV9/10 at 6.0±0.4 and indicating that the nsp9 mutation found in MHVp15-1 was not responsible for its improved fitness relative to the attenuated parent. Introduction of Lys4298Arg into the MHV backbone did not reduce the peak titer of the virus; MHV_{K4298R} attained a titer of 7.5±0.1 $\log_{10}$pfu/ml at 30 h.p.i. which was comparable to wild-type with 7.4±0.1. The combination of K4298R and Q2319T found in the nsp9 of MHVp15-3 were

not sufficient to return the mutant MHV9/10_{K4298R} to wild-type growth, although it did improve growth kinetics relative to the parent MHV9/10. Although MHV9/10_{K4298R} reached a peak titer of 6.5±0.1 $\log_{10}$pfu/ml at 30 h.p.i, similar to MHV9/10 at 6.0±0.4, the virus maintained better growth than the parent mutant from 12 to 24 h.p.i. MHV9/10_{K4298R} reached average titers of 5.1±0.2, 6.1±0.1, and 6.4±0.1 $\log_{10}$pfu/ml at 12, 18, and 24 h.p.i., respectively. In comparison, MHV9/10 had titers of 3.7±0.2, 4.7±0.3, and 5.4±0.3 at the same time-points. The mutation(s) responsible for the increased in vitro fitness of the serially passaged virus at least require the contribution of more distal mutations within the genome that remain to be identified.

Rearranging nsp7/nsp8. The domain order of coronavirus ORF1ab non-structural proteins is conserved. However, it has been possible to recover mutant viruses with deletion and rearrangement of nsp2 ((69)and unpublished data). To test whether the nsp7-10 order must be maintained for efficient replication, the nsp7 and nsp8 genes were rearranged. Transcripts were driven from the cDNA templates and electroporated into cells. Viability was determined by syncitia formation and detection of leader containing transcripts by RTPCR of RNA harvested at each of three passages. Following electroporation of cells with mutant genome RNA containing the nsp8-7 rearrangement, no virus was obtained and no leader-containing transcripts were detected, suggesting that the domain order for nsp7, nsp8, and perhaps the other components of the precursor polyprotein, were essential for replication.

Verification of ablated cleavage sites in viable mutant viruses. Processing of the ORF1a nsp8, 9 and 10 replicase proteins were evaluated in DBT cells infected at a MOI of 1, treated with actinomycin D at 4.5 hpi, and radiolabeled from 6 at 9 hpi. Immunoprecipitation (i.p.)

using either anti-nsp8 (for the MHV7/8 mutants) or anti-nsp9 and anti-nsp10 antibody (for the MHV9/10 and passage 15 mutants) (11) was used to evaluate the impact of the specific cleavage site mutations on ORF1a polyprotein processing. Substitution of the P1-Gln to Ala prevented processing at the cleavage sites for the MHV9/10, MHVp15-1 and MHVp15-3 viruses (**Fig. 23**). Normal processing of nsp8 (22 kDa), nsp9 (12 kDa) and nsp10 (15 kDa) was detected during wildtype MHV infection but not in mock-infected cells. In contrast, nsp10 was absent following MHV9/10 and MHVp15 infection. However, a slower migrating band of approximately 27 kDa, which is the predicted size for an nsp9-10 fusion protein, was present in the mutants, but absent in the wild-type controls. These data indicate that neither the nsp9 P1-Ala110Thr in the MHVp15-1 nor the nsp9 Lys89Arg change in MHVp15-3 restored cleavage at the nsp9-10 junction.

Analysis of MHV7/8A and MHV7/8B infected cultures indicated that both the LQ↓A and LQ↓S sites bordering the nsp7-8 junction are functional cleavage sites. Following immunoprecipitation, 22 kDa proteins were precipitated with anti-nsp8 antibody for the wild-type control, MHV7/8A, and MHV7/8B. Notably, the immunoprecipitated protein from MHV7/8B had slightly slower migration than that of the control or the MHV7/8A mutant, consistent with the prediction that the LQ↓A site was cleaved and yielded an nsp8 protein 3 amino-acids larger (~366Da) than that of the LQ↓S cleaved protein.

Transcriptional profile of viable mutant viruses. With the exception of the attenuated MHV9/10 mutant, viable mutants were found to be similar to MHV in their transcriptional activity and generation of subgenomic RNA (**Fig. 22**). To determine if differences in RNA synthesis were associated with the different growth phenotypes, cultures of DBT cells were

infected with the mutant panel at a MOI of 0.05, and total intracellular RNA was harvested at 12 h p.i. Northern blots hybridized with an RNA probe complementing the 5' end of the N-gene showed no differences in either the pattern or relative amounts of subgenomic to genomic RNA in most mutants when compared to control virus. Consistent with the reduced growth of the mutant virus in vitro relative to MHV, MHV9/10 had significantly reduced amounts of RNA with only the mRNA 6 and 7 bands clearly resolved. Importantly, revertant viruses had restored efficient growth kinetics and transcription of full length and subgenomic mRNAs. We did not identify any significant differences in the relative molar ratios of the viral plus sensed RNAs (data not shown).

Association of mutant proteins with replication complexes. The distribution of the mutant proteins within cells was compared to their wild-type counterparts. The nsp7-10 are known to colocalize with sites of viral replication while being excluded from regions of virion assembly (11, 12). In order to determine if abolition of processing in the mutant viruses affected the distribution, subcellular localization, or the ability of the protein to traffic into the replication complex, we used confocal microscopy to compare the colocalization of wild-type and mutated proteins to sites of replication and assembly. DBT cultures were infected with either MHV-A59, mock, or mutant virus and at 8 hrs postinfection were methanol fixed and dual-stained for either nsp8 or nsp10 (depending on the mutant, as above) and nucleocapsid (N), which colocalizes with sites of active viral replication, or membrane (M), which is targeted to regions of virus assembly. Regardless of the construct, the nsp8 and nsp10 proteins colocalized with N in subcellular compartments that were separate from M

(**Fig. 23**). These results are identical to those for wild-type MHV (not shown) indicating that incorporation of the mutated proteins into the replication complex is not disrupted (11).

Discussion

The nsp7-10 are highly conserved among, and perhaps unique to, the family coronaviridae. Indeed, even the arteriviruses, another family member of the order *Nidovirales*, do not appear to possess homologs to the coronavirus nsp7-nsp10 (146). The roles of these proteins in coronavirus replication are only just beginning to be studied, with the existing body of data suggesting that they are components of the replication complex. However, the details of their involvement in replication and RNA synthesis remain to be determined. This study used an infectious clone of MHV to define fundamental features of the nsp7-10 during viral replication in culture. Each of the four proteins appears to be critical for viral replication, since deletion of any of the four protein domains was lethal for RNA synthesis and productive virus infection. Furthermore, the results indicate that processing of the proteins from each other is necessary for replication, with the one exception of the nsp9-10 cleavage site. Finally, we determined that rearranging two of the replicase proteins, nsp7 and nsp8, was not permissive for virus replication.

To date, only the nsp2 coronavirus replicase protein has been shown to be dispensable for replication in both MHV-A59 and SARS-CoV, albeit attenuating in vitro and in vivo (70). Portions the carboxy-terminal half of MHV nsp1 has also been deleted in viable mutants (19), but otherwise, no full or partial deletions of replicase protein domains has been reported in viable mutants of any coronavirus. In contrast, deletion of each of the nsp7-10 resulted in a lethal phenotype as evidenced by the lack of recoverable viruses and an inability to detect subgenomic mRNAs by RT-PCR. These data suggest that each of the nsp7-10 may

be an indispensable component of the replication complex, which is consistent with the highly conserved nature of these proteins. Alternatively, deletion of nsp coding sequences may sufficiently alter the structure of the polyprotein template to interfere with M^{pro} accessibility to its cleavage sites. Interestingly, an MHV temperature sensitive mutant, LA6, contains a mutation in nsp10 that blocks processing of nsp4-10 at the non-permissive temperature suggesting that mutations or deletions at the c-terminus of ORF1a might disrupt M^{pro} activity (165).

Although it is known that global inhibition of coronavirus proteinases that process the replicase polyproteins prevents replication (103), the requirements for each of the 15 cleavage sites in the ORF1ab polyprotein are not completely determined. Cleavage of nsp1, nsp2 and nsp3 has been abolished in viable MHV mutants (46, 69). Otherwise, little is known of the requirements for processing, including nsp7-nsp10. Our results show that changes at cleavage sites between nsp6-7, nsp7-8, nsp8-9, and nsp10-11 were not replication viable. Lethality could be due to disruption of nsp7-10 proteolytic processing causing a failure of precursor, intermediate, or mature protein function within the replication complex. However, not all of the cleavage site mutants were nonviable. Based on genetic analysis, MHV has two functional nsp7-8 cleavage sites, LQ↓A and LQ↓S, and disruption of either of these potential sites failed to affect replication competence, cleavage patterns, or cellular localization *in vitro*. Interestingly, the LQ↓A site is conserved across all coronavirus families, while the second LQ↓S site is limited to group II coronaviruses, including MHV, BCoV, HKU1, and OC43, but not SARS-CoV. Wild-type replication efficiency when either one or the other site was knocked out suggests that either, or both, sites are cleaved during replication. Although we cannot detect any significant impact on in vitro replication,

variations in N or C-terminal processing of nsp7-8 may influence in vivo pathogenesis or affect cell signaling pathways. However, simultaneous mutation of both sites was lethal, indicating that nsp7 and nsp8 must be fully separated to function in mRNA synthesis.

The only cleavage site that tolerated inactivation was the nsp9-10 cleavage site. The mutant MHV9/10 virus produced a fusion nsp9-10 protein and was highly attenuated in its replication efficiency. Serial passage of this virus restored near wild-type replication fitness, but did so without reverting at the mutated cleavage site or regaining the ability to process nsp9-10, demonstrating that efficient replication can be achieved without nsp9-10 proteolytic processing. The data demonstrate that with the exception of cleavage between the nsp9 and nsp10 proteins, M^{pro} processing of the nsp7-nsp10 are essential in coronavirus RNA transcription and replication.

Previous work has indicated that nsp7 and nsp8 in solution form a complex hexadecameric structure that is proposed to function in processivity and generation of RNA primers for the RNA replicase (89, 234). If these structures represent those seen in during infection, then formation of the structures would require cleavage of nsp7 from nsp8. Similarly, the virus could not replicate when the relative positions of the genes encoding nsp7 and nsp8 were switched. This loss of viability could be due to an alteration of the precursor polyprotein that interfered with processing or prevented a distinct function associated with the uncleaved precursor. It is unclear why only the MHV9/10 mutant was viable. Nsp9 associates with the replication complex, interacting at least with nsp8 (191), and has been shown to possess single-stranded RNA binding affinity (11, 53, 191). Nsp10 is known to associate with several proteins of the replication complex, including nsp1, nsp5, nsp7, nsp8, and nsp12 (18, 19). Nsp10 has been shown to be critical for the formation of

functional replication complexes (165), and has recently been shown to crystallize to form monomers and homodimers as well as a complex dodecameric structure when expressed as an nsp10-11 fusion (97, 187). It is puzzling why this critical protein with broad interactions with other replicase proteins would retain its function without full separation from nsp9. Interestingly, mutation of the nsp10-11 cleavage site was nonviable despite the report that the spherical structure formed by 12 units of nsp10 was crystallized as an nsp10-11 construct (187). Collectively, our data indicates that the C-terminal cleavage site for the nsp10 protein is essential for infectivity, raising doubt about the biological relevance of the reported nsp10-11 crystal structure (187).

Prior to this study, two viable cleavage mutants of coronaviruses had been reported, the PLP1-mediated cleavage sites between nsp1-nsp2 and nsp2-nsp3 were removed in MHV (46, 69). Loss of cleavage site function resulted in attenuated replication and suggested that efficient cleavage of nsp1-2 and nsp2-3 was important, but not required, for replication in tissue culture (46, 69). Indeed, viable mutant virus could be generated even when PLP1, which solely mediates nsp1-2 and nsp2-3 processing in MHV, was inactivated (69). With this report, three cleavage sites in the MHV ORF1a polyprotein have been shown to be dispensable for replication: nsp1-2, nsp2-3 and nsp9-10 (46, 69). It is possible that this reflects the use of these proteins in natural precursors, such as has been reported for nsp2-3 and nsp4-10. Thus the engineered changes may reproduce some component of the normal lifecycle and at least residual function of these proteins. Interestingly, rearrangement of the nsp7 and nsp8 encoding sequences was lethal, a result that lends support to the idea that their may be an independent function in replication associated with the nsp4-10 precursor (165).

There are still many aspects of coronavirus replication that are not clearly understood. Several conserved components of the coronavirus replicase have no known homologs and serve unknown or poorly defined functions. The proteolytic processing of the replicase polyproteins are a critical step in replication of these viruses, and such processing my provide a level of regulation over replication in general, such as providing the molecular switch for altering the output of the replication complex from minus strand RNA to that of positive strand RNA (13, 164). This work will be progressed by experimentally pursuing new questions defined by these results. Although processing of either of the sites at the nsp7-8 boundary had no impact on in vitro growth, work will be done to determine if both sites are required for efficient replication in vivo. Some insight may be gained into nsp7-10 function, such as cis versus trans activity, by determining if lethal cleavage mutants can complement each other to form viable replication complexes to rescue virus. The distal mutation(s) which arose during serial passage to allow the attenuated MHV9/10 mutant to recover will also be identified and may expand our understanding of the interactions that occur between proteins of the replication complex. The presented data supports existing information that the proteins of the 3' c-terminus of ORF1a are critical for replication, establishes the importance of processing in their function, and lays the foundation for future studies.

TABLE 2. Primers, template DNA, and restriction sites used in the generation of deletion and cleavage mutants

Mutant	Amplicon	Primer	Primer Name	Sequence (5'->3')	Template DNA	Restriction Sites
Δnsp7	1	5'	D 3500:	CGGAGGCTTTTGACTTTCTG	MHVD	PstI+NdeI
		3'	D 470c:	AATTTGAGATACTTCAATGACTGG		
	2	5'	5'Δnsp7	GTATCTCAAATTCAAAGTGAATTTGTTAATATGGC	MHVD	
		3'	D 1001c:	GCAGACACTACCTTACTCTTC		
Δnsp8	1	5'	D 3500:	CGGAGGCTTTTGACTTTCTG	MHVD	PstI+HindIII
		3'	D743c	TAAGGCTTGCAAGACAGTATTGTC		
	2	5'	5'Δnsp8	GTCTTGCAAGCCTTACAGAACAATGAGTTGATGCCTCAG	MHVD	
		3'	D 1570c:	CAGTTACGCTGGAGTCTG		
Δnsp9-D	1	5'	D 880:	CAGCAGATTAAGCAGCTAG	MHVD	HindIII+NdeI
		3'	D 1328c:	CAAAACAACAGTAGACACTTC		
	2	5'	5'Δnsp9-D	CTACTGTTGTTTTGCAGCCTAAGAGACGAAGGGCG	MHVD	
		3'	D 1769C	GCGCTCTGCTGAAGCCAG		
Δnsp9-E	1	5'	E 4031	CCACGCTGATGAGCTTTACC	MHVE	ClaI+MscI
		3'	E 1c	TAGGAGAGACGAAGGGC		
	2	5'	5'Δnsp9-E	CCTTCGTCTCTCCTAGCGGGTACGGCAACTGAG	MHVE	
		3'	E 462c:	CCATCAACATCTGGATGTTC		
Δnsp10	1	5'	E 4031	CCACGCTGATGAGCTTTACC	MHVE	ClaI+KpnI
		3'	E 199c:	CAATCTCACTGTCGAGG		
	2	5'	5'Δnsp10	CGACAGTGAGATTGCAGTCAAAAGACACGAACTTTTTAAACG	MHVE	
		3'	E: 1021c:	CATTGCGGTCAAAATGACGC		
nsp6*7	1	5'	D 3500:	CGGAGGCTTTTGACTTTCTG	MHVD	PstI+NdeI
		3'	D 470c:	AATTTGAGATACTTCAATGACTGG		
	2	5'	QAnsp6/7:	GTATCTCAAATTGCATCAAGATTGACG	MHVD	
		3'	D 1001c:	GCAGACACTACCTTACTCTTC		
nsp7*8	1	5'	D 3500:	CGGAGGCTTTTGACTTTCTG	MHVD	PstI+NdeI
		3'	D 1328c:	CAAAACAACAGTAGACACTTC		
	2	5'	QAnsp7/8	CAAGCCTTAGCGAGTGAATTTGTTAATATG	MHVD	
		3'	D 1001c	GCAGACACTACCTTACTCTTC		
nsp8*9	1	5'	D 880:	CAGCAGATTAAGCAGCTAG	MHVD	NdeI+HindIII
		3'	D 1328c	CAAAACAACAGTAGACACTTC		
	2	5'	QAnsp8/9:	CTACTGTTGTTTTGGCGAACAATGAGTTGATGC	MHVD	
		3'	D 1570c:	CAGTTACGCTGGAGTCTG		
nsp9*10	1	5'	E 4373:	GTTCGGTGTAGGTCGTTC	MHVE	ClaI+MscI
		3'	E 199c:	CAATCTCACTGTCGAGG		
	2	5'	QAnsp9/10	GTGAGATTGGCGGCGGGTACGG	MHVE	
		3'	E 462c:	CCATCAACATCTGGATGTTC		
nsp10*11	1	5'	E 4031	CCACGCTGATGAGCTTTACC	MHVE	ClaI+KpnI
		3'	E 606c+:	GCAAACTGGGAGCCTGTGCCTAC		
	2	5'	QAnsp10/nsp11	CCCAGTTTGCGTCAAAAGACACG	MHVE	
		3'	E 1021c:	CATTGCGGTCAAAATGACGC		

TABLE 3. nsp7-10 cleavage sites of wild-type MHV and deletion mutants

	Wild-type amino acid sequence of the nsp7-10 cleavage sites									
	P5	P4	P3	P2	P1	P1'	P2'	P3'	P4'	P5'
nsp6-7	V	S	Q	I	Q	S	R	L	T	D
nsp7-8	**L**	**Q**	**A**	**L**	**Q**	**S**	**E**	**F**	**V**	**N**
nsp8-9	T	V	V	L	Q	N	N	E	L	M
nsp9-10	**T**	**V**	**R**	**L**	**Q**	**A**	**G**	**T**	**A**	**T**
nsp10-11	G	S	Q	F	Q	S	K	D	T	N
	Mutant amino acid sequence of the nsp7-10 cleavage sites									
	P5	P4	P3	P2	P1	P1'	P2'	P3'	P4'	P5'
Δnsp7	V	S	Q	I	Q	**S**	**E**	**F**	**V**	**N**
Δnsp8	**L**	**Q**	**A**	**L**	**Q**	N	N	E	L	M
Δnsp9	T	V	V	L	Q	**A**	**G**	**T**	**A**	**T**
Δsnp10	**T**	**V**	**R**	**L**	**Q**	S	K	D	T	N

TABLE 4. Mutagenesis of the nsp7-10 cleavage sites

	Mutating P1-Q to A at Cleavage Sites									
	P5	P4	P3	P2	P1	P1'	P2'	P3'	P4'	P5'
MHV6/7	V	S	Q	I	**A**	S	R	L	T	D
MHV7/8A[a]	L	**A**	A	L	Q	S	E	F	V	N
MHV7/B[b]	L	Q	A	L	**A**	S	E	F	V	N
MHV7/8AB[c]	L	**A**	A	L	**A**	S	E	F	V	N
MHV8/9	T	V	V	L	**A**	N	N	E	L	M
MHV9/10	T	V	R	L	**A**	A	G	T	A	T
MHV10/11	G	S	Q	F	**A**	S	K	D	T	N

[a] The upstream LQ↓A site is substituted.
[b] The downstream LQ↓S site is substituted.
[c] Both sites are substituted.

TABLE 5. Genomic variation of nsp9 between MHV, MHV9/10, and the passage 15 mutants

Genome Position (aa)	4298	4319
MHV	Lys	Gln
MHV9/10	Lys	Ala
MHVp15-1	Lys	Thr
MHVp15-3	Arg	Ala
MHV_{Q4319T}	Lys	Thr
MHV_{K4298R}	Arg	Gln
$MHV9/10_{K4298R}$	Arg	Ala

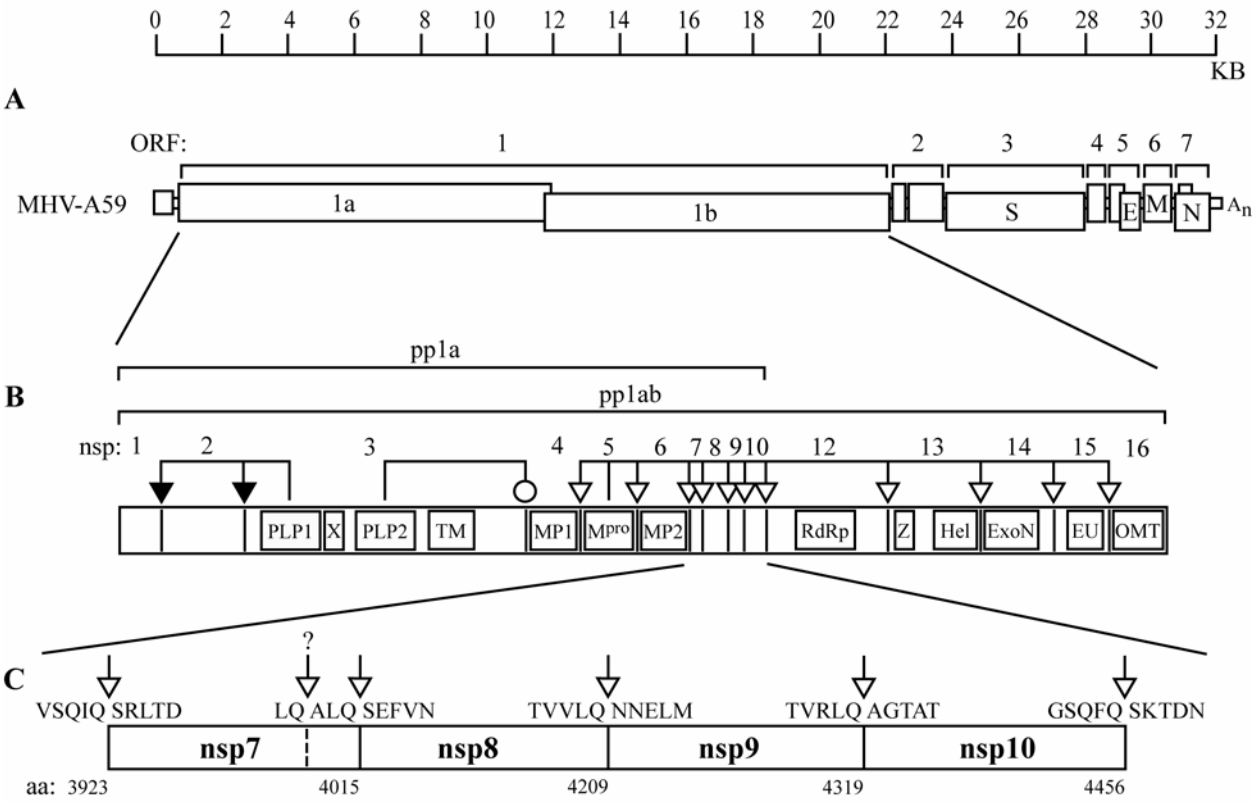

Figure 19. MHV genome organization, proteolytic processing of the replicase polyproteins, and putative cleavage sites of nsp7-10. (A) The 5' two-thirds of the MHV genome encode the ORF1 replicase proteins, pp1a and pp1ab. ORFs 2-7 encode the major structural proteins, S, E, M, and N along with several accessory proteins. (B) The replicase polyproteins are processed by three proteases to produce 16 mature proteins. PLP1 is responsible for cleaving between nsp1-2 and nsp2-3 (black arrows) while PLP2 cleaves between nsp3-4 (open circle). M^{pro} processes the remainder of the polyproteins (open triangles). The replicase proteins include a number of functionally conserved domains including the two PLP proteases, an ADP-ribose-1"-monophosphate processing enzyme (X), three hydrophobic trans-membrane domains (TM, MP1 and MP2), the nsp5 protease (M^{pro}), RNA-dependent RNA polymerase (RdRp), putative zinc-binding domain (Z) and helicase (Hel), exonuclease (ExoN), endoribonuclease (EU), and an S-adenosylmethionine-dependent ribose 2'-O-methyltransferase (OMT). (C) The amino acid sequences of the M^{pro} cleavage sites falling within the nsp7-10 region of the replicase polyproteins are shown (open arrows denote point of cleavage) along with their P1-Gln amino acid positions. A second putative cleavage site falling between nsp7-8 is identified with a question mark and a vertical dotted line illustrating its proposed cleavage site.

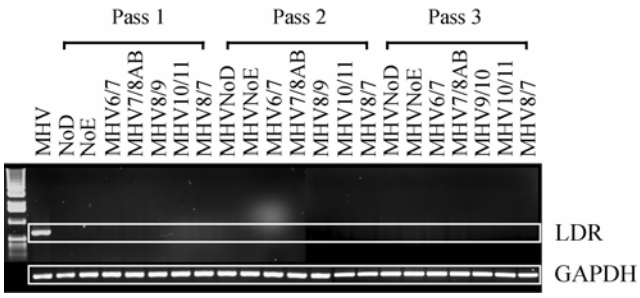

Figure 20. RTPCR verification of the replication deficiency of non syncitia forming cleavage mutant viruses. RNA was extracted from cells over 3 passages of electroporated DBT cells and supernatants. PCR was completed using primers specific for leader containing N-gene transcripts and GAPDH as a control of RNA quality and successful RT reactions. RNA from cells infected with wild-type MHV was used as a positive control.

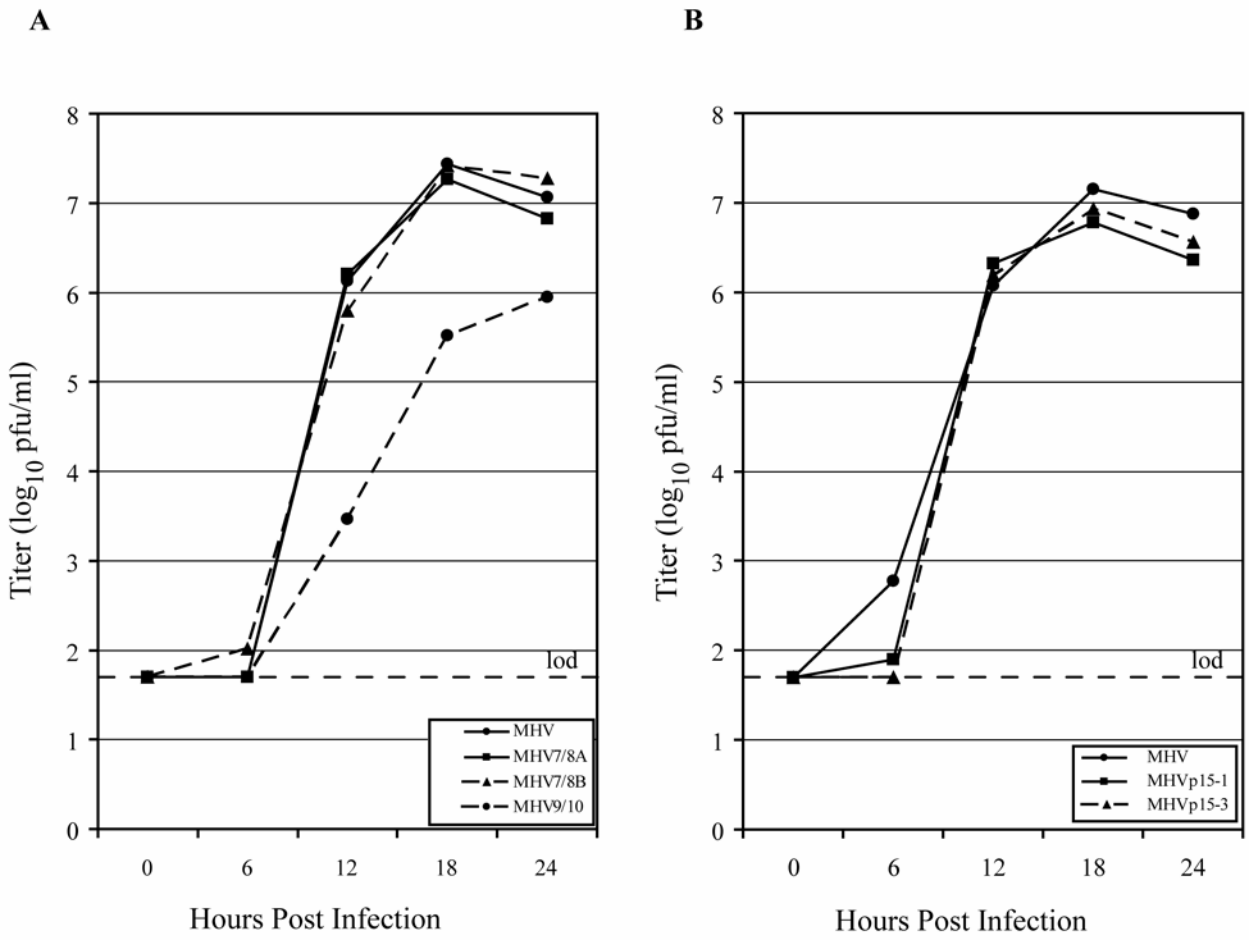

Figure 21. Replication kinetics of the viable cleavage mutants and MHV9/10 revertants. (A) Comparison of the growth curves for MHV (black circle and solid line), MHV7/8A (black square and solid line), MHV7/8B (black triangle and dashed line), and MHV9/10 (black circle and dashed line). (B) Replication fitness of the revertant MHV9/10 passage 15 viruses. Growth curves comparing MHV (black circle and solid line), to the passage-15 isolates, MHVp15-1 (black square and solid line) and MHVp15-3 (black triangle and dashed line). Growth curves were performed on DBT cell monolayers infected at an moi of 0.05 pfu/cell. Supernatants sampled for replicating virus at 0, 6, 12, 18, and 24 hours post infection and titers determined by plaque assay. Data points represent the average of three replicate experiments. The limit of detection (lod) is represented by a horizontal dashed line at 1.7 $\log_{10}$ pfu/ml.

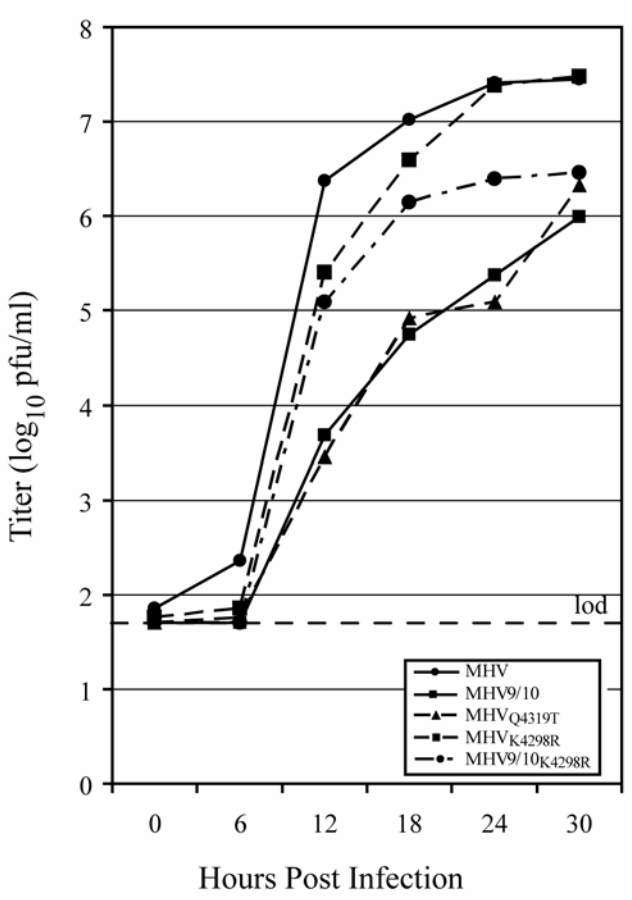

Figure 22. Characterizing the nsp9 genetic components of MHVp15-1 and MHVp15-3. Comparison of MHV (black circle and solid line), the attenuated parent virus MHV9/10 (black square and solid line), MHV_{Q4319T} (black triangle and dotted line), MHV_{K4298R} (black square and dotted line), and $MHV9/10_{K4298R}$ (black circle and dotted line). Growth curves were performed on DBT cell monolayers infected at an moi of 0.05 pfu/cell. Supernatants sampled for replicating virus at 0, 6, 12, 18, and 24 hours post infection and titers determined by plaque assay. Data points represent the average of three replicate experiments. The limit of detection (lod) is represented by a horizontal dashed line at 1.7 log_{10} pfu/ml.

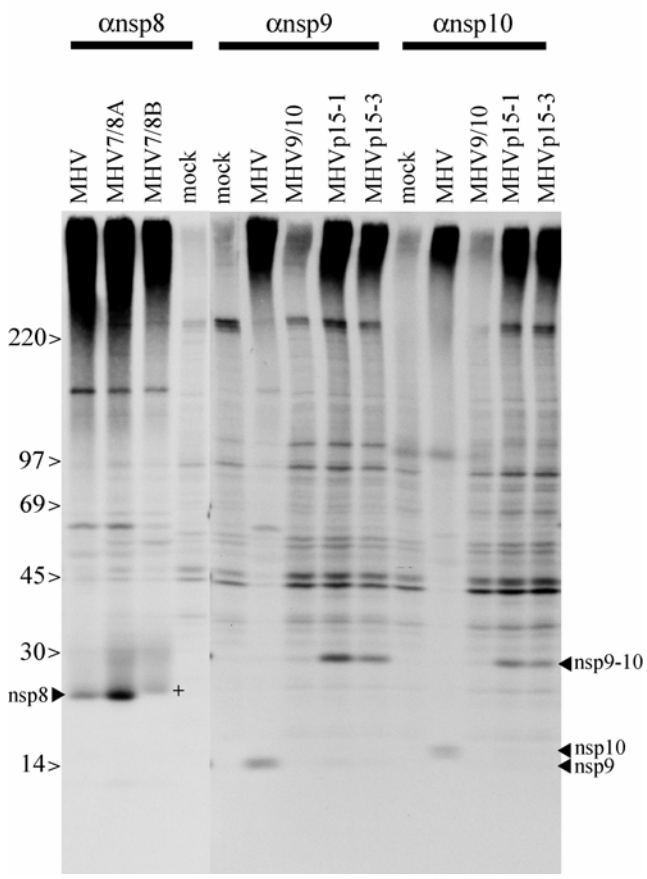

Figure 23. ORF1a Polyprotein Processing in Recombinant Viruses. Cultures of cells were infected with MHV, MHV7/8A, MHV7/8B, MHV9/10, MHVp15-1, or MHVp15-3 for 4.5 hrs. The cultures were radiolabeled for 3 hrs and antisera against nsp8 (22 kDa), nsp 9 (12 kDa) or nsp10 (15 kDa) used for immunoprecipitation . DBT cells were infected at an MOI of 1 pfu/cell and labeled with [^{35}S]-Met/Cys containing medium from 6 to 9 h.p.i. in the presence of actinomycin D. Approximately 9 h.p.i. cells were lysed and immunoprecipitated with polyclonal sera against nsp8, nsp9, or nsp10, then resolved by SDS-PAGE and fluorography. Bands corresponding to nsp8, nsp9, nsp10, and the fused nsp9+nsp10 (nsp9-10) are indicated. The protein corresponding to nsp8 isolated from MHV7/8B infected cells (+) migrated slower than those of MHV or MHV7/8A.

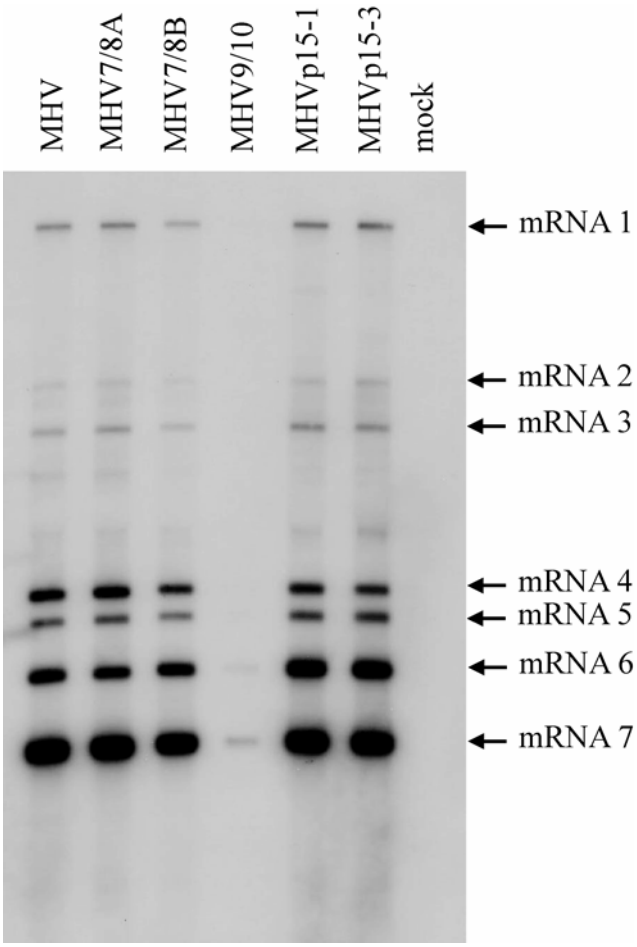

Figure 24. Recombinant and wildtype virus RNA Synthesis. Cultures of cells were infected with the wildtype MHV or recombinant viruses and intracellular RNA harvested from DBT cells at 12 hours post infection. The RNA was separated on a 1% agarose gel, transferred to nylon filters and hybridized with biotinylated RNA probe specific for nucleocapsid. The filters were incubated with a chemi-illuminescent substrate and exposed on film.

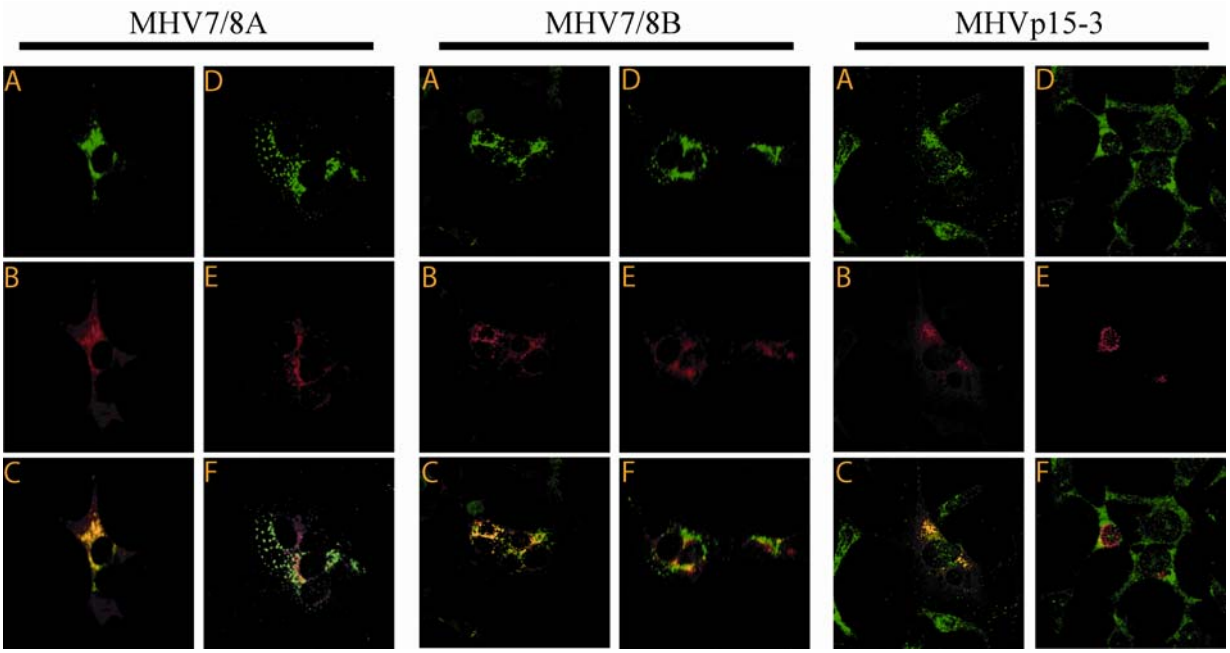

Figure 25. Immunofluoresence of MHV cleavage mutant infected cells. Cells were infected with either MHV7/8A, MHV7/8B, or MHVp15-3, fixed and permeabilized with MeOH, then dual-stained with antibody specific for nsp8 (MHV7/8A and MHV7/8B) or nsp10 (MHVp15-3) and nucleocapsid or membrane protein. The green fluorescent anti-nsp image (A, D) was overlayed with the corresponding red fluorescent anti-N (B) or anti-M image (E) to determine points of co-localization (yellow) between the nsp and either N, representing localization with the replication complexes (C), or M, which is excluded from sites of replication (F).

Chapter IV

Summary

The recently developed coronavirus reverse genetic systems have been a tremendous asset for improving our understanding of the viruses' complex replication strategy, pathogenesis, mechanisms of host-range expansion, and in the development of anti-viral therapies. We completed two studies using coronavirus infectious clones. The work presented in chapter two evaluated the ability of a severe acute respiratory syndrome coronavirus (SARS-CoV) vaccine to protect against an antigenically divergent strain. The study described in chapter three determined the requirement for the highly conserved nsp7-10 replicase proteins and their proteolytic processing by the M^{pro} viral proteinase for efficient replication. This work contributes to the active field of SARS-CoV vaccine development and presents a new animal model for the study of improving vaccine efficacy in an aged population. In the case of the vaccine based on expressing SARS nucleocapsid as an antigen, it also demonstrates a previously undescribed enhanced inflammatory response.

SARS-CoV vaccines, senescent animal models, and a heterologous challenge virus

VRP vaccine vectors have been shown to induce robust mucosal and cellular immune responses against a large number of foreign antigens (40, 41), and in this work have been evaluated as candidate vaccines against SARS-CoV strains in young and senescent animals. Specifically, Venezuelan equine encephalitis virus replicon particles (VRP) expressing either the 2003 epidemic Urbani SARS-CoV strain spike glycoprotein (VRP-S) or nucleocapsid

protein (VRP-N) were tested for their ability to protect young and senescent mice challenged with homologous and heterologous strains of SARS-CoV.

Since the ideal SARS-CoV vaccine will provide long-term protection against emergent strains which might arise from their zoonotic hosts, the evaluation of candidate vaccines should include a challenge virus antigenically similar to newly emergent strains. However, SARS-CoV strain diversity was mostly confined to China where many human and animal isolates were not successfully cultured in vitro (195) and most available experimental strains are nearly identical and do not reflect natural diversity (156, 175). Fortunately, recent advances in synthetic biology allow researchers to reconstruct extinct viruses, or specific genes of those viruses, de novo from their nucleotide sequences (29, 105, 177). Using a comprehensive SARS-CoV genetic database (195, 224), we resurrected the divergent GDO3-S glycoprotein in the Urbani genetic backbone. The icGD03-S recombinant virus was identical to the molecular clone except for the presence of two mutations in S that likely evolved after transfection of full-length RNA and virus passage in Vero cells, similar to the cell culture adaptations reported in S for other SARS-CoV strains isolated from human clinical specimens and passaged in vitro (182). The icGDO3-S CoV's sequence divergence from Urbani, efficient in vitro replication in HAE and Vero cultures, and robust in vivo replication in the mouse model, make it an excellent heterologous challenge inoculum for vaccine studies. The amino acid sequence of the GD03 receptor binding domain (RBD) is found in many zoonotic isolates described in civets and raccoon dogs, supporting its use as a zoonotic model strain (195). Additionally, the reduced replication in human airway epithelial (HAE) cultures of icGDO3-S relative to the Urbani strain is consistent with the reduced pathogenesis noted in the GDO3 human case (35, 88, 195).

Our results were similar to those reported for other SARS-N–expressing DNA and vectored vaccines (20, 155): VRP-N did not protect mice from SARS-CoV replication, and no benefit to vaccination with a cocktail of both VRP-S and VRP-N was observed. We did note about a half-log reduction in viral titers within the lungs of some VRP-N–vaccinated mice, although this was only occasionally observed. Of course, any reduction in SARS-CoV titer can be interpreted as a positive aspect of a potential vaccine, given the relationship between viral titer and SARS disease severity (35, 88), but the increased number of lymphocytic and eosinophilic inflammatory infiltrates, which are also characteristic of the immune pathology observed with respiratory syncytial virus (RSV) infection following vaccination with formalin-inactivated RSV (43, 78), raises concerns that vaccination with N alone will not only fail to effectively protect against SARS-CoV replication, but may result in vaccine-enhanced pulmonary disease (102). This finding has particular significance for SARS-N and inactivated SARS-CoV vaccines currently under development that also induce anti-N antibody and T cell responses (104, 122, 170, 181, 192, 222, 233, 241). SARS-CoV N-induced pathology has not been previously reported, possibly because most studies examined lungs at 2–3 d post-infection, prior to the infiltration of inflammatory cells into the lung. VRP-N–induced pathology was clearly evident by day 4 and persisted for 1–2 weeks following wild-type virus challenge. The passive transfer of anti-N antibody did not contribute to inflammation and suggests that it is the activity of SARS-N–specific T cells in the absence of effective neutralizing anti–SARS-CoV antibody that mediates the adverse response. It is interesting that a T_h2–skewed cytokine profile is a hallmark of the RSV vaccine-enhanced disease, which raises the possibility that the N-specific immune response is skewed in a similar manner (95).

VRP-S alone provided long-term protection in animals when they were vaccinated young and suggests that a simple vaccine regimen could provide effective long-term protection in healthy individuals. The high level of protection conferred to young animals against icGDO3-S also suggests that an Urbani SARS-CoV S vaccine may effectively provide at least short-term protection against more divergent strains, such as newly emergent SARS-CoV. However, only limited protection was seen in vaccinated senescent animals, a limitation most likely due to immunosenescence and an ineffective anti-SARS-S response following vaccine administration (59, 84, 134, 139, 179, 239). The challenge of inducing a protective immune response in the elderly is not limited to developers of coronavirus vaccines and will likely involve utilizing techniques to induce stronger reactions from the senescent immune system to administered vaccines (60).

Consistent with previous work comparing the susceptibility of pseudotyped lentiviruses bearing the S glycoproteins of various SARS strains to neutralization by anti-S (Urbani) IgG (224), anti–VRP-S antibody demonstrated reduced neutralization of icGDO3-S relative to the vaccine strain. In spite of this, the VRP-S vaccine successfully provided short-term protection against the divergent virus, indicating that current vaccines may also provide protection from many zoonotic strains that might emerge in the future. Such cross protection has been observed among other vaccines, such as HA formulations for influenza virus (38) and VRP vaccines against norovirus (123). Vaccination of senescent animals produced significantly reduced antibody responses compared with younger mice, and when challenged with the heterologous icGDO3-S virus, protection was incomplete. However, any animal with a $PRNT_{80}$ value above 1:114 against icSARS showed reduced viral replication within the lungs following challenge with either the vaccine or icGDO3-S strains. As noted for the

homologous challenge studies, the combination of VRP-S+N did not enhance protection from heterologous challenge, but may actually have weakened it, with senescent animals showing even lower anti-S antibody responses and an even higher rate of viral replication, albeit with reduced titers, and increased lung pathology. One possible cause for vaccine failure is the emergence of an escape mutant in an environment of suboptimal neutralization. However, initial data comparing the neutralization susceptibility of viruses isolated from these mice to the challenge stock refute this conjecture (unpublished data). Reduced antibody responses have been described in immunosenescent mice and humans characterized by limited switching to secondary isotypes, lower antibody levels in general, and production of antibody with lower affinities (59, 84, 134, 139, 179, 239). Although we have not tested single-vaccine dose regimens, previous studies have demonstrated that these are efficacious against SARS-CoV challenge in young animals (99). Given the low antibody titers following boost in senescent populations, single-vaccine dose formulations will likely prove ineffective. Rather, improving the VRP-S efficacy in older vaccinees may require additional vaccine boosts, the use of adjuvants, or other additional therapies (60). Another likely contributing factor to vaccine failure in older animals was the resistance of icGDO3-S to neutralization relative to the vaccine strain, icSARS-CoV. At least three neutralizing sites have been identified in the SARS-CoV S glycoprotein, two of which map at the N-terminus and in the RBD of the S glycoprotein, and one to a weak third site near the carboxy-terminus of S. Given that most of the GD03 mutations map in and around the N-terminus and RBD in S1 (224), it is possible that either one or both of these critical epitopes are significantly different in icGD03-S, and likely explains the resistance to neutralization with antisera against Urbani-S.

Earlier work had indicated that antibodies to the Urbani strain of SARS-CoV enhanced the in vitro infectivity of pseudotyped viruses bearing the S glycoprotein of zoonotic strains, primarily with strains SZ16 and SZ3, and raised the specter of S-vaccine–induced complications with newly emergent strains (224). In contrast, it was shown that monoclonal, but not polyclonal, antibodies that neutralized the epidemic strain may enhance the infectivity of pseudotyped viruses bearing GD03-S glycoproteins, although the enhanced infection was marginal at best (224). Our research with antibody directed against Urbani-S indicated that the polyclonal antibody neutralized icGD03-S on Vero cells, although less efficiently than the vaccine strain, which is consistent with the previous report (224). Moreover, in the young and senescent mouse models, VRP-S–vaccinated animals challenged with homologous or heterologous icGD03-S recombinant viruses did not display vaccine-mediated enhancement of virus replication or enhanced pathology. Because VRP-S vaccines induce broad neutralizing antibody responses that likely target multiple epitopes across the S glycoprotein, it is possible that the noted enhancement of infectivity with monoclonal antibodies is nullified. Indeed, recent work showed that antibody specific for the RBD of Tor-2–S, GDO3–S, and SZ3–S glycoproteins did not reproduce enhanced infectivity in pseudotyped viruses bearing SZ3-S and identified conserved epitopes that allowed all three strains to be effectively neutralized, raising hope that a single vaccine could be effective against widely divergent strains of SARS-CoV (80). Of course, additional studies are needed with more heterologous strains in alternative animal models before the possibility of vaccine-induced enhancement of infection and pathology can be discounted.

Future Directions

Two areas of study currently being pursued involve the use of vaccine vectors expressing the S glycoproteins of different strains of SARS-CoV and the generation of new heterologous challenge strains. VRPs expressing the S of zoonotic strains such as GDO3 and SZ16 will be compared to the VRP expressing the Urbani glycoprotein for their ability to induce cross-neutralizing antibody responses. Studies employing a combination of multi-strain SARS-CoV S-antigens as well as multiple challenge strains have not been reported and are likely to make a significant contribution to the field by helping to determine an optimal vaccine design that provides the broadest level of protection. Additionally, a murine-adapted strain of SARS-CoV provides a lethal challenge virus that should provide increased sensitivity for comparing the efficacy of candidate vaccines.

Future work will also be devoted to evaluating whether changes in vaccine design or regimen will improve vaccine efficacy in senescent animals. Based on our work comparing the antibody responses to VRP-S in senescent mice, the vaccine's incomplete protection against icGDO3-S was likely due to insufficient response of the immune system to the S-antigen. The reduced ability of the anti-Urbani S antibody to neutralize the heterologous virus coupled with the reduced response to the vaccine were both likely contributors to the vaccine's limited success. This shortcoming might be overcome by inducing a more robust response from the senescent animals. The use of different vaccine vectors, vaccination with purified protein, adjuvants, killed virus vaccines, and variations in the number and scheduling of boosts are all components of the vaccine that can be tested for improved responses in senescent animals.

Our research provides a model for future experiments designed to characterize the components and inducers of the VRP-N–enhanced pulmonary inflammation. Experiments to characterize and compare the inflammatory infiltrates and cytokine profiles within the lungs of SARS-N, -S, and control vaccinated animals should provide insight into the immunological mechanisms underlying the different responses. It has been noted that a similar reaction in the murine model to RSV vaccines is the result of a Th2 skewed response in those animals. If the cellular components and cytokine profiles of the SARS-CoV N vaccine-induced immunopathology are consistent with this observation, the use of IL-4 knockout mice will be used to verify the connection between a T_h2-skewed response and the characteristic eosinophil-containing inflammation. SARS N vaccines in the hamster, ferret, and primate models in which pathology and clinical disease are more prominent following wild-type virus challenge will also be used to determine if similar immunopathology is limited to the murine model or demonstrable across multiple species.

MHV replicase protein processing in replication

The nsp7-10 of the coronavirus replicase polyprotein are highly conserved among the family coronaviridae (146). The details of their involvement in replication and RNA synthesis are largely unknown. This study used an infectious clone of MHV to define fundamental features of the nsp7-10 during viral replication in culture. Each of the four proteins appears to be critical for viral replication, since deletion of any of the four protein domains was lethal for RNA synthesis and productive virus infection. Furthermore, the results indicate that processing of the proteins from each other is necessary for replication,

with the one exception of the nsp9-10 cleavage site. Finally, we determined that rearranging two of the replicase proteins, nsp7 and nsp8, was not permissive for virus replication.

Only the nsp2 coronavirus replicase protein has been shown to be dispensable for replication in both MHV-A59 and SARS-CoV, although its omission is attenuating both in vitro and in vivo (70). Portions the carboxy-terminal half of MHV nsp1 has also been deleted in viable mutants (19), but otherwise, no full or partial deletions of replicase protein domains has been reported in viable mutants of any coronavirus. In contrast, deletion of each of the nsp7-10 resulted in a lethal phenotype as evidenced by the lack of recoverable viruses and an inability to detect subgenomic mRNAs by RT-PCR, suggesting that each of the nsp7-10 may be an indispensable component of the replication complex. Alternatively, deletion of nsp coding sequences may sufficiently alter the structure of the polyprotein template to interfere with M^{pro} accessibility to its cleavage sites. Interestingly, an MHV temperature sensitive mutant, LA6, contains a mutation in nsp10 that blocks processing of nsp4-10 at the non-permissive temperature suggesting that mutations or deletions at the c-terminus of ORF1a might disrupt M^{pro} activity (165).

Although it is known that global inhibition of coronavirus proteinases that process the replicase polyproteins prevents replication (103), the requirements for each of the 15 cleavage sites in the ORF1ab polyprotein are not completely determined. Cleavage of nsp1, nsp2 and nsp3 has been abolished in viable MHV mutants (46, 69). Otherwise, little is known of the requirements for processing, including nsp7-nsp10. Our results show that changes at cleavage sites between nsp6-7, nsp7-8, nsp8-9, and nsp10-11 were not replication viable. Lethality could be due to disruption of nsp7-10 proteolytic processing causing a failure of precursor, intermediate or mature protein function within the replication complex.

However, not all of the cleavage site mutants were nonviable. Based on genetic analysis, MHV has two functional nsp7-8 cleavage sites, LQ↓A and LQ↓S, and disruption of either of these potential sites failed to affect replication competence, cleavage patterns, or cellular localization *in vitro*. Interestingly, the LQ↓A site is conserved across all coronavirus families, while the second LQ↓S site is limited to group II coronaviruses, including MHV, BCoV, HKU1, and OC43, but not SARS-CoV. Wild-type replication efficiency when either one or the other site was knocked out suggests that either, or both, sites are cleaved during replication. Although we cannot detect any significant impact on in vitro replication, variations in N or C-terminal processing of nsp7-8 may influence in vivo pathogenesis or affect cell signaling pathways. However, simultaneous mutation of both sites was lethal, indicating that nsp7 and nsp8 must be fully separated to function in mRNA synthesis.

The only cleavage site that tolerated inactivation was the nsp9-10 cleavage site. The mutant MHV9/10 virus produced a fusion nsp9-10 protein and was highly attenuated in its replication efficiency. Serial passage of this virus restored near wild-type replication fitness, but did so without reverting at the mutated cleavage site or regaining the ability to process nsp9-10, demonstrating that efficient replication can be achieved without nsp9-10 proteolytic processing. The data demonstrate that with the exception of cleavage between the nsp9 and nsp10 proteins, M^{pro} processing of the nsp7-nsp10 are essential in coronavirus RNA transcription and replication.

Previous work has indicated that nsp7 and nsp8 in solution form a complex hexadecameric structure that is proposed to function in processivity and generation of RNA primers for the RNA replicase (89, 234). If these structures represent those seen in during infection, then formation of the structures would require cleavage of nsp7 from nsp8.

Similarly, the virus could not replicate when the relative positions of the genes encoding nsp7 and nsp8 were switched. This loss of viability could be due to an alteration of the precursor polyprotein that interfered with processing or prevented a distinct function associated with the uncleaved precursor. It is unclear why only the MHV9/10 mutant was viable. Nsp9 associates with the replication complex, interacting at least with nsp8 (191), and has been shown to possess single-stranded RNA binding affinity (11, 53, 191). Nsp10 is known to associate with several proteins of the replication complex, including nsp1, nsp5, nsp7, nsp8, and nsp12 (18, 19). Nsp10 has been shown to be critical for the formation of functional replication complexes (165), and has recently been shown to crystallize to form monomers and homodimers as well as a complex dodecameric structure when expressed as an nsp10-11 fusion (97, 187). It is puzzling why this critical protein with broad interactions with other replicase proteins would retain its function without full separation from nsp9. Interestingly, mutation of the nsp10-11 cleavage site was nonviable despite the report that the spherical structure formed by 12 units of nsp10 was crystallized as an nsp10-11 construct (187). Collectively, our data indicates that the C-terminal cleavage site for the nsp10 protein is essential for infectivity, raising doubt about the biological relevance of the reported nsp10-11 crystal structure (187).

Prior to this study, two viable cleavage mutants of coronaviruses had been reported, the PLP1-mediated cleavage sites between nsp1-nsp2 and nsp2-nsp3 were removed in MHV (46, 69). Loss of cleavage site function resulted in attenuated replication and suggested that efficient cleavage of nsp1-2 and nsp2-3 was important, but not required, for replication in tissue culture (46, 69). Indeed, viable mutant virus could be generated even when PLP1, which solely mediates nsp1-2 and nsp2-3 processing in MHV, was inactivated (69). With

this report, three cleavage sites in the MHV ORF1a polyprotein have been shown to be dispensable for replication: nsp1-2, nsp2-3 and nsp9-10 (46, 69). It is possible that this reflects the use of these proteins in natural precursors, such as has been reported for nsp2-3 and nsp4-10. Thus the engineered changes may reproduce some component of the normal lifecycle and at least residual function of these proteins. Interestingly, rearrangement of the nsp7 and nsp8 encoding sequences was lethal, a result that lends support to the idea that their may be an independent function in replication associated with the nsp4-10 precursor (165).

Future Directions

Although we have demonstrated that coronavirus replication depends upon the presence of the nsp7-10 coding sequences and, with one exception, their full processing by M^{pro}, there are still many aspects of the nsp7-10 proteins' role in replication that remain to be answered. One aspect of this research, defining the fundamental role that these small proteins play in coronavirus replication, will be advanced by introducing mutations across the proteins. By altering the amino acid sequence of the proteins their function may be perturbed to various degrees and allow us to determine a specific function in replication based on the point at which attenuation occurs.

The mutations which arose in MHVp15-1 and MHVp15-3 during serial passage of the highly attenuated MHV9/10 mutant may provide valuable insight into interactions between nsp9-10 and other components of the replicase proteins. Mutations that arise to offset the diminished replication efficiency as a result of inhibiting nsp9-10 processing could identify new interactions between individual proteins of the replication complex. Sequencing the genomes of MHVp15-1 and MHVp15-3 has been completed and the notable mutations

are listed in Table 6. These mutations are currently being added to the MHV infectious clone and will be used to generate recombinant viruses and allow us to determine the relative contributions each alteration makes to the MHV9/10 replication efficiency. The mutations in nsp3 and S are particularly attractive as they are present in both passage 15 isolates.

Other avenues of research are also available to further our understanding of the roles nsp7-10 play in coronavirus replication. Although processing of either of the sites at the nsp7-8 boundary permitted efficient in vitro growth, the MHV mouse model can be used to determine if use of both, or preferential use of a single site, has an effect in vivo. Furthermore, distinct roles in replication for both fully processed and precursor forms of the proteins could be identified by determining if lethal cleavage mutants can complement each other to form viable replication complexes. Of course, a system limiting the chance of simple rescue by recombination, such as through use of expression vectors or stable cell expression systems would need to be established; and not a trivial task given the notable instability of MHV replicase cDNA in *E. coli* plasmid amplification vectors. Still, such a system could allow us to determine the minimum unit of a functional replicase polyprotein required for trans rescue of a lethal mutant and identify the specific replicase precursor needed for efficient replication. Similar answers could be found with further use of the rearrangement mutants. Other combinations of rearrangements within the nsp4-10 polyprotein could provide evidence that subcomponents of the precursor are required thereby identifying a functional unit within the precursor protein.

The development of coronavirus reverse genetics systems has provided a valuable tool for aspects of applied and basic coronavirus research. Through use of the SARS-CoV

and MHV infectious clones, we have developed systems for the rigorous testing of candidate vaccines as well as for elucidating fundamental aspects of coronavirus biology. Although many questions remain to be answered, we have developed model systems with which we -- and other researchers -- can address them and continue to contribute to the development of anti-coronaviral therapies and expand our understanding of the viruses' complex replication strategy.

Table 6. Genomic variation between MHV, MHV9/10, MHVp15-1, and MHVp15-3.

Genome position (nt)	65-69	1628	3874	10428	13102	13164-5	16793	22741	26738	28607
Gene	5'UTR	nsp2	nsp3	nsp5	nsp9	nsp9	nsp13	ORF2a	S	ORF6
MHV		Met	His	Ser	Lys	Gln	Phe	Gln	Phe	Ser
MHV9/10	tctaa	Met	His	Ser	Lys	Ala	Phe	Gln	Phe	Ser
MHVp15-1	tctaa	Leu	**Leu**	Ser	Lys	Thr	Val	stop	**Tyr**	Ile
MHVp15-3	tctaa	Met	**Leu**	Gly	Arg	Ala	Phe	Gln	**Tyr**	Ser

References

1. **Almazan, F., M. L. Dediego, C. Galan, D. Escors, E. Alvarez, J. Ortego, I. Sola, S. Zuniga, S. Alonso, J. L. Moreno, A. Nogales, C. Capiscol, and L. Enjuanes.** 2006. Construction of a severe acute respiratory syndrome coronavirus infectious cDNA clone and a replicon to study coronavirus RNA synthesis. J Virol **80:**10900-6.

2. **Almazan, F., J. M. Gonzalez, Z. Penzes, A. Izeta, E. Calvo, J. Plana-Duran, and L. Enjuanes.** 2000. Engineering the largest RNA virus genome as an infectious bacterial artificial chromosome. Proc Natl Acad Sci U S A **97:**5516-21.

3. **Baric, R. S., K. Fu, W. Chen, and B. Yount.** 1995. High recombination and mutation rates in mouse hepatitis virus suggest that coronaviruses may be potentially important emerging viruses. Adv Exp Med Biol **380:**571-6.

4. **Baric, R. S., K. Fu, M. C. Schaad, and S. A. Stohlman.** 1990. Establishing a genetic recombination map for murine coronavirus strain A59 complementation groups. Virology **177:**646-56.

5. **Baric, R. S., E. Sullivan, L. Hensley, B. Yount, and W. Chen.** 1999. Persistent infection promotes cross-species transmissibility of mouse hepatitis virus. J Virol **73:**638-49.

6. **Baric, R. S., B. Yount, L. Hensley, S. A. Peel, and W. Chen.** 1997. Episodic evolution mediates interspecies transfer of a murine coronavirus. J Virol **71:**1946-55.

7. **Bhardwaj, K., L. Guarino, and C. C. Kao.** 2004. The severe acute respiratory syndrome coronavirus Nsp15 protein is an endoribonuclease that prefers manganese as a cofactor. J Virol **78:**12218-24.

8. **Biebricher, C. K., and M. Eigen.** 2006. What is a quasispecies? Curr Top Microbiol Immunol **299:**1-31.

9. **Bisht, H., A. Roberts, L. Vogel, A. Bukreyev, P. L. Collins, B. R. Murphy, K. Subbarao, and B. Moss.** 2004. Severe acute respiratory syndrome coronavirus spike protein expressed by attenuated vaccinia virus protectively immunizes mice. Proc Natl Acad Sci U S A **101:**6641-6.

10. **Bonilla, P. J., S. A. Hughes, J. D. Pinon, and S. R. Weiss.** 1995. Characterization of the leader papain-like proteinase of MHV-A59: identification of a new in vitro cleavage site. Virology **209:**489-97.

11. **Bost, A. G., R. H. Carnahan, X. T. Lu, and M. R. Denison.** 2000. Four proteins processed from the replicase gene polyprotein of mouse hepatitis virus colocalize in the cell periphery and adjacent to sites of virion assembly. J Virol **74:**3379-87.

12. **Bost, A. G., E. Prentice, and M. R. Denison.** 2001. Mouse hepatitis virus replicase protein complexes are translocated to sites of M protein accumulation in the ERGIC at late times of infection. Virology **285:**21-9.

13. **Brayton, P. R., M. M. Lai, C. D. Patton, and S. A. Stohlman.** 1982. Characterization of two RNA polymerase activities induced by mouse hepatitis virus. J Virol **42:**847-53.

14. **Bredenbeek, P. J., C. J. Pachuk, A. F. Noten, J. Charite, W. Luytjes, S. R. Weiss, and W. J. Spaan.** 1990. The primary structure and expression of the second open reading frame of the polymerase gene of the coronavirus MHV-A59; a highly conserved polymerase is expressed by an efficient ribosomal frameshifting mechanism. Nucleic Acids Res **18:**1825-32.

15. **Bridgen, A., M. Duarte, K. Tobler, H. Laude, and M. Ackermann.** 1993. Sequence determination of the nucleocapsid protein gene of the porcine epidemic diarrhoea virus confirms that this virus is a coronavirus related to human coronavirus 229E and porcine transmissible gastroenteritis virus. J Gen Virol **74 (Pt 9):**1795-804.

16. **Brierley, I., P. Digard, and S. C. Inglis.** 1989. Characterization of an efficient coronavirus ribosomal frameshifting signal: requirement for an RNA pseudoknot. Cell **57:**537-47.

17. **Britton, P., S. Evans, B. Dove, M. Davies, R. Casais, and D. Cavanagh.** 2005. Generation of a recombinant avian coronavirus infectious bronchitis virus using transient dominant selection. J Virol Methods **123:**203-11.

18. **Brockway, S. M., C. T. Clay, X. T. Lu, and M. R. Denison.** 2003. Characterization of the expression, intracellular localization, and replication complex association of the putative mouse hepatitis virus RNA-dependent RNA polymerase. J Virol **77:**10515-27.

19. **Brockway, S. M., X. T. Lu, T. R. Peters, T. S. Dermody, and M. R. Denison.** 2004. Intracellular localization and protein interactions of the gene 1 protein p28 during mouse hepatitis virus replication. J Virol **78:**11551-62.

20. **Buchholz, U. J., A. Bukreyev, L. Yang, E. W. Lamirande, B. R. Murphy, K. Subbarao, and P. L. Collins.** 2004. Contributions of the structural proteins of severe acute respiratory syndrome coronavirus to protective immunity. Proc Natl Acad Sci U S A **101:**9804-9.

21. **Bukreyev, A., E. W. Lamirande, U. J. Buchholz, L. N. Vogel, W. R. Elkins, M. St Claire, B. R. Murphy, K. Subbarao, and P. L. Collins.** 2004. Mucosal immunisation of African green monkeys (Cercopithecus aethiops) with an attenuated parainfluenza virus expressing the SARS coronavirus spike protein for the prevention of SARS. Lancet **363:**2122-7.

22. **Campanacci, V., M. P. Egloff, S. Longhi, F. Ferron, C. Rancurel, A. Salomoni, C. Durousseau, F. Tocque, N. Bremond, J. C. Dobbe, E. J. Snijder, B. Canard, and C. Cambillau.** 2003. Structural genomics of the SARS coronavirus: cloning, expression, crystallization and preliminary crystallographic study of the Nsp9 protein. Acta Crystallogr D Biol Crystallogr **59:**1628-31.

23. **Casais, R., B. Dove, D. Cavanagh, and P. Britton.** 2003. Recombinant avian infectious bronchitis virus expressing a heterologous spike gene demonstrates that the spike protein is a determinant of cell tropism. J Virol **77:**9084-9.

24. **Casais, R., V. Thiel, S. G. Siddell, D. Cavanagh, and P. Britton.** 2001. Reverse genetics system for the avian coronavirus infectious bronchitis virus. J Virol **75:**12359-69.

25. **Cavanagh, D.** 2005. Coronaviruses in poultry and other birds. Avian Pathol **34:**439-48.

26. **Cavanagh, D., P. Davis, J. Cook, and D. Li.** 1990. Molecular basis of the variation exhibited by avian infectious bronchitis coronavirus (IBV). Adv Exp Med Biol **276:**369-72.

27. **(CDC), C. f. D. C. a. P.** 1995. From the Centers for Disease Control and Prevention. Pneumonia and influenza death rates--United States, 1979-1994. Jama **274:**532.

28. **(CDC), C. f. D. C. a. P.** 2003. Prevalence of IgG antibody to SARS-associated coronavirus in animal traders--Guangdong Province, China, 2003. MMWR Morb Mortal Wkly Rep **52:**986-7.

29. **Cello, J., A. V. Paul, and E. Wimmer.** 2002. Chemical synthesis of poliovirus cDNA: generation of infectious virus in the absence of natural template. Science **297:**1016-8.

30. **Chen, W., and R. S. Baric.** 1996. Molecular anatomy of mouse hepatitis virus persistence: coevolution of increased host cell resistance and virus virulence. J Virol **70:**3947-60.

31. **Chen, Z., L. Zhang, C. Qin, L. Ba, C. E. Yi, F. Zhang, Q. Wei, T. He, W. Yu, J. Yu, H. Gao, X. Tu, A. Gettie, M. Farzan, K. Y. Yuen, and D. D. Ho.** 2005. Recombinant modified vaccinia virus Ankara expressing the spike glycoprotein of severe acute respiratory syndrome coronavirus induces protective neutralizing antibodies primarily targeting the receptor binding region. J Virol **79:**2678-88.

32. **Cheng, A., W. Zhang, Y. Xie, W. Jiang, E. Arnold, S. G. Sarafianos, and J. Ding.** 2005. Expression, purification, and characterization of SARS coronavirus RNA polymerase. Virology **335:**165-76.

33. **Chenna, R., H. Sugawara, T. Koike, R. Lopez, T. J. Gibson, D. G. Higgins, and J. D. Thompson.** 2003. Multiple sequence alignment with the Clustal series of programs. Nucleic Acids Res **31:**3497-500.

34. **Chou, T. H., S. Wang, P. V. Sakhatskyy, I. Mboudoudjeck, J. M. Lawrence, S. Huang, S. Coley, B. Yang, J. Li, Q. Zhu, and S. Lu.** 2005. Epitope mapping and biological function analysis of antibodies produced by immunization of mice with an inactivated Chinese isolate of severe acute respiratory syndrome-associated coronavirus (SARS-CoV). Virology **334:**134-43.

35. **Chu, C. M., L. L. Poon, V. C. Cheng, K. S. Chan, I. F. Hung, M. M. Wong, K. H. Chan, W. S. Leung, B. S. Tang, V. L. Chan, W. L. Ng, T. C. Sim, P. W. Ng, K. I. Law, D. M. Tse, J. S. Peiris, and K. Y. Yuen.** 2004. Initial viral load and the outcomes of SARS. Cmaj **171:**1349-52.

36. **Coley, S. E., E. Lavi, S. G. Sawicki, L. Fu, B. Schelle, N. Karl, S. G. Siddell, and V. Thiel.** 2005. Recombinant mouse hepatitis virus strain A59 from cloned, full-length cDNA replicates to high titers in vitro and is fully pathogenic in vivo. J Virol **79:**3097-106.

37. **Compton, S. R., C. B. Stephensen, S. W. Snyder, D. G. Weismiller, and K. V. Holmes.** 1992. Coronavirus species specificity: murine coronavirus binds to a mouse-specific epitope on its carcinoembryonic antigen-related receptor glycoprotein. J Virol **66:**7420-8.

38. **Couch, R. B.** 2003. An overview of serum antibody responses to influenza virus antigens. Dev Biol (Basel) **115:**25-30.

39. **Cowley, J. A., C. M. Dimmock, K. M. Spann, and P. J. Walker.** 2000. Gill-associated virus of Penaeus monodon prawns: an invertebrate virus with ORF1a and ORF1b genes related to arteri- and coronaviruses. J Gen Virol **81:**1473-84.

40. **Davis, N. L., I. J. Caley, K. W. Brown, M. R. Betts, D. M. Irlbeck, K. M. McGrath, M. J. Connell, D. C. Montefiori, J. A. Frelinger, R. Swanstrom, P. R. Johnson, and R. E. Johnston.** 2000. Vaccination of macaques against pathogenic simian immunodeficiency virus with Venezuelan equine encephalitis virus replicon particles. J Virol **74:**371-8.

41. **Davis, N. L., A. West, E. Reap, G. MacDonald, M. Collier, S. Dryga, M. Maughan, M. Connell, C. Walker, K. McGrath, C. Cecil, L. H. Ping, J. Frelinger, R. Olmsted, P. Keith, R. Swanstrom, C. Williamson, P. Johnson, D. Montefiori, and R. E. Johnston.** 2002. Alphavirus replicon particles as candidate HIV vaccines. IUBMB Life **53:**209-11.

42. **de Haan, C. A., P. S. Masters, X. Shen, S. Weiss, and P. J. Rottier.** 2002. The group-specific murine coronavirus genes are not essential, but their deletion, by reverse genetics, is attenuating in the natural host. Virology **296:**177-89.

43. **De Swart, R. L., T. Kuiken, H. H. Timmerman, G. van Amerongen, B. G. Van Den Hoogen, H. W. Vos, H. J. Neijens, A. C. Andeweg, and A. D. Osterhaus.** 2002. Immunization of macaques with formalin-inactivated respiratory syncytial virus (RSV) induces interleukin-13-associated hypersensitivity to subsequent RSV infection. J Virol **76:**11561-9.

44. **Delmas, B., J. Gelfi, R. L'Haridon, L. K. Vogel, H. Sjostrom, O. Noren, and H. Laude.** 1992. Aminopeptidase N is a major receptor for the entero-pathogenic coronavirus TGEV. Nature **357:**417-20.

45. **Denison, M. R., J. C. Kim, and T. Ross.** 1995. Inhibition of coronavirus MHV-A59 replication by proteinase inhibitors. Adv Exp Med Biol **380:**391-7.

46. **Denison, M. R., B. Yount, S. M. Brockway, R. L. Graham, A. C. Sims, X. Lu, and R. S. Baric.** 2004. Cleavage between replicase proteins p28 and p65 of mouse hepatitis virus is not required for virus replication. J Virol **78:**5957-65.

47. **Dennis, D. E., and D. A. Brian.** 1982. RNA-dependent RNA polymerase activity in coronavirus- infected cells. J Virol **42:**153-64.

48. **Draker, R., R. L. Roper, M. Petric, and R. Tellier.** 2006. The complete sequence of the bovine torovirus genome. Virus Res **115:**56-68.

49. **Drosten, C., S. Gunther, W. Preiser, S. van der Werf, H. R. Brodt, S. Becker, H. Rabenau, M. Panning, L. Kolesnikova, R. A. Fouchier, A. Berger, A. M. Burguiere, J. Cinatl, M. Eickmann, N. Escriou, K. Grywna, S. Kramme, J. C. Manuguerra, S. Muller, V. Rickerts, M. Sturmer, S. Vieth, H. D. Klenk, A. D. Osterhaus, H. Schmitz, and H. W. Doerr.** 2003. Identification of a novel coronavirus in patients with severe acute respiratory syndrome. N Engl J Med **348:**1967-76.

50. **Duan, J., X. Yan, X. Guo, W. Cao, W. Han, C. Qi, J. Feng, D. Yang, G. Gao, and G. Jin.** 2005. A human SARS-CoV neutralizing antibody against epitope on S2 protein. Biochemical and Biophysical Research Communications **333:**186-193.

51. **Duarte, M., and H. Laude.** 1994. Sequence of the spike protein of the porcine epidemic diarrhoea virus. J Gen Virol **75 (Pt 5):**1195-200.

52. **Dveksler, G. S., M. N. Pensiero, C. B. Cardellichio, R. K. Williams, G. S. Jiang, K. V. Holmes, and C. W. Dieffenbach.** 1991. Cloning of the mouse hepatitis virus (MHV) receptor: expression in human and hamster cell lines confers susceptibility to MHV. J Virol **65:**6881-91.

53. **Egloff, M. P., F. Ferron, V. Campanacci, S. Longhi, C. Rancurel, H. Dutartre, E. J. Snijder, A. E. Gorbalenya, C. Cambillau, and B. Canard.** 2004. The severe acute respiratory syndrome-coronavirus replicative protein nsp9 is a single-stranded RNA-binding subunit unique in the RNA virus world. Proc Natl Acad Sci U S A **101:**3792-6.

54. **Erles, K., C. Toomey, H. W. Brooks, and J. Brownlie.** 2003. Detection of a group 2 coronavirus in dogs with canine infectious respiratory disease. Virology **310:**216-23.

55. **Esper, F., C. Weibel, D. Ferguson, M. L. Landry, and J. S. Kahn.** 2005. Evidence of a novel human coronavirus that is associated with respiratory tract disease in infants and young children. J Infect Dis **191:**492-8.

56. **Faber, M., E. W. Lamirande, A. Roberts, A. B. Rice, H. Koprowski, B. Dietzschold, and M. J. Schnell.** 2005. A single immunization with a rhabdovirus-based vector expressing severe acute respiratory syndrome coronavirus (SARS-CoV) S protein results in the production of high levels of SARS-CoV-neutralizing antibodies. J Gen Virol **86:**1435-40.

57. **Fischer, F., D. Peng, S. T. Hingley, S. R. Weiss, and P. S. Masters.** 1997. The internal open reading frame within the nucleocapsid gene of mouse hepatitis virus encodes a structural protein that is not essential for viral replication. J Virol **71:**996-1003.

58. **Fouchier, R. A., N. G. Hartwig, T. M. Bestebroer, B. Niemeyer, J. C. de Jong, J. H. Simon, and A. D. Osterhaus.** 2004. A previously undescribed coronavirus associated with respiratory disease in humans. Proc Natl Acad Sci U S A **101:**6212-6.

59. **Frasca, D., R. L. Riley, and B. B. Blomberg.** 2005. Humoral immune response and B-cell functions including immunoglobulin class switch are downregulated in aged mice and humans. Semin Immunol **17:**378-84.

60. **Frech, S. A., R. T. Kenney, C. A. Spyr, H. Lazar, J.-F. Viret, C. Herzog, R. Gluck, and G. M. Glenn.** 2005. Improved immune responses to influenza vaccination in the elderly using an immunostimulant patch. Vaccine **23:**946-950.

61. **Fu, K., and R. S. Baric.** 1992. Evidence for variable rates of recombination in the MHV genome. Virology **189:**88-102.

62. **Fu, K., and R. S. Baric.** 1994. Map locations of mouse hepatitis virus temperature-sensitive mutants: confirmation of variable rates of recombination. J Virol **68:**7458-66.

63. **Gallagher, T. M., M. J. Buchmeier, and S. Perlman.** 1992. Cell receptor-independent infection by a neurotropic murine coronavirus. Virology **191:**517-22.

64. **Goebel, S. J., J. Taylor, and P. S. Masters.** 2004. The 3' cis-acting genomic replication element of the severe acute respiratory syndrome coronavirus can function in the murine coronavirus genome. J Virol **78:**7846-51.

65. **Gorbalenya, A. E., A. P. Donchenko, V. M. Blinov, and E. V. Koonin.** 1989. Cysteine proteases of positive strand RNA viruses and chymotrypsin-like serine proteases. A distinct protein superfamily with a common structural fold. FEBS Lett **243:**103-14.

66. **Gorbalenya, A. E., L. Enjuanes, J. Ziebuhr, and E. J. Snijder.** 2006. Nidovirales: evolving the largest RNA virus genome. Virus Res **117:**17-37.

67. **Gorbalenya, A. E., E. V. Koonin, A. P. Donchenko, and V. M. Blinov.** 1989. Coronavirus genome: prediction of putative functional domains in the non-structural polyprotein by comparative amino acid sequence analysis. Nucleic Acids Res **17:**4847-61.

68. **Gosert, R., A. Kanjanahaluethai, D. Egger, K. Bienz, and S. C. Baker.** 2002. RNA replication of mouse hepatitis virus takes place at double-membrane vesicles. J Virol **76:**3697-708.

69. **Graham, R. L., and M. R. Denison.** 2006. Replication of murine hepatitis virus is regulated by papain-like proteinase 1 processing of nonstructural proteins 1, 2, and 3. J Virol **80:**11610-20.

70. **Graham, R. L., A. C. Sims, S. M. Brockway, R. S. Baric, and M. R. Denison.** 2005. The nsp2 replicase proteins of murine hepatitis virus and severe acute respiratory syndrome coronavirus are dispensable for viral replication. J Virol **79:**13399-411.

71. **Greenough, T. C., G. J. Babcock, A. Roberts, H. J. Hernandez, W. D. Thomas, Jr., J. A. Coccia, R. F. Graziano, M. Srinivasan, I. Lowy, R. W. Finberg, K. Subbarao, L. Vogel, M. Somasundaran, K. Luzuriaga, J. L. Sullivan, and D. M. Ambrosino.** 2005. Development and characterization of a severe acute respiratory syndrome-associated coronavirus-neutralizing human monoclonal antibody that provides effective immunoprophylaxis in mice. J Infect Dis **191:**507-14.

72. **Guan, Y., B. J. Zheng, Y. Q. He, X. L. Liu, Z. X. Zhuang, C. L. Cheung, S. W. Luo, P. H. Li, L. J. Zhang, Y. J. Guan, K. M. Butt, K. L. Wong, K. W. Chan, W. Lim, K. F. Shortridge, K. Y. Yuen, J. S. Peiris, and L. L. Poon.** 2003. Isolation and characterization of viruses related to the SARS coronavirus from animals in southern China. Science **302:**276-8.

73. **Haijema, B. J., H. Volders, and P. J. Rottier.** 2004. Live, attenuated coronavirus vaccines through the directed deletion of group-specific genes provide protection against feline infectious peritonitis. J Virol **78:**3863-71.

74. **Haijema, B. J., H. Volders, and P. J. Rottier.** 2003. Switching species tropism: an effective way to manipulate the feline coronavirus genome. J Virol **77:**4528-38.

75. **Hamre D, P. J.** 1966. A new virus isolated from the human respiratory tract. Proc Soc Exp Biol Med **121:**190-193.

76. **Han, M. G., D. S. Cheon, X. Zhang, and L. J. Saif.** 2006. Cross-protection in gnotobiotic calves between a human enteric coronavirus and a virulent bovine enteric coronavirus. J Virol **80:**12350-6.

77. **Han, Y., H. Geng, W. Feng, X. Tang, A. Ou, Y. Lao, Y. Xu, H. Lin, H. Liu, and Y. Li.** 2003. A follow-up study of 69 discharged SARS patients. J Tradit Chin Med **23:**214-7.

78. **Hancock, G. E., D. J. Speelman, K. Heers, E. Bortell, J. Smith, and C. Cosco.** 1996. Generation of atypical pulmonary inflammatory responses in BALB/c mice after immunization with the native attachment (G) glycoprotein of respiratory syncytial virus. J Virol **70:**7783-91.

79. **Harcourt, B. H., D. Jukneliene, A. Kanjanahaluethai, J. Bechill, K. M. Severson, C. M. Smith, P. A. Rota, and S. C. Baker.** 2004. Identification of severe acute respiratory syndrome coronavirus replicase products and characterization of papain-like protease activity. J Virol **78:**13600-12.

80. **He, Y., J. Li, W. Li, S. Lustigman, M. Farzan, and S. Jiang.** 2006. Cross-neutralization of human and palm civet severe acute respiratory syndrome coronaviruses by antibodies targeting the receptor-binding domain of spike protein. J Immunol **176:**6085-92.

81. **He, Y., Y. Zhou, P. Siddiqui, and S. Jiang.** 2004. Inactivated SARS-CoV vaccine elicits high titers of spike protein-specific antibodies that block receptor binding and virus entry. Biochem Biophys Res Commun **325:**445-52.

82. **He, Y., Q. Zhu, S. Liu, Y. Zhou, B. Yang, J. Li, and S. Jiang.** 2005. Identification of a critical neutralization determinant of severe acute respiratory syndrome (SARS)-associated coronavirus: importance for designing SARS vaccines. Virology **334:**74-82.

83. **Heise, M. T., D. A. Simpson, and R. E. Johnston.** 2000. A single amino acid change in nsP1 attenuates neurovirulence of the Sindbis-group alphavirus S.A.AR86. J Virol **74:**4207-13.

84. **Herrera, E., A. C. Martinez, and M. A. Blasco.** 2000. Impaired germinal center reaction in mice with short telomeres. Embo J **19:**472-81.

85. **Herrewegh, A. A., I. Smeenk, M. C. Horzinek, P. J. Rottier, and R. J. de Groot.** 1998. Feline coronavirus type II strains 79-1683 and 79-1146 originate from a double recombination between feline coronavirus type I and canine coronavirus. J Virol **72:**4508-14.

86. **Holland, J. J.** 2006. Transitions in understanding of RNA viruses: a historical perspective. Curr Top Microbiol Immunol **299:**371-401.

87. **Huelsenbeck, J. P., and F. Ronquist.** 2001. MRBAYES: Bayesian inference of phylogenetic trees. Bioinformatics **17:**754-5.

88. **Hung, I. F., V. C. Cheng, A. K. Wu, B. S. Tang, K. H. Chan, C. M. Chu, M. M. Wong, W. T. Hui, L. L. Poon, D. M. Tse, K. S. Chan, P. C. Woo, S. K. Lau, J. S. Peiris, and K. Y. Yuen.** 2004. Viral loads in clinical specimens and SARS manifestations. Emerg Infect Dis **10:**1550-7.

89. **Imbert, I., J. C. Guillemot, J. M. Bourhis, C. Bussetta, B. Coutard, M. P. Egloff, F. Ferron, A. E. Gorbalenya, and B. Canard.** 2006. A second, non-canonical RNA-dependent RNA polymerase in SARS Coronavirus. Embo J **25:**4933-42.

90. **Ishii, K., H. Hasegawa, N. Nagata, T. Mizutani, S. Morikawa, T. Suzuki, F. Taguchi, M. Tashiro, T. Takemori, T. Miyamura, and Y. Tsunetsugu-Yokota.** 2006. Induction of protective immunity against severe acute respiratory syndrome coronavirus (SARS-CoV) infection using highly attenuated recombinant vaccinia virus DIs. Virology **351:**368-80.

91. **Ivanov, K. A., T. Hertzig, M. Rozanov, S. Bayer, V. Thiel, A. E. Gorbalenya, and J. Ziebuhr.** 2004. Major genetic marker of nidoviruses encodes a replicative endoribonuclease. Proc Natl Acad Sci U S A **101:**12694-9.

92. **Ivanov, K. A., V. Thiel, J. C. Dobbe, Y. van der Meer, E. J. Snijder, and J. Ziebuhr.** 2004. Multiple enzymatic activities associated with severe acute respiratory syndrome coronavirus helicase. J Virol **78:**5619-32.

93. **Ivanov, K. A., and J. Ziebuhr.** 2004. Human coronavirus 229E nonstructural protein 13: characterization of duplex-unwinding, nucleoside triphosphatase, and RNA 5'-triphosphatase activities. J Virol **78:**7833-8.

94. **Jia, W., K. Karaca, C. R. Parrish, and S. A. Naqi.** 1995. A novel variant of avian infectious bronchitis virus resulting from recombination among three different strains. Arch Virol **140:**259-71.

95. **Johnson, T. R., S. M. Varga, T. J. Braciale, and B. S. Graham.** 2004. Vbeta14(+) T cells mediate the vaccine-enhanced disease induced by immunization with respiratory syncytial virus (RSV) G glycoprotein but not with formalin-inactivated RSV. J Virol **78:**8753-60.

96. **Jones, D. T., W. R. Taylor, and J. M. Thornton.** 1992. The rapid generation of mutation data matrices from protein sequences. Comput Appl Biosci **8:**275-82.

97. **Joseph, J. S., K. S. Saikatendu, V. Subramanian, B. W. Neuman, A. Brooun, M. Griffith, K. Moy, M. K. Yadav, J. Velasquez, M. J. Buchmeier, R. C. Stevens, and P. Kuhn.** 2006. Crystal structure of nonstructural protein 10 from the severe acute respiratory syndrome coronavirus reveals a novel fold with two zinc-binding motifs. J Virol **80:**7894-901.

98. **Kan, B., M. Wang, H. Jing, H. Xu, X. Jiang, M. Yan, W. Liang, H. Zheng, K. Wan, Q. Liu, B. Cui, Y. Xu, E. Zhang, H. Wang, J. Ye, G. Li, M. Li, Z. Cui, X. Qi, K. Chen, L. Du, K. Gao, Y. T. Zhao, X. Z. Zou, Y. J. Feng, Y. F. Gao, R. Hai, D. Yu, Y. Guan, and J. Xu.** 2005. Molecular evolution analysis and geographic investigation of severe acute respiratory syndrome coronavirus-like virus in palm civets at an animal market and on farms. J Virol **79:**11892-900.

99. **Kapadia, S. U., J. K. Rose, E. Lamirande, L. Vogel, K. Subbarao, and A. Roberts.** 2005. Long-term protection from SARS coronavirus infection conferred by a single immunization with an attenuated VSV-based vaccine. Virology **340:**174-82.

100. **Keck, J. G., G. K. Matsushima, S. Makino, J. O. Fleming, D. M. Vannier, S. A. Stohlman, and M. M. Lai.** 1988. In vivo RNA-RNA recombination of coronavirus in mouse brain. J Virol **62:**1810-3.

101. **Keng, C. T., A. Zhang, S. Shen, K. M. Lip, B. C. Fielding, T. H. Tan, C. F. Chou, C. B. Loh, S. Wang, J. Fu, X. Yang, S. G. Lim, W. Hong, and Y. J. Tan.** 2005. Amino acids 1055 to 1192 in the S2 region of severe acute respiratory syndrome coronavirus S protein induce neutralizing antibodies: implications for the development of vaccines and antiviral agents. J Virol **79:**3289-96.

102. **Kim, H. W., J. G. Canchola, C. D. Brandt, G. Pyles, R. M. Chanock, K. Jensen, and R. H. Parrott.** 1969. Respiratory syncytial virus disease in infants despite prior administration of antigenic inactivated vaccine. Am J Epidemiol **89:**422-34.

103. **Kim, J. C., R. A. Spence, P. F. Currier, X. Lu, and M. R. Denison.** 1995. Coronavirus protein processing and RNA synthesis is inhibited by the cysteine proteinase inhibitor E64d. Virology **208:**1-8.

104. **Kim, T. W., J. H. Lee, C. F. Hung, S. Peng, R. Roden, M. C. Wang, R. Viscidi, Y. C. Tsai, L. He, P. J. Chen, D. A. Boyd, and T. C. Wu.** 2004. Generation and

characterization of DNA vaccines targeting the nucleocapsid protein of severe acute respiratory syndrome coronavirus. J Virol **78:**4638-45.

105. **Kobasa, D., A. Takada, K. Shinya, M. Hatta, P. Halfmann, S. Theriault, H. Suzuki, H. Nishimura, K. Mitamura, N. Sugaya, T. Usui, T. Murata, Y. Maeda, S. Watanabe, M. Suresh, T. Suzuki, Y. Suzuki, H. Feldmann, and Y. Kawaoka.** 2004. Enhanced virulence of influenza A viruses with the haemagglutinin of the 1918 pandemic virus. Nature **431:**703-7.

106. **Kottier, S. A., D. Cavanagh, and P. Britton.** 1995. Experimental evidence of recombination in coronavirus infectious bronchitis virus. Virology **213:**569-80.

107. **Ksiazek, T. G., D. Erdman, C. S. Goldsmith, S. R. Zaki, T. Peret, S. Emery, S. Tong, C. Urbani, J. A. Comer, W. Lim, P. E. Rollin, S. F. Dowell, A. E. Ling, C. D. Humphrey, W. J. Shieh, J. Guarner, C. D. Paddock, P. Rota, B. Fields, J. DeRisi, J. Y. Yang, N. Cox, J. M. Hughes, J. W. LeDuc, W. J. Bellini, and L. J. Anderson.** 2003. A novel coronavirus associated with severe acute respiratory syndrome. N Engl J Med **348:**1953-66.

108. **Kuiken, T., R. Fouchier, G. Rimmelzwaan, and A. Osterhaus.** 2003. Emerging viral infections in a rapidly changing world. Curr Opin Biotechnol **14:**641-6.

109. **Kuo, L., G. J. Godeke, M. J. Raamsman, P. S. Masters, and P. J. Rottier.** 2000. Retargeting of coronavirus by substitution of the spike glycoprotein ectodomain: crossing the host cell species barrier. J Virol **74:**1393-406.

110. **Kusters, J. G., E. J. Jager, H. G. Niesters, and B. A. van der Zeijst.** 1990. Sequence evidence for RNA recombination in field isolates of avian coronavirus infectious bronchitis virus. Vaccine **8:**605-8.

111. **Lai, M. M., R. S. Baric, S. Makino, J. G. Keck, J. Egbert, J. L. Leibowitz, and S. A. Stohlman.** 1985. Recombination between nonsegmented RNA genomes of murine coronaviruses. J Virol **56:**449-56.

112. **Lassnig, C., A. Kolb, B. Strobl, L. Enjuanes, and M. Muller.** 2005. Studying human pathogens in animal models: fine tuning the humanized mouse. Transgenic Res **14:**803-6.

113. **Lau, S. K., P. C. Woo, K. S. Li, Y. Huang, H. W. Tsoi, B. H. Wong, S. S. Wong, S. Y. Leung, K. H. Chan, and K. Y. Yuen.** 2005. Severe acute respiratory syndrome coronavirus-like virus in Chinese horseshoe bats. Proc Natl Acad Sci U S A **102:**14040-14045.

114. **Lee, C. W., and M. W. Jackwood.** 2000. Evidence of genetic diversity generated by recombination among avian coronavirus IBV. Arch Virol **145:**2135-48.

115. **Lee, C. W., and M. W. Jackwood.** 2001. Spike gene analysis of the DE072 strain of infectious bronchitis virus: origin and evolution. Virus Genes **22:**85-91.

116. **Lee, H. J., C. K. Shieh, A. E. Gorbalenya, E. V. Koonin, N. La Monica, J. Tuler, A. Bagdzhadzhyan, and M. M. Lai.** 1991. The complete sequence (22 kilobases) of murine coronavirus gene 1 encoding the putative proteases and RNA polymerase. Virology **180:**567-82.

117. **Levis, R., C. B. Cardellichio, C. A. Scanga, S. R. Compton, and K. V. Holmes.** 1995. Multiple receptor-dependent steps determine the species specificity of HCV-229E infection. Adv Exp Med Biol **380:**337-43.

118. **Li, W., Z. Shi, M. Yu, W. Ren, C. Smith, J. H. Epstein, H. Wang, G. Crameri, Z. Hu, H. Zhang, J. Zhang, J. McEachern, H. Field, P. Daszak, B. T. Eaton, S. Zhang, and L. F. Wang.** 2005. Bats are natural reservoirs of SARS-like coronaviruses. Science **310:**676-9.

119. **Li, W., C. Zhang, J. Sui, J. H. Kuhn, M. J. Moore, S. Luo, S. K. Wong, I. C. Huang, K. Xu, N. Vasilieva, A. Murakami, Y. He, W. A. Marasco, Y. Guan, H. Choe, and M. Farzan.** 2005. Receptor and viral determinants of SARS-coronavirus adaptation to human ACE2. Embo J **24:**1634-43.

120. **Liang, P. H.** 2006. Characterization and inhibition of SARS-coronavirus main protease. Curr Top Med Chem **6:**361-76.

121. **Liu, L., S. Hagglund, M. Hakhverdyan, S. Alenius, L. E. Larsen, and S. Belak.** 2006. Molecular epidemiology of bovine coronavirus on the basis of comparative analyses of the S gene. J Clin Microbiol **44:**957-60.

122. **Liu, S. J., C. H. Leng, S. P. Lien, H. Y. Chi, C. Y. Huang, C. L. Lin, W. C. Lian, C. J. Chen, S. L. Hsieh, and P. Chong.** 2006. Immunological characterizations of the nucleocapsid protein based SARS vaccine candidates. Vaccine **24:**3100-8.

123. **LoBue, A. D., L. Lindesmith, B. Yount, P. R. Harrington, J. M. Thompson, R. E. Johnston, C. L. Moe, and R. S. Baric.** 2006. Multivalent norovirus vaccines induce strong mucosal and systemic blocking antibodies against multiple strains. Vaccine **24:**5220-34.

124. **Louz, D., H. E. Bergmans, B. P. Loos, and R. C. Hoeben.** 2005. Cross-species transfer of viruses: implications for the use of viral vectors in biomedical research, gene therapy and as live-virus vaccines. J Gene Med **7:**1263-74.

125. **Lu, X., Y. Lu, and M. R. Denison.** 1996. Intracellular and in vitro-translated 27-kDa proteins contain the 3C-like proteinase activity of the coronavirus MHV-A59. Virology **222:**375-82.

126. **Lu, X. T., A. C. Sims, and M. R. Denison.** 1998. Mouse hepatitis virus 3C-like protease cleaves a 22-kilodalton protein from the open reading frame 1a polyprotein in virus-infected cells and in vitro. J Virol **72:**2265-71.

127. **Lu, Y., X. Lu, and M. R. Denison.** 1995. Identification and characterization of a serine-like proteinase of the murine coronavirus MHV-A59. J Virol **69:**3554-9.

128. **Majhdi, F., H. C. Minocha, and S. Kapil.** 1997. Isolation and characterization of a coronavirus from elk calves with diarrhea. J Clin Microbiol **35:**2937-42.

129. **Makino, S., J. G. Keck, S. A. Stohlman, and M. M. Lai.** 1986. High-frequency RNA recombination of murine coronaviruses. J Virol **57:**729-37.

130. **Manrubia, S. C., C. Escarmis, E. Domingo, and E. Lazaro.** 2005. High mutation rates, bottlenecks, and robustness of RNA viral quasispecies. Gene **347:**273-82.

131. **Masters, P. S.** 2006. The molecular biology of coronaviruses. Adv Virus Res **66:**193-292.

132. **Masters, P. S., and P. J. Rottier.** 2005. Coronavirus reverse genetics by targeted RNA recombination. Curr Top Microbiol Immunol **287:**133-59.

133. **Matthes, N., J. R. Mesters, B. Coutard, B. Canard, E. J. Snijder, R. Moll, and R. Hilgenfeld.** 2006. The non-structural protein Nsp10 of mouse hepatitis virus binds zinc ions and nucleic acids. FEBS Lett **580:**4143-9.

134. **McElhaney, J. E.** 2005. The unmet need in the elderly: Designing new influenza vaccines for older adults. Vaccine **23:**S10-S25.

135. **McIntosh, K., J. H. Dees, W. B. Becker, A. Z. Kapikian, and R. M. Chanock.** 1967. Recovery in tracheal organ cultures of novel viruses from patients with respiratory disease. Proc Natl Acad Sci U S A **57:**933-40.

136. **Meulenberg, J. J., J. N. Bos-de Ruijter, R. van de Graaf, G. Wensvoort, and R. J. Moormann.** 1998. Infectious transcripts from cloned genome-length cDNA of porcine reproductive and respiratory syndrome virus. J Virol **72:**380-7.

137. **Minskaia, E., T. Hertzig, A. E. Gorbalenya, V. Campanacci, C. Cambillau, B. Canard, and J. Ziebuhr.** 2006. Discovery of an RNA virus 3'->5' exoribonuclease that is critically involved in coronavirus RNA synthesis. Proc Natl Acad Sci U S A **103:**5108-13.

138. **Molenkamp, R., S. Greve, W. J. Spaan, and E. J. Snijder.** 2000. Efficient homologous RNA recombination and requirement for an open reading frame during replication of equine arteritis virus defective interfering RNAs. J Virol **74:**9062-70.

139. **Murasko, D. M., E. D. Bernstein, E. M. Gardner, P. Gross, G. Munk, S. Dran, and E. Abrutyn.** 2002. Role of humoral and cell-mediated immunity in protection from influenza disease after immunization of healthy elderly. Exp Gerontol **37:**427-39.

140. **Murray, K., S. Baraniuk, M. Resnick, R. Arafat, C. Kilborn, K. Cain, R. Shallenberger, T. L. York, D. Martinez, J. S. Hellums, D. Hellums, M. Malkoff, N. Elgawley, W. McNeely, S. A. Khuwaja, and R. B. Tesh.** 2006. Risk factors for encephalitis and death from West Nile virus infection. Epidemiol Infect**:**1-8.

141. **Normile, D.** 2004. Infectious diseases. Mounting lab accidents raise SARS fears. Science **304:**659-61.

142. **Normile, D.** 2004. Infectious diseases. Viral DNA match spurs China's civet roundup. Science **303:**292.

143. **Olsen, C. W., W. V. Corapi, C. K. Ngichabe, J. D. Baines, and F. W. Scott.** 1992. Monoclonal antibodies to the spike protein of feline infectious peritonitis virus mediate antibody-dependent enhancement of infection of feline macrophages. J Virol **66:**956-65.

144. **Ontiveros, E., L. Kuo, P. S. Masters, and S. Perlman.** 2001. Inactivation of expression of gene 4 of mouse hepatitis virus strain JHM does not affect virulence in the murine CNS. Virology **289:**230-8.

145. **Ortego, J., I. Sola, F. Almazan, J. E. Ceriani, C. Riquelme, M. Balasch, J. Plana, and L. Enjuanes.** 2003. Transmissible gastroenteritis coronavirus gene 7 is not essential but influences in vivo virus replication and virulence. Virology **308:**13-22.

146. **Pasternak, A. O., W. J. Spaan, and E. J. Snijder.** 2006. Nidovirus transcription: how to make sense...? J Gen Virol **87:**1403-21.

147. **Peiris, J. S., C. M. Chu, V. C. Cheng, K. S. Chan, I. F. Hung, L. L. Poon, K. I. Law, B. S. Tang, T. Y. Hon, C. S. Chan, K. H. Chan, J. S. Ng, B. J. Zheng, W. L. Ng, R. W. Lai, Y. Guan, and K. Y. Yuen.** 2003. Clinical progression and viral load in a community outbreak of coronavirus-associated SARS pneumonia: a prospective study. Lancet **361:**1767-72.

148. **Pensaert, M. B., and P. de Bouck.** 1978. A new coronavirus-like particle associated with diarrhea in swine. Arch Virol **58:**243-7.

149. **Poon, L. L., D. K. Chu, K. H. Chan, O. K. Wong, T. M. Ellis, Y. H. Leung, S. K. Lau, P. C. Woo, K. Y. Suen, K. Y. Yuen, Y. Guan, and J. S. Peiris.** 2005. Identification of a novel coronavirus in bats. J Virol **79:**2001-9.

150. **Poon, L. L., Y. Guan, J. M. Nicholls, K. Y. Yuen, and J. S. Peiris.** 2004. The aetiology, origins, and diagnosis of severe acute respiratory syndrome. Lancet Infect Dis **4:**663-71.

151. **Prentice, E., J. McAuliffe, X. Lu, K. Subbarao, and M. R. Denison.** 2004. Identification and characterization of severe acute respiratory syndrome coronavirus replicase proteins. J Virol **78:**9977-86.

152. **Putics, A., W. Filipowicz, J. Hall, A. E. Gorbalenya, and J. Ziebuhr.** 2005. ADP-ribose-1"-monophosphatase: a conserved coronavirus enzyme that is dispensable for viral replication in tissue culture. J Virol **79:**12721-31.

153. **Putics, A., A. E. Gorbalenya, and J. Ziebuhr.** 2006. Identification of protease and ADP-ribose 1"-monophosphatase activities associated with transmissible gastroenteritis virus non-structural protein 3. J Gen Virol **87:**651-6.

154. **Qin, C., J. Wang, Q. Wei, M. She, W. A. Marasco, H. Jiang, X. Tu, H. Zhu, L. Ren, H. Gao, L. Guo, L. Huang, R. Yang, Z. Cong, Y. Wang, Y. Liu, Y. Sun, S. Duan, J. Qu, L. Chen, W. Tong, L. Ruan, P. Liu, H. Zhang, J. Zhang, D. Liu, Q. Liu, T. Hong, and W. He.** 2005. An animal model of SARS produced by infection of Macaca mulatta with SARS coronavirus. J Pathol **206:**251-259.

155. **Qiu, M., Y. Shi, Z. Guo, Z. Chen, R. He, R. Chen, D. Zhou, E. Dai, X. Wang, B. Si, Y. Song, J. Li, L. Yang, J. Wang, H. Wang, X. Pang, J. Zhai, Z. Du, Y. Liu, Y. Zhang, L. Li, B. Sun, and R. Yang.** 2005. Antibody responses to individual proteins of SARS coronavirus and their neutralization activities. Microbes Infect **7:**882-9.

156. **Radun, D., M. Niedrig, A. Ammon, and K. Stark.** 2003. SARS: retrospective cohort study among German guests of the Hotel 'M', Hong Kong. Euro Surveill **8:**228-30.

157. **Rest, J. S., and D. P. Mindell.** 2003. SARS associated coronavirus has a recombinant polymerase and coronaviruses have a history of host-shifting. Infect Genet Evol **3:**219-25.

158. **Roberts, A., C. Paddock, L. Vogel, E. Butler, S. Zaki, and K. Subbarao.** 2005. Aged BALB/c mice as a model for increased severity of severe acute respiratory syndrome in elderly humans. J Virol **79:**5833-8.

159. **Ronquist, F., and J. P. Huelsenbeck.** 2003. MrBayes 3: Bayesian phylogenetic inference under mixed models. Bioinformatics **19:**1572-4.

160. **Rottier, P. J., K. Nakamura, P. Schellen, H. Volders, and B. J. Haijema.** 2005. Acquisition of macrophage tropism during the pathogenesis of feline infectious peritonitis is determined by mutations in the feline coronavirus spike protein. J Virol **79:**14122-30.

161. **Saif, L. J.** 2004. Animal coronavirus vaccines: lessons for SARS. Dev Biol (Basel) **119:**129-40.

162. **Saif, L. J.** 1996. Mucosal immunity: an overview and studies of enteric and respiratory coronavirus infections in a swine model of enteric disease. Vet Immunol Immunopathol **54:**163-9.

163. **Saikatendu, K. S., J. S. Joseph, V. Subramanian, T. Clayton, M. Griffith, K. Moy, J. Velasquez, B. W. Neuman, M. J. Buchmeier, R. C. Stevens, and P. Kuhn.** 2005. Structural basis of severe acute respiratory syndrome coronavirus ADP-ribose-1"-phosphate dephosphorylation by a conserved domain of nsP3. Structure (Camb) **13:**1665-75.

164. **Sawicki, S. G., and D. L. Sawicki.** 1986. Coronavirus minus-strand RNA synthesis and effect of cycloheximide on coronavirus RNA synthesis. J Virol **57:**328-34.

165. **Sawicki, S. G., D. L. Sawicki, D. Younker, Y. Meyer, V. Thiel, H. Stokes, and S. G. Siddell.** 2005. Functional and genetic analysis of coronavirus replicase-transcriptase proteins. PLoS Pathog **1:**e39.

166. **Schickli, J. H., L. B. Thackray, S. G. Sawicki, and K. V. Holmes.** 2004. The N-terminal region of the murine coronavirus spike glycoprotein is associated with the extended host range of viruses from persistently infected murine cells. J Virol **78:**9073-83.

167. **Schickli, J. H., B. D. Zelus, D. E. Wentworth, S. G. Sawicki, and K. V. Holmes.** 1997. The murine coronavirus mouse hepatitis virus strain A59 from persistently infected murine cells exhibits an extended host range. J Virol **71:**9499-507.

168. **Schiller, J. J., A. Kanjanahaluethai, and S. C. Baker.** 1998. Processing of the coronavirus MHV-JHM polymerase polyprotein: identification of precursors and proteolytic products spanning 400 kilodaltons of ORF1a. Virology **242:**288-302.

169. **Schwarz, B., E. Routledge, and S. G. Siddell.** 1990. Murine coronavirus nonstructural protein ns2 is not essential for virus replication in transformed cells. J Virol **64:**4784-91.

170. **See, R. H., A. N. Zakhartchouk, M. Petric, D. J. Lawrence, C. P. Mok, R. J. Hogan, T. Rowe, L. A. Zitzow, K. P. Karunakaran, M. M. Hitt, F. L. Graham, L. Prevec, J. B. Mahony, C. Sharon, T. C. Auperin, J. M. Rini, A. J. Tingle, D. W. Scheifele, D. M. Skowronski, D. M. Patrick, T. G. Voss, L. A. Babiuk, J. Gauldie, R. L. Roper, R. C. Brunham, and B. B. Finlay.** 2006. Comparative evaluation of two severe acute respiratory syndrome (SARS) vaccine candidates in mice challenged with SARS coronavirus. J Gen Virol **87:**641-50.

171. **Seybert, A., C. C. Posthuma, L. C. van Dinten, E. J. Snijder, A. E. Gorbalenya, and J. Ziebuhr.** 2005. A complex zinc finger controls the enzymatic activities of nidovirus helicases. J Virol **79:**696-704.

172. **Shi, S. T., and M. M. Lai.** 2005. Viral and cellular proteins involved in coronavirus replication. Curr Top Microbiol Immunol **287:**95-131.

173. **Shi, S. T., J. J. Schiller, A. Kanjanahaluethai, S. C. Baker, J. W. Oh, and M. M. Lai.** 1999. Colocalization and membrane association of murine hepatitis virus gene 1 products and De novo-synthesized viral RNA in infected cells. J Virol **73:**5957-69.

174. **Sims, A. C., R. S. Baric, B. Yount, S. E. Burkett, P. L. Collins, and R. J. Pickles.** 2005. Severe acute respiratory syndrome coronavirus infection of human ciliated airway epithelia: role of ciliated cells in viral spread in the conducting airways of the lungs. J Virol **79:**15511-24.

175. **Skowronski, D. M., C. Astell, R. C. Brunham, D. E. Low, M. Petric, R. L. Roper, P. J. Talbot, T. Tam, and L. Babiuk.** 2005. Severe acute respiratory syndrome (SARS): a year in review. Annu Rev Med **56:**357-81.

176. **Smati, R., A. Silim, C. Guertin, M. Henrichon, M. Marandi, M. Arella, and A. Merzouki.** 2002. Molecular characterization of three new avian infectious bronchitis virus (IBV) strains isolated in Quebec. Virus Genes **25:**85-93.

177. **Smith, H. O., C. A. Hutchison, 3rd, C. Pfannkoch, and J. C. Venter.** 2003. Generating a synthetic genome by whole genome assembly: phiX174 bacteriophage from synthetic oligonucleotides. Proc Natl Acad Sci U S A **100:**15440-5.

178. **Snijder, E. J., P. J. Bredenbeek, J. C. Dobbe, V. Thiel, J. Ziebuhr, L. L. Poon, Y. Guan, M. Rozanov, W. J. Spaan, and A. E. Gorbalenya.** 2003. Unique and conserved features of genome and proteome of SARS-coronavirus, an early split-off from the coronavirus group 2 lineage. J Mol Biol **331:**991-1004.

179. **Song, H., P. W. Price, and J. Cerny.** 1997. Age-related changes in antibody repertoire: contribution from T cells. Immunol Rev **160:**55-62.

180. **Song, H. D., C. C. Tu, G. W. Zhang, S. Y. Wang, K. Zheng, L. C. Lei, Q. X. Chen, Y. W. Gao, H. Q. Zhou, H. Xiang, H. J. Zheng, S. W. Chern, F. Cheng, C. M. Pan, H. Xuan, S. J. Chen, H. M. Luo, D. H. Zhou, Y. F. Liu, J. F. He, P. Z. Qin, L. H. Li, Y. Q. Ren, W. J. Liang, Y. D. Yu, L. Anderson, M. Wang, R. H. Xu, X. W. Wu, H. Y. Zheng, J. D. Chen, G. Liang, Y. Gao, M. Liao, L. Fang, L. Y. Jiang, H. Li, F. Chen, B. Di, L. J. He, J. Y. Lin, S. Tong, X. Kong, L. Du, P. Hao, H. Tang, A. Bernini, X. J. Yu, O. Spiga, Z. M. Guo, H. Y. Pan, W. Z. He, J. C. Manuguerra, A. Fontanet, A. Danchin, N. Niccolai, Y. X. Li, C. I. Wu, and G. P. Zhao.** 2005. Cross-host evolution of severe acute respiratory syndrome coronavirus in palm civet and human. Proc Natl Acad Sci U S A **102:**2430-5.

181. **Spruth, M., O. Kistner, H. Savidis-Dacho, E. Hitter, B. Crowe, M. Gerencer, P. Bruhl, L. Grillberger, M. Reiter, C. Tauer, W. Mundt, and P. N. Barrett.** 2006. A double-inactivated whole virus candidate SARS coronavirus vaccine stimulates neutralising and protective antibody responses. Vaccine **24:**652-61.

182. **Srikantiah, P., M. D. Charles, S. Reagan, T. A. Clark, M. W. Pletz, P. R. Patel, R. M. Hoekstra, J. Lingappa, J. A. Jernigan, and M. Fischer.** 2005. SARS clinical features, United States, 2003. Emerg Infect Dis **11:**135-8.

183. **Stadler, K., A. Roberts, S. Becker, L. Vogel, M. Eickmann, L. Kolesnikova, H. D. Klenk, B. Murphy, R. Rappuoli, S. Abrignani, and K. Subbarao.** 2005. SARS vaccine protective in mice. Emerg Infect Dis **11:**1312-4.

184. **Stanhope, M. J., J. R. Brown, and H. Amrine-Madsen.** 2004. Evidence from the evolutionary analysis of nucleotide sequences for a recombinant history of SARS-CoV. Infect Genet Evol **4:**15-9.

185. **Stavrinides, J., and D. S. Guttman.** 2004. Mosaic evolution of the severe acute respiratory syndrome coronavirus. J Virol **78:**76-82.

186. **St-Jean, J. R., M. Desforges, F. Almazan, H. Jacomy, L. Enjuanes, and P. J. Talbot.** 2006. Recovery of a neurovirulent human coronavirus OC43 from an infectious cDNA clone. J Virol **80:**3670-4.

187. **Su, D., Z. Lou, F. Sun, Y. Zhai, H. Yang, R. Zhang, A. Joachimiak, X. C. Zhang, M. Bartlam, and Z. Rao.** 2006. Dodecamer structure of severe acute respiratory syndrome coronavirus nonstructural protein nsp10. J Virol **80:**7902-8.

188. **Subbarao, K., J. McAuliffe, L. Vogel, G. Fahle, S. Fischer, K. Tatti, M. Packard, W. J. Shieh, S. Zaki, and B. Murphy.** 2004. Prior infection and passive transfer of neutralizing antibody prevent replication of severe acute respiratory syndrome coronavirus in the respiratory tract of mice. J Virol **78:**3572-7.

189. **Subbarao, K., and A. Roberts.** 2006. Is there an ideal animal model for SARS? Trends Microbiol **14:**299-303.

190. **Sui, J., W. Li, A. Murakami, A. Tamin, L. J. Matthews, S. K. Wong, M. J. Moore, A. S. Tallarico, M. Olurinde, H. Choe, L. J. Anderson, W. J. Bellini, M. Farzan, and W. A. Marasco.** 2004. Potent neutralization of severe acute respiratory syndrome (SARS) coronavirus by a human mAb to S1 protein that blocks receptor association. Proc Natl Acad Sci U S A **101:**2536-41.

191. **Sutton, G., E. Fry, L. Carter, S. Sainsbury, T. Walter, J. Nettleship, N. Berrow, R. Owens, R. Gilbert, A. Davidson, S. Siddell, L. L. Poon, J. Diprose, D.**

Alderton, M. Walsh, J. M. Grimes, and D. I. Stuart. 2004. The nsp9 replicase protein of SARS-coronavirus, structure and functional insights. Structure **12:**341-53.

192. **Takasuka, N., H. Fujii, Y. Takahashi, M. Kasai, S. Morikawa, S. Itamura, K. Ishii, M. Sakaguchi, K. Ohnishi, M. Ohshima, S. Hashimoto, T. Odagiri, M. Tashiro, H. Yoshikura, T. Takemori, and Y. Tsunetsugu-Yokota.** 2004. A subcutaneously injected UV-inactivated SARS coronavirus vaccine elicits systemic humoral immunity in mice. Int Immunol **16:**1423-30.

193. **Thackray, L. B., and K. V. Holmes.** 2004. Amino acid substitutions and an insertion in the spike glycoprotein extend the host range of the murine coronavirus MHV-A59. Virology **324:**510-24.

194. **Thackray, L. B., B. C. Turner, and K. V. Holmes.** 2005. Substitutions of conserved amino acids in the receptor-binding domain of the spike glycoprotein affect utilization of murine CEACAM1a by the murine coronavirus MHV-A59. Virology **334:**98-110.

195. **The Chinese SARS Molecular Epidemiology Consortium.** 2004. Molecular Evolution of the SARS Coronavirus During the Course of the SARS Epidemic in China. Science **303:**1666-1669.

196. **Thiel, V., J. Herold, B. Schelle, and S. G. Siddell.** 2001. Infectious RNA transcribed in vitro from a cDNA copy of the human coronavirus genome cloned in vaccinia virus. J Gen Virol **82:**1273-81.

197. **Thiel, V., and S. G. Siddell.** 2005. Reverse genetics of coronaviruses using vaccinia virus vectors. Curr Top Microbiol Immunol **287:**199-227.

198. **Tibbles, K. W., I. Brierley, D. Cavanagh, and T. D. Brown.** 1996. Characterization in vitro of an autocatalytic processing activity associated with the predicted 3C-like proteinase domain of the coronavirus avian infectious bronchitis virus. J Virol **70:**1923-30.

199. **Tresnan, D. B., R. Levis, and K. V. Holmes.** 1996. Feline aminopeptidase N serves as a receptor for feline, canine, porcine, and human coronaviruses in serogroup I. J Virol **70:**8669-74.

200. **Tripp, R. A., L. M. Haynes, D. Moore, B. Anderson, A. Tamin, B. H. Harcourt, L. P. Jones, M. Yilla, G. J. Babcock, and T. Greenough.** 2005. Monoclonal antibodies to SARS-associated coronavirus (SARS-CoV): Identification of neutralizing and antibodies reactive to S, N, M and E viral proteins. Journal of Virological Methods **128:**21-28.

201. **Tsunemitsu, H., Z. R. el-Kanawati, D. R. Smith, H. H. Reed, and L. J. Saif.** 1995. Isolation of coronaviruses antigenically indistinguishable from bovine coronavirus from wild ruminants with diarrhea. J Clin Microbiol **33:**3264-9.

202. **Tu, C., G. Crameri, X. Kong, J. Chen, Y. Sun, M. Yu, H. Xiang, X. Xia, S. Liu, T. Ren, Y. Yu, B. T. Eaton, H. Xuan, and L. F. Wang.** 2004. Antibodies to SARS coronavirus in civets. Emerg Infect Dis **10:**2244-8.

203. **van der Hoek, L., K. Pyrc, M. F. Jebbink, W. Vermeulen-Oost, R. J. Berkhout, K. C. Wolthers, P. M. Wertheim-van Dillen, J. Kaandorp, J. Spaargaren, and B. Berkhout.** 2004. Identification of a new human coronavirus. Nat Med **10:**368-73.

204. **van der Meer, Y., E. J. Snijder, J. C. Dobbe, S. Schleich, M. R. Denison, W. J. Spaan, and J. K. Locker.** 1999. Localization of mouse hepatitis virus nonstructural proteins and RNA synthesis indicates a role for late endosomes in viral replication. J Virol **73:**7641-57.

205. **van Dinten, L. C., J. A. den Boon, A. L. Wassenaar, W. J. Spaan, and E. J. Snijder.** 1997. An infectious arterivirus cDNA clone: identification of a replicase point mutation that abolishes discontinuous mRNA transcription. Proc Natl Acad Sci U S A **94:**991-6.

206. **van Dinten, L. C., S. Rensen, A. E. Gorbalenya, and E. J. Snijder.** 1999. Proteolytic processing of the open reading frame 1b-encoded part of arterivirus replicase is mediated by nsp4 serine protease and Is essential for virus replication. J Virol **73:**2027-37.

207. **Vega, V. B., Y. Ruan, J. Liu, W. H. Lee, C. L. Wei, S. Y. Se-Thoe, K. F. Tang, T. Zhang, P. R. Kolatkar, E. E. Ooi, A. E. Ling, L. W. Stanton, P. M. Long, and E. T. Liu.** 2004. Mutational dynamics of the SARS coronavirus in cell culture and human populations isolated in 2003. BMC Infect Dis **4:**32.

208. **Vennema, H.** 1999. Genetic drift and genetic shift during feline coronavirus evolution. Vet Microbiol **69:**139-41.

209. **Vennema, H., A. Poland, J. Foley, and N. C. Pedersen.** 1998. Feline infectious peritonitis viruses arise by mutation from endemic feline enteric coronaviruses. Virology **243:**150-7.

210. **Vignuzzi, M., J. K. Stone, J. J. Arnold, C. E. Cameron, and R. Andino.** 2006. Quasispecies diversity determines pathogenesis through cooperative interactions in a viral population. Nature **439:**344-8.

211. **Vijgen, L., E. Keyaerts, P. Lemey, P. Maes, K. Van Reeth, H. Nauwynck, M. Pensaert, and M. Van Ranst.** 2006. Evolutionary history of the closely related group

2 coronaviruses: porcine hemagglutinating encephalomyelitis virus, bovine coronavirus, and human coronavirus OC43. J Virol **80:**7270-4.

212. **von Grotthuss, M., L. S. Wyrwicz, and L. Rychlewski.** 2003. mRNA cap-1 methyltransferase in the SARS genome. Cell **113:**701-2.

213. **Wang, L., D. Junker, and E. W. Collisson.** 1993. Evidence of natural recombination within the S1 gene of infectious bronchitis virus. Virology **192:**710-6.

214. **Wang, S., T. H. Chou, P. V. Sakhatskyy, S. Huang, J. M. Lawrence, H. Cao, X. Huang, and S. Lu.** 2005. Identification of two neutralizing regions on the severe acute respiratory syndrome coronavirus spike glycoprotein produced from the mammalian expression system. J Virol **79:**1906-10.

215. **Wang, Z., Z. Yuan, M. Matsumoto, U. R. Hengge, and Y. F. Chang.** 2005. Immune responses with DNA vaccines encoded different gene fragments of severe acute respiratory syndrome coronavirus in BALB/c mice. Biochem Biophys Res Commun **327:**130-5.

216. **Weingartl, H., M. Czub, S. Czub, J. Neufeld, P. Marszal, J. Gren, G. Smith, S. Jones, R. Proulx, Y. Deschambault, E. Grudeski, A. Andonov, R. He, Y. Li, J. Copps, A. Grolla, D. Dick, J. Berry, S. Ganske, L. Manning, and J. Cao.** 2004. Immunization with modified vaccinia virus Ankara-based recombinant vaccine against severe acute respiratory syndrome is associated with enhanced hepatitis in ferrets. J Virol **78:**12672-6.

217. **Weiss, S. R., P. W. Zoltick, and J. L. Leibowitz.** 1993. The ns 4 gene of mouse hepatitis virus (MHV), strain A 59 contains two ORFs and thus differs from ns 4 of the JHM and S strains. Arch Virol **129:**301-9.

218. **Wentworth, D. E., D. B. Tresnan, B. C. Turner, I. R. Lerman, B. Bullis, E. M. Hemmila, R. Levis, L. H. Shapiro, and K. V. Holmes.** 2005. Cells of human aminopeptidase N (CD13) transgenic mice are infected by human coronavirus-229E in vitro, but not in vivo. Virology **335:**185-97.

219. **Woo, P. C., S. K. Lau, C. M. Chu, K. H. Chan, H. W. Tsoi, Y. Huang, B. H. Wong, R. W. Poon, J. J. Cai, W. K. Luk, L. L. Poon, S. S. Wong, Y. Guan, J. S. Peiris, and K. Y. Yuen.** 2005. Characterization and complete genome sequence of a novel coronavirus, coronavirus HKU1, from patients with pneumonia. J Virol **79:**884-95.

220. **Woo, P. C., S. K. Lau, C. C. Yip, Y. Huang, H. W. Tsoi, K. H. Chan, and K. Y. Yuen.** 2006. Comparative analysis of 22 coronavirus HKU1 genomes reveals a novel genotype and evidence of natural recombination in coronavirus HKU1. J Virol **80:**7136-45.

221. **Woolhouse, M. E., and S. Gowtage-Sequeria.** 2005. Host range and emerging and reemerging pathogens. Emerg Infect Dis **11:**1842-7.

222. **Xiong, S., Y. F. Wang, M. Y. Zhang, X. J. Liu, C. H. Zhang, S. S. Liu, C. W. Qian, J. X. Li, J. H. Lu, Z. Y. Wan, H. Y. Zheng, X. G. Yan, M. J. Meng, and J. L. Fan.** 2004. Immunogenicity of SARS inactivated vaccine in BALB/c mice. Immunol Lett **95:**139-43.

223. **Yang, Z. Y., W. P. Kong, Y. Huang, A. Roberts, B. R. Murphy, K. Subbarao, and G. J. Nabel.** 2004. A DNA vaccine induces SARS coronavirus neutralization and protective immunity in mice. Nature **428:**561-4.

224. **Yang, Z. Y., H. C. Werner, W. P. Kong, K. Leung, E. Traggiai, A. Lanzavecchia, and G. J. Nabel.** 2005. Evasion of antibody neutralization in emerging severe acute respiratory syndrome coronaviruses. Proc Natl Acad Sci U S A **102:**797-801.

225. **Yeager, C. L., R. A. Ashmun, R. K. Williams, C. B. Cardellichio, L. H. Shapiro, A. T. Look, and K. V. Holmes.** 1992. Human aminopeptidase N is a receptor for human coronavirus 229E. Nature **357:**420-2.

226. **Yeh, S. H., H. Y. Wang, C. Y. Tsai, C. L. Kao, J. Y. Yang, H. W. Liu, I. J. Su, S. F. Tsai, D. S. Chen, and P. J. Chen.** 2004. Characterization of severe acute respiratory syndrome coronavirus genomes in Taiwan: molecular epidemiology and genome evolution. Proc Natl Acad Sci U S A **101:**2542-7.

227. **Yokomori, K., and M. M. Lai.** 1991. Mouse hepatitis virus S RNA sequence reveals that nonstructural proteins ns4 and ns5a are not essential for murine coronavirus replication. J Virol **65:**5605-8.

228. **Youn, S., J. L. Leibowitz, and E. W. Collisson.** 2005. In vitro assembled, recombinant infectious bronchitis viruses demonstrate that the 5a open reading frame is not essential for replication. Virology **332:**206-15.

229. **Yount, B., K. M. Curtis, and R. S. Baric.** 2000. Strategy for systematic assembly of large RNA and DNA genomes: transmissible gastroenteritis virus model. J Virol **74:**10600-11.

230. **Yount, B., K. M. Curtis, E. A. Fritz, L. E. Hensley, P. B. Jahrling, E. Prentice, M. R. Denison, T. W. Geisbert, and R. S. Baric.** 2003. Reverse genetics with a full-length infectious cDNA of severe acute respiratory syndrome coronavirus. Proc Natl Acad Sci U S A **100:**12995-3000.

231. **Yount, B., M. R. Denison, S. R. Weiss, and R. S. Baric.** 2002. Systematic assembly of a full-length infectious cDNA of mouse hepatitis virus strain A59. J Virol **76:**11065-78.

232. **Yount, B., R. S. Roberts, L. Lindesmith, and R. S. Baric.** 2006. Rewiring the severe acute respiratory syndrome coronavirus (SARS-CoV) transcription circuit: Engineering a recombination-resistant genome. Proc Natl Acad Sci U S A **103:**12546-51.

233. **Zakhartchouk, A. N., Q. Liu, M. Petric, and L. A. Babiuk.** 2005. Augmentation of immune responses to SARS coronavirus by a combination of DNA and whole killed virus vaccines. Vaccine **23:**4385-91.

234. **Zhai, Y., F. Sun, X. Li, H. Pang, X. Xu, M. Bartlam, and Z. Rao.** 2005. Insights into SARS-CoV transcription and replication from the structure of the nsp7-nsp8 hexadecamer. Nat Struct Mol Biol.

235. **Zhang, J. S., J. T. Chen, Y. X. Liu, Z. S. Zhang, H. Gao, Y. Liu, X. Wang, Y. Ning, Y. F. Liu, Q. Gao, J. G. Xu, C. Qin, X. P. Dong, and W. D. Yin.** 2005. A serological survey on neutralizing antibody titer of SARS convalescent sera. J Med Virol **77:**147-50.

236. **Zhang, X. M., W. Herbst, K. G. Kousoulas, and J. Storz.** 1994. Biological and genetic characterization of a hemagglutinating coronavirus isolated from a diarrhoeic child. J Med Virol **44:**152-61.

237. **Zhang, X. W., Y. L. Yap, and A. Danchin.** 2005. Testing the hypothesis of a recombinant origin of the SARS-associated coronavirus. Arch Virol **150:**1-20.

238. **Zhao, P., J. S. Ke, Z. L. Qin, H. Ren, L. J. Zhao, J. G. Yu, J. Gao, S. Y. Zhu, and Z. T. Qi.** 2004. DNA vaccine of SARS-Cov S gene induces antibody response in mice. Acta Biochim Biophys Sin (Shanghai) **36:**37-41.

239. **Zheng, B., S. Han, Y. Takahashi, and G. Kelsoe.** 1997. Immunosenescence and germinal center reaction. Immunol Rev **160:**63-77.

240. **Zheng, B. J., K. H. Wong, J. Zhou, K. L. Wong, B. W. Young, L. W. Lu, and S. S. Lee.** 2004. SARS-related virus predating SARS outbreak, Hong Kong. Emerg Infect Dis **10:**176-8.

241. **Zhu, M. S., Y. Pan, H. Q. Chen, Y. Shen, X. C. Wang, Y. J. Sun, and K. H. Tao.** 2004. Induction of SARS-nucleoprotein-specific immune response by use of DNA vaccine. Immunol Lett **92:**237-43.

242. **Ziebuhr, J.** 2005. The coronavirus replicase. Curr Top Microbiol Immunol **287:**57-94.

243. **Ziebuhr, J., E. J. Snijder, and A. E. Gorbalenya.** 2000. Virus-encoded proteinases and proteolytic processing in the Nidovirales. J Gen Virol **81:**853-79.